

An Emerging Era: Conformable Ultrasound Electronics

Lin Zhang, Wenya Du, Jin-Hoon Kim, Chia-Chen Yu, and Canan Dagdeviren*

Conformable electronics are regarded as the next generation of personal healthcare monitoring and remote diagnosis devices. In recent years, piezoelectric-based conformable ultrasound electronics (cUSE) have been intensively studied due to their unique capabilities, including nonradiative monitoring, soft tissue imaging, deep signal decoding, wireless power transfer, portability, and compatibility. This review provides a comprehensive understanding of cUSE for use in biomedical and healthcare monitoring systems and a summary of their recent advancements. Following an introduction to the fundamentals of piezoelectrics and ultrasound transducers, the critical parameters for transducer design are discussed. Next, five types of cUSE with their advantages and limitations are highlighted, and the fabrication of cUSE using advanced technologies is discussed. In addition, the working function, acoustic performance, and accomplishments in various applications are thoroughly summarized. It is noted that application considerations must be given to the tradeoffs between material selection, manufacturing processes, acoustic performance, mechanical integrity, and the entire integrated system. Finally, current challenges and directions for the development of cUSE are highlighted, and research flow is provided as the roadmap for future research. In conclusion, these advances in the fields of piezoelectric materials, ultrasound transducers, and conformable electronics spark an emerging era of biomedicine and personal healthcare.

real-time analysis of bodily vital signs have assumed paramount importance in safeguarding individuals from the onset and progression of diseases. On the one hand, those who rely on conventional centralized healthcare services are required to physically visit hospitals in order to access medical treatment, hence potentially experiencing delays in meeting their healthcare needs. In contrast, it is important to acknowledge that the diverse range of rigid tools and diagnostic techniques present a number of limitations, including suboptimal biocompatibility, reliance on skilled operators, and uncomfortable patient experiences.^[2] It is highly desired to have medical equipment or systems that allow patients to monitor and control their own health problems by themselves. In recent decades, conformable electronics have garnered significant interest and will transform traditional healthcare monitoring and diagnosis through the incorporation of qualities such as portability, wearability, remote access, and timelines.^[3] A variety of flexible electronics with different substrates and matrices (i.e., polymers,^[4] elastomers,^[5] textiles,^[6] aerogels,^[7] hydrogels^[8])—have


1. Introduction

Healthcare and medical systems have been facing tremendous challenges in recent decades, due to the ever-increasing health requirements of society as well as the unanticipated health problems that have arisen around the world.^[1] More and more individuals are realizing that most non-communicable diseases are caused by physical inactivity, poor nutrition, and low-quality lifestyle choices. In modern society, the regular collection and

been demonstrated for monitoring a wide range of health-relevant parameters—such as electrophysiological (e.g., electrocardiogram (ECG), electroencephalogram (EEG), electromyography (EMG), electrooculogram (EOG)),^[9] physiological (e.g., blood pressure,^[10] pulse,^[11] temperature^[12]), thermal (e.g., thermal conductivity, temperature distribution^[13]), mechanical^[14] (e.g., strain,^[15] pressure^[16]) and biochemical information (e.g., glucose/lactate,^[17] hydration,^[18] pH,^[19] sweat,^[20] local field potential^[21]), have continuously emanated from the human body. However, the majority of these devices tended to concentrate on physiological signals from the human body's surface or the tissue/organ's surface, offering limited information on or inside deep tissues/organs. Decoding data from deep tissue, which plays a crucial role in the intricate processes at the root of many disease forms, is of great interest.

Ultrasound technology, one of the most widely used and quickly evolving diagnosis and treatment modalities, has been extensively explored for medical diagnosis in deep tissue. It has numerous advantages over magnetic resonance imaging (MRI), which lacks real-time imaging and is expensive, as well as computed tomography (CT), which is ionizing and dangerous. Ultrasonic waves are typically produced by a number of physical phenomena, such as magnetostrictive, electrostatic, electrodynamic,

L. Zhang, W. Du, J.-H. Kim, C.-C. Yu, C. Dagdeviren
Media Lab
Massachusetts Institute of Technology
Cambridge, MA 02139, USA
E-mail: canand@mit.edu

 The ORCID identification number(s) for the author(s) of this article can be found under <https://doi.org/10.1002/adma.202307664>

© 2023 The Authors. Advanced Materials published by Wiley-VCH GmbH. This is an open access article under the terms of the Creative Commons Attribution-NonCommercial License, which permits use, distribution and reproduction in any medium, provided the original work is properly cited and is not used for commercial purposes.

DOI: 10.1002/adma.202307664

piezoelectric, and capacitive effects.^[22] The piezoelectric effect is the most common operating principle for actuating and sensing ultrasonic signals.^[23] This review will concentrate solely on piezoelectric-based ultrasound systems. The ultrasonic method is an ideal technology for non-destructive testing (NDT), biomedical, and healthcare applications because of its special characteristics, such as its excellent precision, powerful deep tissue penetrating capability, tremendous sensitivity, and non-ion radiative nature. The design principle, materials, configurations, fabrication, and applications of traditional ultrasound transducers have been widely investigated in recent decades.^[23] Despite the advantages offered by ultrasound technologies, traditional ultrasound probes are large and heavy, and an operator is required to hold them steady to achieve a solid acoustic coupling interface, a sufficient field of view, or a desired penetration direction. In particular, it is still not possible for an ultrasound probe to cover the full curved surface of a human body part such as elbow, skull, knee, or large parts of the body such as breast, abdomen, or fetus.^[24] Therefore, mechanically deformed ultrasonic transducers that may seamlessly adhere to the skin and still contain ultrasound function are significantly needed for accurate imaging, long-term monitoring, precise therapy, and other applications. In this review, we used conformable ultrasound electronics (cUSE) to represent all types of attachable, wearable, flexible, and soft ultrasound sensors, transducers, and patches. The concept of cUSE was first put forth before 2010,^[24,25] then intensively investigated in the past six years,^[26] which not only solved some current limitations of rigid and bulky ultrasound probes, but also developed various designs and technologies of conformable electronics for healthcare to a new level. In recent studies, numerous cUSE were proposed and fabricated using several fabrication strategies for NDT and biomedical applications (**Figure 1**), including stretchable^[27] and bendable^[28] devices imaging on complex surfaces, long-term monitoring with bio-adhesion^[29] or intergated system,^[30] large organ monitoring (breast tissue,^[31] bladder volume),^[32] cardiac monitoring,^[33] blood pressure monitoring,^[34] blood flow monitoring,^[35] energy harvesting^[36] and power transfer for implant device,^[37] tissue repair,^[38] chronic wound healing,^[39] retinal stimulating,^[40] peripheral nerve stimulation,^[41] brain stimulation,^[42] drug delivery on faces,^[43] transdermal cosmeceutical delivery,^[44] and several other biomedical applications.

In this review, we provide an overview of the most current advancements and innovations in piezoelectric-based cUSE, including the selection of materials, device performance, mechanical conformability, and applications in biomedical and health monitoring systems (**Figure 2**). A brief outline of this review is as follows. Section 2 introduces the fundamentals and configurations of ultrasound transducers, including single-element transducers, 1D arrays, and 2D matrix arrays for 3D images, and the properties of different types of piezoelectric materials, particularly the specifications needed for high-performance ultrasound transducers. Strategies for cUSE are outlined in Section 3, along with different types, several technical requirements, substrates, and interfaces, beamforming, and data acquisition systems. Section 4 exhibits the cUSE for various biomedical applications, including wearable large patches for tissue imaging, health monitoring, brain/neural stimulation, energy harvesting and power transfer, therapeutics, drug delivery, and CUSE hybrids with other electronics. Finally,

in Section 5, we provide a summary of the current status of cUSE, and discuss the challenges and prospects for the future.

2. Piezoelectric Materials and Ultrasound Transducers

In recent years, piezoelectric materials, as the smart materials that link electrical and mechanical energy, have been extensively utilized in a variety of electronic devices. Recent developments in mechanical engineering and material fabrication technology have made it possible to realize high-performance piezoelectric devices in conformable configurations and given them unique prospects for usage in bio-integrated applications.^[14,46] Piezoelectric conformable electronics, fabricated from ceramics, crystals, composites,^[7,47] thin film, polymers, fibers,^[48] have demonstrated real-time and continuous signal monitoring and decoding for diverse soft tissue biomedical and healthcare applications, ranging from sensing^[46a,49] to energy harvesting^[14a,50] and human-machine interactions,^[51] including in understanding body motion, facial motion,^[5,52] skin modulus,^[15,53] heart motion,^[54] gastrointestinal motility,^[4] tactile stimuli,^[55] blood pressure,^[16b,34] and blood flow.^[35] In addition, through quantitative imaging, piezoelectric ultrasound transducers can provide insight into deep tissues and curved organs, improving our understanding of soft tissue illnesses. Because there are numerous piezoelectric materials, it is necessary to have an in-depth summary of available materials to choose the appropriate one for creating ultrasonic transducers. In the first half of this section, various well-known piezoelectric ceramics, single crystals, thin films, and composites are introduced. The critical parameters and equations of piezoelectric materials are summarized in **Table 1**. Some novel piezoelectric materials are also discussed to illustrate the most recent piezoelectric material fabrication technologies. In the second half of this section, the design and configuration of ultrasound transducers are summarized, and important parameters are listed in **Table 2**. A large range of piezoelectric materials have been developed because of the great variety of piezoelectric transducers, as listed in **Table 3**.

2.1. Traditional Piezoelectric Materials for Ultrasound Transducers

2.1.1. Critical Parameters of Piezoelectric Materials

Piezoelectricity is a unique property of certain non-centrally symmetric crystalline materials.^[56] The piezoelectric effect is a reversible process that exhibits two effects: direct piezoelectric effect (generating electric polarization after applying mechanical stress) and the converse piezoelectric effect (generating mechanical strain after applying an electric field), which are fundamental for a number of electronic devices, including transducers, actuators, and sensors (**Figure 3a,b**).^[23b,57] The piezoelectric coefficient for each material has its own value with respect to its crystal orientation.^[56] An appropriate material must be polarized by using a strong electric field in order to create piezoelectric characteristics. Two digits are frequently used to subscript or describe piezoelectric characteristics. The direction of the created charge

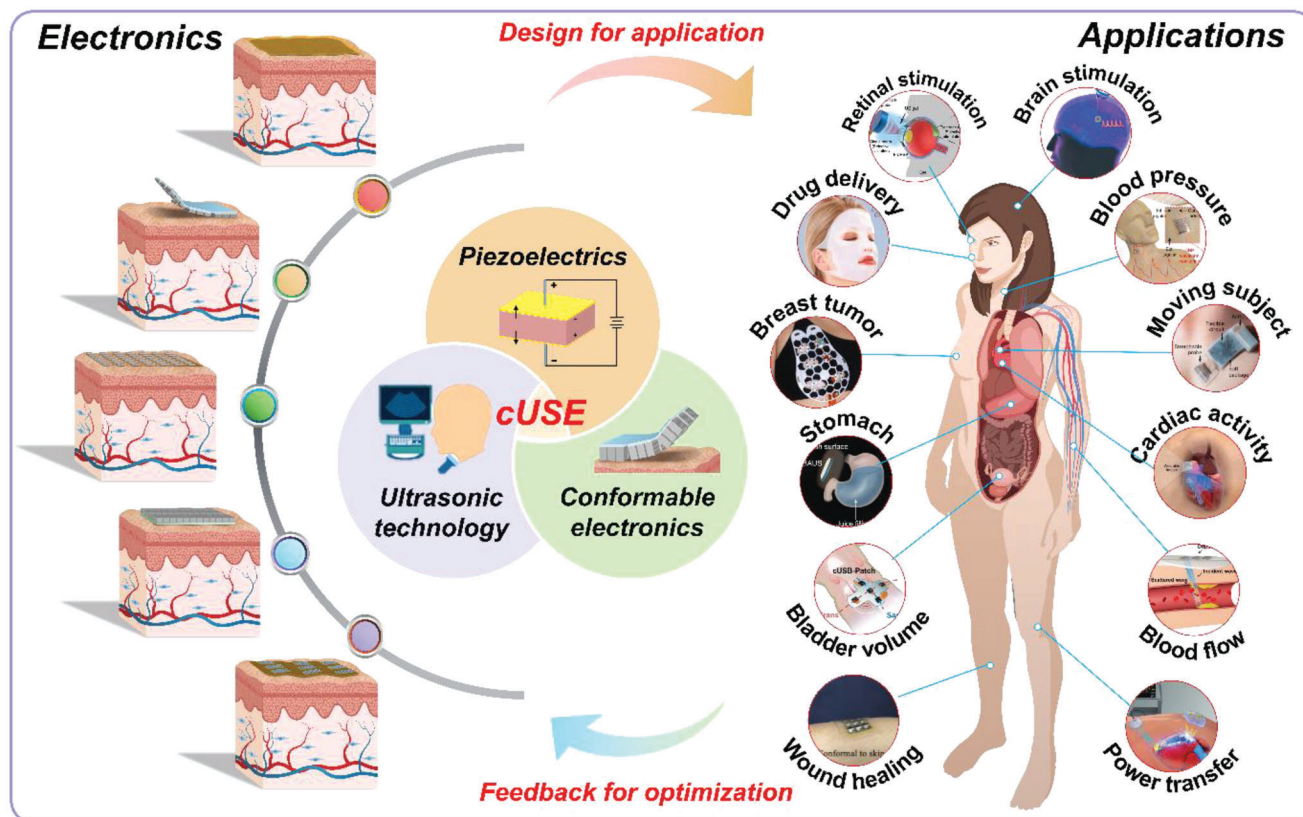


Figure 1. Overview of conformable ultrasound electronics (cUSE) and their biomedical applications. The cUSE is the research domain that encompasses the study of piezoelectric materials, ultrasonic technology, and conformable electronics. The representative biomedical applications included: imaging the dynamics of the stomach (Reproduced with permission.^[29] Copyright 2022, American Association for the Advancement of Science), imaging the moving subject (Reproduced with permission.^[30] Copyright 2023, Springer Nature Limited), cardiac activity monitoring (Reproduced under the terms of the Creative Commons License.^[45] Copyright 2023, The Authors, Published by Springer Nature Limited), imaging on breast tumors (Reproduced under the terms of the Creative Commons License.^[31] Copyright 2023, The Authors, Published by American Association for the Advancement of Science), bladder volume monitoring (Reproduced with permission.^[32] Copyright 2023, Springer Nature Limited.), blood pressure monitoring (Reproduced with permission.^[34] Copyright 2021, Springer Nature Limited), blood flow monitoring (Reproduced under the terms of the Creative Commons License.^[35] Copyright 2021, The Authors, Published by American Association for the Advancement of Science), energy harvesting and power transfer (Reproduced under the terms of the Creative Commons License.^[36] Copyright 2021, The Authors, Published by American Association for the Advancement of Science), wound healing (Reproduced with permission.^[39] Copyright 2021, Wiley-VCH), retinal electrical stimulation (Reproduced under the terms of the Creative Commons License.^[40] Copyright 2022, The Authors, Published by Springer Nature Limited), drug delivery (Reproduced with permission.^[44] Copyright 2023, Wiley-VCH), brain stimulation (Reproduced under the terms of the Creative Commons License.^[42] Copyright 2022, The Authors, Published by Springer Nature Limited).

or the applied electric field is indicated by the first subscript. The direction of the mechanical stress or strain is indicated by the second subscript. The polarizing direction, or applied polarization field direction, has traditionally been abbreviated as “3”. The direction “3” refers to other instructions. Although a piezoelectric material can have a wide range of characteristics and piezoelectric coefficients, it is chosen based on the intended vibration mode. Consider a vibrational mode in which thickness plays a significant role. For applications requiring thickness or out-of-plane vibration monitoring, a piezoelectric element with a higher d_{33} property is chosen.

In the field of materials science, many parameters must be defined to describe the properties of piezoelectric materials. Dielectric, piezoelectric, electromechanical, and acoustic properties are the four most important material properties when designing an ultrasonic transducer, including the piezoelectric coefficient

(d_{33}), dielectric permittivity (ϵ_r), electromechanical coupling coefficient (k), and acoustic impedance (Z). In addition, the use of piezoelectric composites has attracted a great deal of interest due to the material’s enhanced electromechanical coupling, which can help broaden bandwidths and increase energy transfer, resulting in a substantial improvement in signal-to-noise ratio (SNR). Temperature and high electric field stability are also important for ultrasound transducers, since the dielectric permittivity changes as a function of temperature and electric field, resulting in a variation of electrical impedance of the device.

Because the piezoelectric material is a capacitor, the related electrical port of an ultrasonic transducer is a capacitor structure, which is the dielectric between two parallel electrodes.^[58] A dielectric is an electrical insulator that can respond to external electric stimulation.^[59] When an AC electric field is applied to the dielectric material, the dielectric permittivity (ϵ'') shows a complex

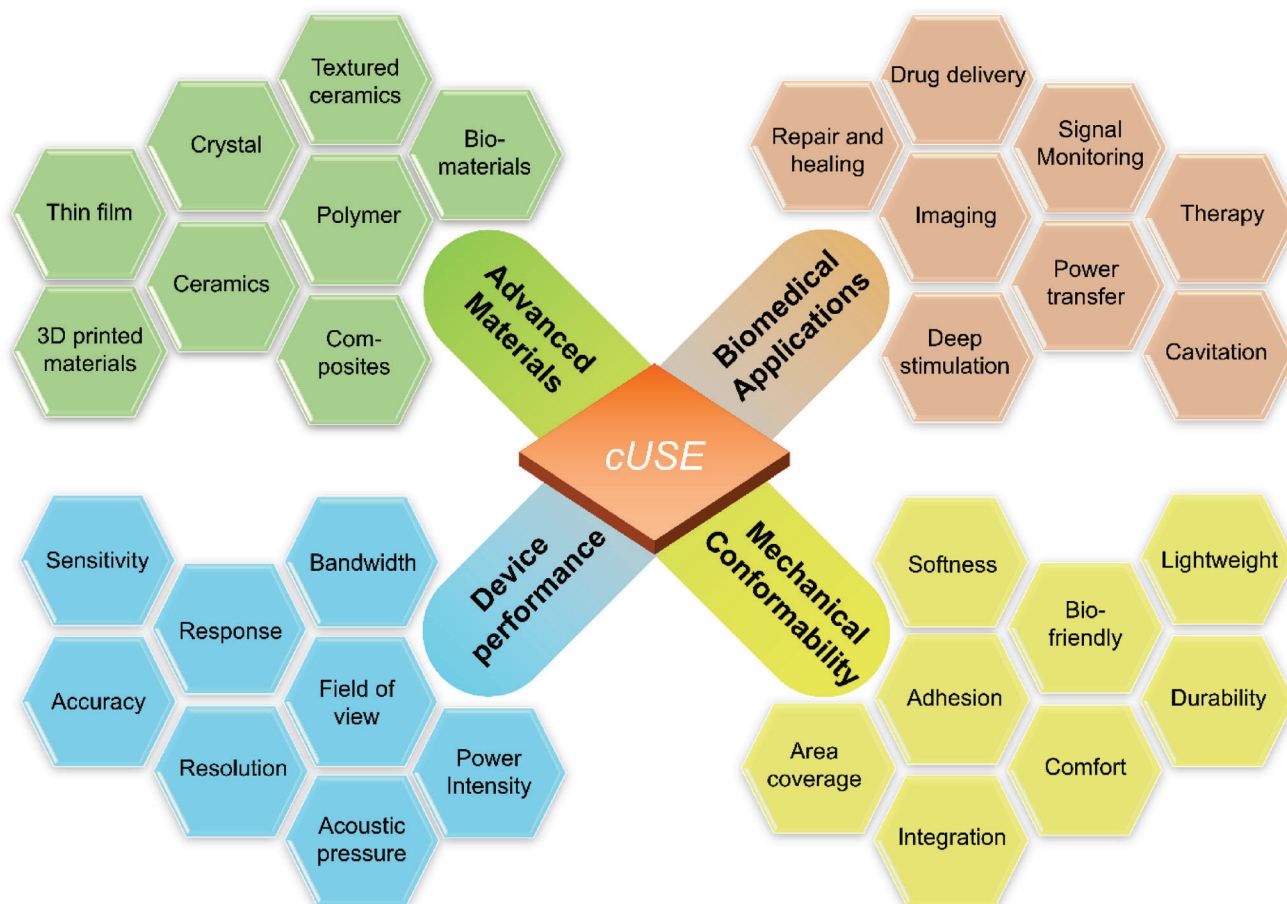


Figure 2. The overview of the key aspects in piezoelectric-based cUSE, including the selection of materials, device performance, mechanical conformability, and applications in biomedical and health monitoring systems.

form.^[60] The phase difference between D and E is defined as the dielectric loss ($\tan\delta$), which can be considered as the process by which a portion of the electric energy is changed into thermal energy under an external electric field. The clamped capacitance of an ultrasonic transducer is determined by the clamped dielectric permittivity, area, and thickness of the piezoelectric material. In addition, dielectric permittivity is a critical parameter in order to match the electrical impedance of the transducer to that of the driving electronics. To achieve maximum power transfer, the ultrasonic transducer's input electrical impedance at the intended frequency must be real, and its input resistance must equal the source's electrical impedance (typically 50 Ω in termination).

The electromechanical coupling factor is an important parameter for measuring the ability of piezoelectric materials to convert energy between electrical and mechanical forms. It depends on the geometry of the material rather than being a constant material property. For instance, a material's k coefficient is higher in a rod shape than it is in a plate form.^[56] A high k value in transducer design is preferred for greater energy conversion, increased bandwidth, and higher sensitivity. Depending on the vibration mode at which the element is excited, the coupling factor can be estimated using the measured resonance and anti-resonance frequencies of a piezoelectric element. The res-

onant frequency and the acoustic impedance of a material are determined by the speed of sound inside itself, which is an inherent property of the material. It is mentioned above that the impedance matching between the transducer and the propagating medium is very important to improve the transducer's performance. The most prevalent coupling variables for vibration in a circular disk along the radial and thickness axes are typically denoted as k_{33} or k_p and k_t , which are described and summarized in Table 1 with other critical parameters and equations of piezoelectric materials. The configuration of the piezoelectric element can be adjusted to approach the desired transducer performance, in addition to choosing the proper piezoelectric material for a particular transducer.^[23b] A trade-off in other features is typically necessary because the majority of applications want a combination of properties.^[61]

2.1.2. Lead-Based Ceramics

Piezoelectric lead zirconate titanate $\text{Pb}(\text{Zr}_{1-x}\text{Ti}_x)\text{O}_3$ (PZT) ceramics have been widely used as the transducers' active components in commercial ultrasound probe applications due to their low cost and well-developed and stable piezoelectric properties with

Table 1. Critical parameters and equations of piezoelectric materials.

Properties	Symbol	Name	Equation	Notes
Piezoelectric properties	s^E	Compliance under a constant electrical field	$\begin{bmatrix} S \\ D \end{bmatrix} = \begin{bmatrix} s^E & d \\ d & \epsilon^T \end{bmatrix} \begin{bmatrix} T \\ E \end{bmatrix}$	Direct/converse piezoelectric effect
	ϵ^T	Dielectric permittivity under a constant stress		
	d_{ij}	Piezoelectric charge coefficient or piezoelectric strain coefficient	$d_{ij} = k_{ij} \cdot \sqrt{s^E \cdot \epsilon^T}$	d_{33} can be directly measured by the d_{33} meter.
	g_{ij}	piezoelectric voltage coefficient	$g_{ij} = d_{ij} / \epsilon^T$	–
	d_h	Hydrostatic piezoelectric charge coefficient	$d_h = d_{31} + d_{32} + d_{33}$	–
Dielectric properties	$\epsilon_{ij}, \epsilon_r$	Dielectric permittivity	$D_{ij} = \epsilon_{ij} \cdot E_j, C = \frac{\epsilon_0 \epsilon_r A}{d}$	D is the electrical displacement
	$\tan \delta$	Dielectric loss	$\tan \delta = \frac{\epsilon_r''}{\epsilon_r'}, \epsilon_r^* = \frac{\epsilon_r^*}{\epsilon_0} = \epsilon_r' - j\epsilon_r''$	–
	Z	Electrical impedance	$Z \propto \frac{1}{j\omega C} = \frac{t}{j2\pi A \epsilon_r'}$	Transducer's input Z must equal the source's Z .
	E_c	Coercive field	–	A large coercive field is critical for high-power transducers
Electromechanical properties	k	Electromechanical coefficient	$k^2 = \frac{\text{converted mechanical energy}}{\text{input electric energy}} = \frac{\text{converted electric energy}}{\text{input mechanical energy}}$	
	k_p	electromechanical coupling factors	$k_p^2 = \frac{1}{p} \frac{f_a^2 - f_r^2}{f_a^2}$	Thin disk-shape samples
	k_t	electromechanical coupling factors	$k_t^2 = \frac{\pi}{2} \frac{f_r}{f_a} \cot\left(\frac{\pi}{2} \frac{f_r}{f_a}\right)$	Thin disk-shape samples
	k_{33}	electromechanical coupling factors	$k_{33}^2 = \frac{\pi}{2} \frac{f_r}{f_a} \cot\left(\frac{\pi}{2} \frac{f_r}{f_a}\right)$	Longitudinal mode
	k_{31}	electromechanical coupling factors	$\frac{k_{31}^2}{k_{31}^2 - 1} = \frac{\pi}{2} \frac{f_a}{f_r} \cot\left(\frac{\pi}{2} \frac{f_a}{f_r}\right)$	Transverse mode
	Q_m	Mechanical quality factor	$Q_m = \frac{f_r}{\Delta f}$	Δf is the frequency difference at -3 dB of the maximum admittance.
Acoustic properties	ν_{33}	longitudinal acoustic velocity	$\nu_{33} = 2f_a \cdot t$	t is controlling dimension of the piezoelectric element (thickness)
	Z_p	Acoustic impedance	$Z_p = \rho \cdot \nu_{33}$	ρ is the density of the sample
	N	Frequency constant	$N = f_a \cdot t$	f_a is the anti-resonance frequency.
Temperature	T_c	Curie temperature	$\epsilon = \frac{C}{T - T_c}$	C is the Curie-Weiss constant. A greater T_c can guarantee transducer a wider temperature operating range.

compositions near the morphotropic phase boundary (MPB) ($d_{33} < 700$ pC N⁻¹, $k_{33} < 0.7$).^[62] The majority of conformable ultrasound devices use commercial PZT.^[27,33–35,63] Due to their higher polarizability—which results from the coupling between two equivalent energy states, namely the tetragonal and rhombohedral phases—MPB compositions have abnormally high dielectric and piezoelectric characteristics.^[64] This allows for the most efficient possible domain reorientation during the poling process. In addition to PZT, researchers also focused on a wide variety of piezoelectric compositions due to further alterations employing acceptor and donor dopants.^[65] Several complex lead-based relaxor materials Pb(B'B'')O₃ and Pb(B'B'')O₃ – PbTiO₃ (B' = Mg²⁺, Zn²⁺, In³⁺, Ni²⁺ · · ·, B'' = Nb⁵⁺, Ta⁵⁺, W⁶⁺ · · ·) have been intensively studied,^[66] among them, PMN-PT and PbMg_{1/3}Nb_{2/3}O₃-PbTiO₃ (PMN-PT), PbZn_{1/3}Nb_{2/3}O₃-PbTiO₃ (PZN-PT) and x Pb(In_{1/2}Nb_{1/2})O₃- y Pb(Mg_{1/3}Nb_{2/3})O₃- z PbTiO₃ materials are most attractive ceramics due to their exceptional piezoelectric performance.^[67] In addition, conventional piezoceramics, which have grain sizes in the range of 5–10 μ m, are not the best choice for high-frequency transducer applications because the active components' sizes can reach tens of micrometers. PMN-PT-based ceramics, which are particularly suited for

array transducers due to their high clamped dielectric permittivity, are now being manufactured in fine grain versions, which is critical to the high-frequency transducer and the requirement of the dicing operation.^[68] Furthermore, Zhang's and Li's groups successfully addressed the long-standing challenge of synthesizing new piezoelectric ceramics by introducing dopants into the local structural heterogeneity for a specific ferroelectric system, and achieved record-high dielectric and piezoelectric properties of the newly designed ceramics.^[69] After that, rare-earth (RE) single-doped or co-doped element (RE = La³⁺, Sm³⁺, Pr³⁺, Yb³⁺, Eu³⁺) doped or co-doped PMN-PT and PZN-PT ceramics have attracted the interest of researchers due to their ultrahigh d_{33} and k_{33} . Very recently, RE-doped PMN-PT and RE-doped PIN-PMN-PT based transducers have been developed for piezoelectric transducer design,^[70] which achieved enhanced acoustic performance for imaging.

2.1.3. Lead-Based Crystals

Single crystal relaxors have received attention in recent years due to their advantages over PZT systems,^[71] including easier

Table 2. Critical parameters and equations of ultrasound transducers.

Properties	Symbol	Name	Equation	Notes
Basic parameters	f	Resonance frequency of the element	$f = n \frac{\nu_p}{2t}$	ν_p is the acoustic velocity of piezoelectric element, and n is an odd integer with the lowest resonant frequency of $n = 1$
	λ	Wavelength of the transducer	$\lambda = \frac{\nu_l}{f}$	ν_l is the sound velocity in the loading medium (1540 m/s for water or tissue).
	Z_m	Acoustic impedance of the matching layer (Z_p and Z_l are the acoustic impedances of piezoelectric material and the loading medium, respectively)	$Z_m = (Z_p Z_l)^{1/2}$ $Z_m = (Z_p Z_l^2)^{1/3}$ $Z_{m1} = (Z_p^3 Z_l^3)^{1/7}$ $Z_{m2} = (Z_p Z_l^6)^{1/7}$	Single matching layer Single matching layer for wideband signal. Two matching layers: 1 st (inner) and 2 nd (outer)
	t_m	Thickness of the matching layer	$t_m = \frac{\lambda_m}{4}$	λ_m is the wavelength in the matching layer
	f_c	Center frequency	$f_c = \frac{f_2 + f_1}{2}$	The center frequency of the Fast Fourier Transforms (FFT) spectrum at -6 dB
Evaluation of transducers	BW	Bandwidth	$BW = \frac{f_2 - f_1}{f_c}$	f_2 and f_1 is the upper and lower frequency on the magnitude of the FFT of the echo at -6 dB value, respectively.
	k_{eff}	Effective electromechanical coupling factor	$k_{\text{eff}}^2 = \frac{f_a^2 - f_r^2}{f_a^2}$	f_a and f_r is the anti-resonance and resonance frequency, respectively.
	IL	Insertion loss	$IL = 20 \log(\frac{V_o}{V_i})$	V_o and V_i are the echo voltage and excitation voltage, respectively.
	V_{p-p}	Peak-to-peak voltage	–	Peak-to-peak amplitude of the output voltage signal
Other performances	R_{axial}	Axial resolution (-6dB)	$R_{\text{axial}} = \frac{\lambda}{2BW} = \frac{c}{2f_c \cdot BW}$	BW is the bandwidth
	R_{lateral}	Lateral resolution	$R_{\text{lateral}} = \lambda \cdot F_{\#} = \frac{c}{f_c} \cdot F_{\#}$	$F_{\#}$ the f-number (the ratio of focal distance to aperture dimension)
	F_d	Doppler shift frequency	$F_d = F_e - F_o = \frac{2F_o V \cos \theta}{c}$	F_e : echo of reflected frequency, F_o : operating frequency, V : speed of the reflector, c : speed of sound, θ : angle between flow and sound propagation
	M.I	Mechanical index	$M.I. = \frac{PNP}{\sqrt{f_c}}$	PNP is the peak negative pressure

crystal growth around MPB compositions and superior piezoelectric and electromechanical properties obtained through domain engineering.^[56,72] For example, due to improved polarizability brought on by the connection between two equivalent energy levels, PMN-PT single crystals possess very good piezoelectric characteristics ($k_{33} > 85\%$ and $d_{33} = 1200\text{--}2500 \text{ pC N}^{-1}$). Furthermore, the application of domain engineering techniques, involving the manipulation and alignment of crystal domains in directions other than the spontaneous polarization direction of single crystals, has significantly contributed to the enhancement of their electrical properties.^[56] In bulky transducers with single elements or phased arrays, it has been proven that PMN-PT single crystal based transducers exhibit superior acoustic performance compared to PZT-based transducers, including greater bandwidth, reduced pulse length, and improved axial and lateral resolutions.^[23b,73] However, the Curie temperature T_c ($\approx 150 \text{ }^\circ\text{C}$) and rhombohedral to tetragonal phase transition temperature T_{r-t} ($70\text{--}90 \text{ }^\circ\text{C}$) are quite low for PMN-PT solid solutions.^[72a] It is widely acknowledged that thermal stability and outstanding electromechanical performance cannot be achieved simultaneously. Therefore, it is essential to discover alternative solutions to the limitations of piezoelectric materials.^[56,65] Moreover, in numerous electromechanical applications, such as those involving high-power transducers and high-field actuators, the combination of strong piezoelectric responsiveness with a substantial coercive field (E_c) facilitates enhanced operational efficiency and a wide range of operational capabilities. Therefore, the pursuit

of novel relaxor-PT systems that satisfy the subsequent criteria poses a pressing endeavor: i) high T_c and T_{r-t} , ii) high d_{33} , or iii) large E_c .^[74] In one research direction, researchers found that PIN-PMN-PT single crystals near MPB composition with a high T_c of $200 \text{ }^\circ\text{C}$ have comparable piezoelectric performance to that of the PMN-PT single crystals. There has been a notable inclination towards the utilization of ternary single crystals in the realm of ultrasound transducer applications. Similarly to ceramics, the thermal stability and piezoelectric characteristics can be enhanced simultaneously with the incorporation of RE elements as dopants.

Besides the design of the components, post-treatment is also critical to the performance of the crystals. The alternating current poling (ACP) was intensively used recently due to its low cost, time saving, and high efficiency to improve the electromechanical properties of the composites and enhance the bandwidth and insertion loss of the transducers, making the ACP a potential and advantageous technology to improve the transducer performances.^[75] In addition, ACP was also used to improve the transparency of piezoelectrics. It was possible to get extremely high optical transmittance or exceptionally high piezoelectric characteristics by doping appropriate RE elements into PMN-PT ceramics. Due to the light scattering at ferroelectric domain walls and grain boundaries, it was still difficult to achieve high piezoelectricity and flawless transparency at the same time before the report on ACP PMN-28PT crystals.^[76] The ultra-high piezoelectric coefficient d_{33} ($>2100 \text{ pC N}^{-1}$), excellent

Table 3. Piezoelectric properties and acoustic performance of selected single element transducers.

Piezoelectric materials	Properties of materials					Performance of transducers				Refs.
	d_{33} [pC N ⁻¹]	$\epsilon_{33}^T/\epsilon_0$	Z [Mrayls]	k_t	f_c [MHz]	Thickness [μ m]	Aperture [mm \times mm]	-6dB BW [%]	IL [dB]	
Leas-based ceramics										
PZT-5H	515	2500	–	0.51	3.03	310	12 \times 0.5	66.4	-44.4	[331]
Sm-PMN-PT	1200	3500	–	0.55	39	–	0.4 \times 0.4	80	-13	[70b]
Sm-PbZrTiO ₃	462	1512	32.8	0.50	2.40	800	$\varnothing = 11$	54.4	-29.3	[332]
Sm-PbBaZrTiO ₃	533	1850	33.7	0.52	2.31	800	$\varnothing = 11$	61.3	-23.2	[332]
PNN-PZT	760	3409	30.2	0.6	42	41	$\varnothing = 0.33$	79	-19.6	[333]
Lead-based crystals										
PMN-PT	1500	5350	27.5	–	3.1	380	15 \times 0.19	90.0	-24.6	[73a]
PMN-31PT	1883	7699	35	0.59	9.93	200	0.5 \times 0.5	35.1	-17.0	[334]
PZN-PT	2009	5265	34.3	–	3.11	360	20 \times 0.2	72.5	-46	[335]
PIN-PMN-PT	1510	4400	36.0	0.57	2.08	–	10 \times 10	77.3	-29.6	[336]
Yb/Bi-PIN-PMN-PT	2800	7000	29.2	0.61	7.5	240	8 \times 0.09	71	–	[31]
Lead-free ceramics										
KNN-3	306	–	26.9	–	24.5	100	$\varnothing = 2.0$	97	-17	[337]
Co-NBT	32	148	30	0.35	70.4	–	0.7 \times 0.7	52.7	–	[338]
BS-PT	450	777	26.5	0.58	10.57	200	–	24.3	–	[339]
BS-64PT	450	1253	–	0.54	4	500	$\varnothing = 10$	9	–	[340]
BZT-50BCT	600	2817	26.7	0.41	30	75	0.8 \times 0.8	53	-18.7	[341]
Lead-free crystal										
LiNbO ₃	–	44	34.0	0.49	22	90	$\varnothing = 10$	72	-19.5	[342]
KNLN	490	466	–	0.55	82	28	0.4 \times 0.4	57.3	–	[343]
NBT-BT	210	80	30	0.52	25	87	0.6 \times 0.6	46.2	-31.9	[344]
Mn-KNN	300	512	–	0.64	50	–	–	70.2	–	[345]
Textured ceramics										
PMN-PZT	1100	2310	29.4	0.69	15	80	$\varnothing = 2.5$	67	-21	[101a]
PNN-PZT	920	2230	29.4	0.55	3	750	$\varnothing = 11.5$	63.6	-14.4	[101b]
KNLN	150	550	–	0.44	52	35	0.4 \times 0.4	61.5	–	[346]
KNLN-BZ-BNT	319	1651	25.2	0.4	81	30	0.4 \times 0.4	52	–	[347]
BCTZ	570	1241	29	0.53	2.9	310	12 \times 0.5	80.5	-47.1	[331]
1-3 composites										
PZT/epoxy	610	1211	15.8	0.58	2.98	560	$\varnothing = 10$	136.8	-21.3	[161]
PIMNT/epoxy	1283	2423	18.9	0.83	1.81	650	$\varnothing = 12$	107	-24.3	[348]
PMN-PT/Epoxy	1230	822	15.9	0.81	3.06	560	$\varnothing = 10$	174.7	-20.3	[161]
PMN-PT/Epoxy	1412	1358	22.5	0.88	3.1	630	$\varnothing = 10$	142.8	-16.1	[124a]
PIN-PMN-PT/epoxy	1100	1813	19.5	0.83	2.24	610	10 \times 10	97.8	-25.9	[336]
Sm-PMN-PT/epoxy	1065	–	–	0.77	2.3	–	–	135.9	-18.7	[118]
BS-PT/epoxy	–	–	16.2	0.61	8.93	200	3.4 \times 3.4	41.6	–	[339]
KNN/epoxy	332	–	12	–	23.4	100	$\varnothing = 2.5$	75.4	-16.7	[349]
KNNS-BNZH/epoxy	350	1342	15.8	0.70	5.0	450	$\Phi = 8$	80	-30	[350]
2-2 composites										
PZT5H/epoxy	–	1237	–	0.66	40	130	–	–	–	[351]
PZT5H/Epo-tek301	–	787	22	0.70	14.4	70	12.8 \times 4	69.4	-33.9	[352]
PMN-PT/Epo-tek301	359	588	24.8	0.58	8.75	–	–	35.5	–	[353]
PIN-PMN-PT/epoxy	1200	2902	21.6	0.86	2.24	590	10 \times 10	96.4	-25.8	[336]
PIN-PMN-PT/epoxy	1200	2902	21.6	0.86	10.18	140	15 \times 1	140	–	[354]

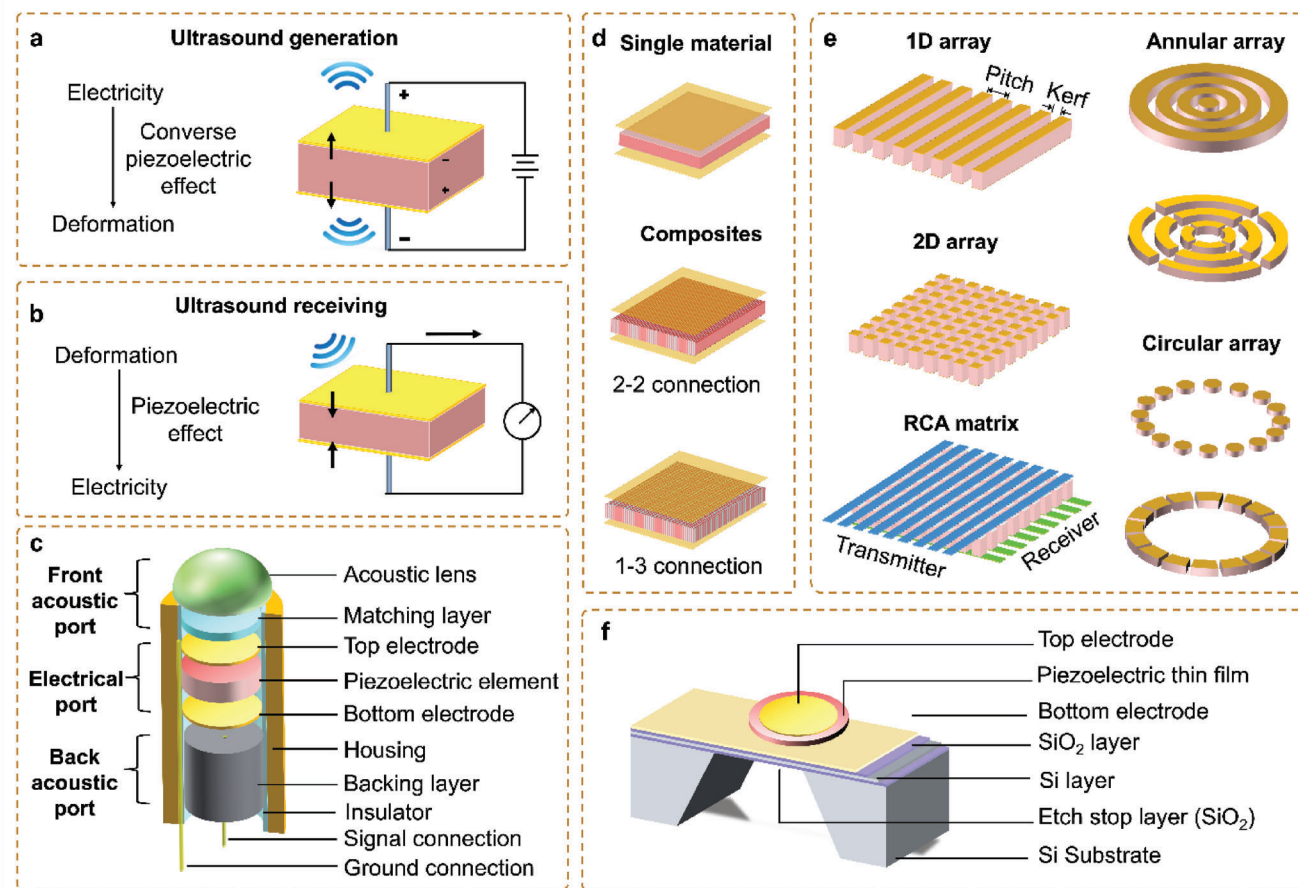


Figure 3. The basic information of ultrasound transducers. a) Principle of ultrasonic generation based on converse piezoelectric effect. c) Schematic of ultrasound transducers in three port model. d) Schematic of active elements for single transducers, including single material and composites (i.e., 2-2 connection and 1-3 connection). e) Schematic of array transducers, including 1D array, 2D array, 2D array with RCA, annular array, and circular array. f) Schematic of pMUT.

electromechanical coupling factor k_{33} (94%) and large electro-optical coefficient γ_{33} ($\approx 220 \text{ pm V}^{-1}$), are far beyond the performance of the commonly used transparent ferroelectric crystal LiNbO_3 . Following this work, many new transparent piezoelectrics were reported (Table 4),^[77] and various sensors, actuators, and ultrasound transducers have been proposed.^[78] Especially for photoacoustic imaging, the transducer with PMN-PT transparent crystal exhibited higher sensitivity, a larger photoacoustic amplitude, and enhanced resolution.

2.1.4. Lead-Free Ceramics

The most important motivation for the investigation on lead-free ceramics is the poisonous element Pb used in the lead-based materials. The growing demand for environmental protection and sustainable development has sped up the development of lead-free piezoceramics.^[64,72b,79] Lead-free piezoelectric ceramics can be divided into three categories: perovskite, zinc oxide, tungsten bronze, and bismuth layered structures.^[80] The ABO_3 -type family of perovskites is one of the most well-known classes of lead-free piezoelectric materials, including BaTiO_3 (BT),^[81] $\text{K}_{1/2}\text{Na}_{1/2}\text{NbO}_3$

(KNN),^[82] $\text{Bi}_{1/2}\text{Na}_{1/2}\text{TiO}_3$ (BNT),^[83] and BiFeO_3 (BFO).^[84] Researchers also focused on their different combinations of binary systems to achieve improved piezoelectric performance.^[85]

For device applications, besides the mass-production processing limitations,^[86] lead-free ceramics also meet a similar challenge, which is to gain the comprehensive properties of both high piezoelectricity and good thermal stability. Due to this reason, many researchers developed various binary and ternary solid solutions in the vicinity of the MPB in order to enhance T_c and improve the dependence of piezoelectric and ferroelectric properties on temperature.^[87] Several compositions showed relatively large piezoelectric coefficients and were fabricated into the low and high-frequency transducers as listed in Table 4. Clearly, in contrast to the lead-based ceramics and crystals that have been extensively employed for various transducer configurations, the majority of research is still in the early stages and focuses on evaluating the acoustic capabilities of lead-based ceramics utilizing single-element probe designs.^[88] For ultrahigh frequency needle transducers, KNN- and BNT-based ceramics were selected, which achieved sufficient bandwidth, but were still not comparable to lead-based piezoelectrics. There is no information reported about bulky lead-based ceramics for cUSE, despite the fact

Table 4. Comparison of representative piezoelectrics for ultrasound transducers.

Comparison aspects		Ceramics ^[65,80]	Lead-based crystals ^[57c,355]	Lead-free films ^[23a]	PVDF based polymers ^[110d]	Composites ^[117a]	3D printed materials ^[145,146,356]
Preparation	Method	Solid state reaction	Bridgman crystal growth	Sol-gel, sputtering	Casting and various treatments	Dice-and-fill, mixing, template, etc.	3D printing
	Fabrication	Difficult	Difficult	Medium	Easy	Easy	Easy
	Cost	High	Very high	Medium	Low	High	Low
Dielectric, piezoelectric, and acoustic properties	d_{33} (pC N ⁻¹)	< 1,000	> 1,500	3–10	10–30	400–1400	60/500
	k_t	0.5–0.6	0.5–0.6	–	Low (< 0.2)	High (0.6–0.8)	Medium (0.4–0.6)
	$\tan\delta$	< 2%	< 0.5%	< 2%	> 1%	Medium	< 2%
	ϵ^T	High	High	Medium	Low	Medium	Medium
	d_h	Low (negative d_{31})	Low	Low	Low	Low	High (positive d_{31})
Physical properties	g_h	Low	Low	Low	Low	High	Medium
	Elastic modulus	High	High	Medium	Low	Medium	Medium
	Density (g cm ⁻³)	High	High	High	Low	Medium	Medium
	Flexibility	Low	Low	High	High	Medium	Medium
	Z (MRayl)	30–35	30–35	20–35	4–5	10–20	3–8

that large lead-based ceramics have been utilized for conformable electronics.^[89]

2.1.5. Lead-Free Crystals

LiNbO₃ (LN) single crystal is a widely known piezoelectric oxide material with a single crystal structure.^[23b] LN single crystal is extensively utilized in acoustic and electro-optical applications due to its stable and robust electro-mechanical and electro-optical coupling properties.^[23b] Compared to lead-based PZT materials, a 36° rotated Y-cut LN single crystal exhibits a comparable electromechanical coupling coefficient, a significantly lower dielectric permittivity, a higher longitudinal sound speed, and a higher Curie temperature.^[90] This makes the LN single crystal an ideal and promising active element for sensitive large aperture single-element transducers. The KNN systems have been regarded as one of the most promising candidates. The KNN-based single crystal exhibited superior piezoelectric response ($d_{33} \approx 690$ pC N⁻¹), high Curie temperature ($T_c \approx 420$ °C), and a large electromechanical coupling coefficient ($k_t \approx 0.55$).^[91] Recently, a major breakthrough has been made in KNN-based single crystals with superior performance (measured $d_{33} > 9000$ C N⁻¹ and strain of 0.9% at 1 kV mm⁻¹).^[92] Therefore, the creation of single crystal thick films based on KNN may be a good option to replace the electrical device's piezoelectric layer that contains lead. Unfortunately, due to its brittleness, it is extremely difficult to produce KNN-based single-crystal thick films with a thickness below 30 μm using the traditional lapping down procedure. Furthermore, it is yet unclear if KNN-based single-crystal thick films can maintain excellent electrical performance. In light of this, investigating KNN-based single-crystal thick films and future applications would be worthwhile.

Numerous initiatives have been taken to develop lead-free piezoelectrics as single crystals,^[90] which take use of the designed domain arrangement to achieve electromechanical cou-

pling factors of up to 90%. The growth and properties of lead-free single crystals, however, suffer from difficulties due to the volatile nature of the constituent elements, inhomogeneous components, poor quality, small size, low ϵ_r , and consequently low d_{33} , low T_c , and low E_c , all of which will restrict their use. In order to further enhance their piezoelectric properties, utilizing the engineered domain configurations, without compromising the temperature usage range or field drive stability, many efforts must be concentrated on the crystal growth and thorough understanding of lead-free piezoelectric materials.

2.1.6. Textured Ceramics

Texture defines the preferred orientation of crystallographic grains in polycrystalline materials, which were created to bridge the disparity between single crystals and polycrystalline ceramics as the primary impetus.^[93] The aforementioned characteristics made single crystals very well-suited for an extensive range of advanced electromechanical applications, however, the poor mechanical properties and challenges associated with producing consistently high-quality crystals of higher dimensions render the utilization of single crystals impracticable in numerous scenarios.^[94] On the other hand, it should be noted that polycrystalline ceramics exhibit mechanical strength, but they generally lack anisotropy, save for their significantly reduced directional characteristics when compared to single crystals. Textured materials have anisotropic qualities akin to those of single crystals due to their grain-oriented morphology and polycrystalline structure and offer mechanical reliability with a wide range of compositional variations. Advancements in the field of texture engineering have facilitated the production of ferroelectric ceramics that exhibit exceptional alignment and possess electromechanical capabilities akin to those found in single crystals. Researchers investigated several textured ceramics,

including PIN-PMN-PT,^[95] doped PIN-PMN-PT ceramics,^[96] PIN-PSN-PT,^[97] BiScO₃-PbTiO₃,^[98] Sm-PMN-26PT,^[99] and PMN-PZT with a near ideal k_{33} value (≈ 0.93).^[100] Very recently, some textured have been fabricated into ultrasound transducers (Table 4),^[101] which exhibited enhanced acoustic performance compared to ceramics.

2.1.7. Inorganic Films

Inorganic piezoelectric thin films provide an advantage over bulk crystals in terms of price, reduced material consumption, compact cell size, energy efficiency, and simplicity of integration in Si semiconductor technology.^[102] A new option for piezoelectric materials for ultra-high frequency ultrasonic transducers has emerged with the advancement of microelectromechanical systems (MEMS) technology and piezoelectric film fabrication technologies.^[103] The thickness control technology is well developed, and the piezoelectric capabilities of films based on conventional ferroelectric materials are outstanding. Thin film piezoelectric materials are used for ultrasonic generation and detection in recent studies as one of the most crucial parts of a PMUT architecture.^[104]

PZT and PMN-PT are the most widely used lead-based thin films, which have been created using a variety of techniques, including sol-gel, radio frequency magnetron sputtering, ion beam sputtering, pulsed laser deposition, chemical vapor deposition, chemical solution deposition (CSD), and others.^[105] Very recently, similar to bulky materials, RE-doped thin films have also been synthesized, such as La-doped PZT film,^[106] Pr-doped PMN-PT film,^[107] and RE-doped PMN-PT film,^[108] to obtain high remanent polarization, low leakage current, and high transmittance, indicating the potential application in a multifunctional ultrasound and optoelectronic device. AlN and ZnO are lead-free thin films, which are wurtzite structured materials, a kind of hexagonal crystal system that illustrates a piezoelectric response along [0001]. AlN is particularly appealing in sensors and resonator applications because of its benefits, including strong electrical resistivity, compatibility with CMOS processing, and high-frequency constant.^[5,109] AlN is better suited for CMOS than ZnO because ZnO has a significantly higher diffusion rate and more contamination problems. Meanwhile, ZnO is used in MEMS and NEMS devices more commonly than AlN due to its superior availability and less demanding vacuum conditions.^[105]

2.1.8. Organic Films

Organic piezoelectric materials have been gaining popularity for sensors, actuators, transducers, and energy storage devices due to their superior mechanical flexibility, design diversity, low processing temperatures, and ease of fabrication as compared to inorganic counterparts.^[54b,110] Polyvinylidene (PVDF) and its copolymer with trifluoroethylene (TrFE) have been widely used for conformable electronics for biomedical and healthcare applications.^[16a,110a,111] As previously noted, a low dielectric permittivity allows for improved electrical matching to the electronics in large area high-frequency devices. Thus, PVDF and re-

lated polymers were also discovered to be useful in the production of high-frequency transducers and an extraordinarily wide band width (up to 100 MHz). Following the polymerization, stretching, and poling procedures, a thin sheet of PVDF with a thickness ranging from 5 to 25 μm can be employed as a transducer material. PVDF has a high degree of flexibility, a low density, and a low acoustic impedance (4 MRayl), transparent, allowing it to match impedance with media such as water and biological tissues.^[112] In addition, PVDF-based polymers are potentially complementary metal oxide semiconductor (CMOS) compatible piezoelectric materials due to their easy fabrication and low annealing temperature.^[54b,113] However, due to its low electromechanical coupling coefficient, PVDF is not an ideal transmitting material, which is the primary reason why PVDF-based cUSE is typically employed for bio-signal detection and not high-resolution imaging. More information about the PVDF base cUSE will be discussed in Section 2.2.4 and Section 3.2.1.

2.1.9. Composites

Piezocomposites can be classified into two types: ceramic-matrix and polymer-matrix composites.^[114] To decouple the piezoelectric and dielectric properties, a bulk piezoelectric ceramic with a high piezoelectric charge coefficient and relative permittivity is substituted by a low permittivity second phase (e.g., air/polymers) in the former. The goal is to drastically lower permittivity while retaining high piezoelectric qualities; the greatest decoupling of these properties is normally observed in soft ferroelectrics, which typically have a high permittivity. The latter entails introducing a piezoelectrically active phase into a polymer with the goal of achieving reasonably high d_{33} values through microstructural design. Porous ferroelectric ceramics will be treated as ceramic-matrix composite systems. For ultrasound transducers, the composites are usually made of a piezoelectric ceramic and a polymer, which are intriguing materials due to their excellently customizable features.^[115] The geometry and boundary conditions of the piezoelectric materials will have a significant impact on the piezoelectric properties. For transducer design, the composite can attain greater piezoelectric and electromechanical coefficients, reduced acoustic impedance, and superior mechanical stability when compared to crystals or ceramics.^[116] According to the connection of each phase in one, two, or three dimensions, the geometry for two-phase composites can be divided into ten different forms. The most practical piezocomposite is thought to be a 0-3, 1-3, 2-2, and 3-3 piezocomposite for different piezoelectric devices.

Especially 1-3 piezocomposites are the most widely used because they wisely utilize the geometry of the piezoelectrics to achieve high coupling factors, low acoustic impedance, good matching to water or human tissue, mechanical flexibility, and broad bandwidth combined with a low mechanical quality factor (Tables 4 and 5).^[117] In recent studies, researchers mainly focused on the following three directions on piezocomposites. First, introducing new piezoelectric ceramics/crystal to fabricate new composites is still the main research direction to improve the acoustic performance of the transducers, such as 2.5Sm-PMN-30PT 1-3 composites (2.3 MHz, -6 dB bandwidth of 135.9%),^[118] NBBT

Table 5. Mechanical properties of materials for substrates.

Substrate	Modulus (MPa)	Dielectric constant	Transparency	Maximum operating temperature [°C]	Mechanical performance	Elastic stretchability [%]	Refs.
Si wafer	130–190 · 10 ³	12	No	1000	Rigid	–	[357]
Metal foil (stainless steel)	190–203 · 10 ³	–	No	1000	Bendable	–	[358]
Polyimide (PI)	2300–2500	2.8–3.5	Yellowish	360–450	Bendable	–	[2, 357–359]
Polyethylene terephthalate (PET)	2000–2700	2.5–3.5	High	100–140	Bendable	–	[2, 358–360]
Polyethylene naphthalate (PEN)	4000–5000	2.9–3.2	High	155–180	Bendable	–	[2, 358–360]
SU-8	4000	4	High	380	Bendable	–	[361]
Parylene-C	3200	3.1	High	110	Bendable	–	[357]
Thermoplastic Polyurethane (TPU)	6	8.2	Opaque to transparent	100	Stretchable	110	[362]
Polydimethylsiloxane (PDMS)	0.5–3	2.65	High	150	Stretchable	100–200	[358–360]
Ecoflex	0.05–0.1	2.8	Opaque	232	Stretchable	900	[359, 363]
Acrylic (3M VHB)	0.01–3	3.2	High	150	Stretchable	900	[364]
Poly(styrene-ethylene/butylene-styrene) block copolymer (SEBS)	0.43	2.4	High	100	Stretchable	800	[365]

1–3 composite ($k_t > 71\%$),^[119] PNN-PZT composites,^[120] textured PMN-PZT composites,^[101a] etc. Second, proposing new structure designs and using new fabrication methods to tune the volume fraction and the vibration of the elements, including a cold ablation process method for PMN-PT 1–3 composites,^[121] a multiple-layer-design to achieve larger transmission efficiency,^[122] non-periodic composites breaking the limits of the lateral mode,^[123] etc. Third, even though the 1–3 composites were investigated, researchers still found some new external methods or treatments to improve their performance. The ACP was intensively used recently due to its low-cost, time-saving, and high-efficiency to improve the electromechanical properties of the composites and enhance the bandwidth and insertion loss of the transducers, making the ACP a potential and advantageous technology to improve the transducer's performances.^[124] A change in the configuration of the domain is responsible for the improvement of the piezoelectric characteristics following ACP. Although it is still unknown, it is generally believed that the contributions of the domain wall motion represent an extrinsic contribution.^[125]

2.2. Recent Advances on Conformable Piezoelectric Materials

In recent years, some novel conformable piezoelectrics have been synthesized and produced owing to advanced preparation technologies and amazing methods. These piezoelectrics not only have exceptional piezoelectric capabilities, but also show promise as candidates for ultrasound transducers; some of these have been fabricated for the cUSE. The hot research covers three main directions based on the varied manufacturing and design purposes: flexible/conformal composites, piezoelectric biomaterials, and 3D printed piezoelectrics.

2.2.1. Flexible/Conformal Piezoelectric Composites

Besides the planar geometries of piezoelectric composites, curved, bendable, and flexible 0–3 and 1–3 composites were proposed to accommodate various surface and application requirements. 0–3 composites usually mix piezoelectric particles with the flexible matrix, showing limited acoustic performance.^[126] Therefore, researchers spent more efforts on the 1–3 curved/flexible composites, which can be fabricated by reshaping the plane elements using different methods, such as hard-pressing on ceramics,^[127] or used bendable or stretchable matrix to replace the Epoxy, such as silicone rubber^[128] and polydimethylsiloxane (PDMS).^[129] Jiang's group reported several PDMS-based 1–3 composites with stretchable electrodes, which exhibited robust mechanical flexibility with promising acoustic performance, and have been conducted for blood pressure monitoring.^[130] Li's group modified the 3D-printing-assisted inserting method to achieve large-area and conformal single crystal piezocomposites (**Figure 4a–d**).^[131] The single-crystal piezocomposite exhibits a high k_t of 85% and a large d_{33} of 1150 pC N⁻¹ with a bending angle of 162°, which will benefit the future design and fabrication of high-performance and complex-shape piezoelectric composites as key materials for cUSE. Besides the single flexible elements, 1–3 composites have also been fabricated as the array, which can conform to irregular surfaces to obtain precise images.^[132] Very recently, Shen's group reported a highly stretchable/compressible piezoelectric composite using ferroelectric relaxor as the skeleton and elastomer as the matrix, which exhibited a ultrahigh d_{33} (250 pC N⁻¹), high k_{eff} ($\approx 65\%$), ultra-low acoustic impedance of 3 MRyl, and high cyclic stability under 50% compression strain.^[133]

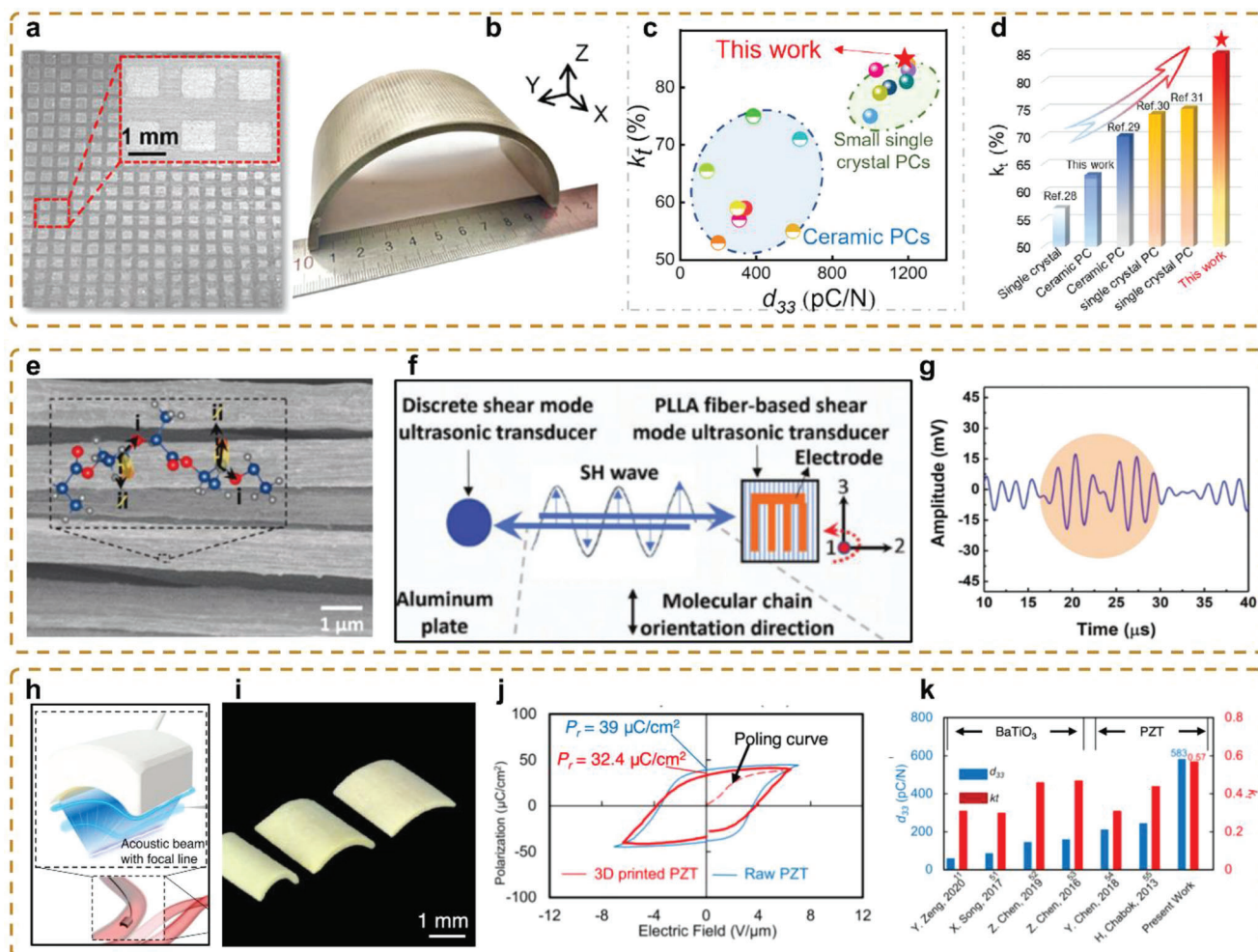


Figure 4. Recent advances on conformable piezoelectric materials. Conformally large-area single-crystal piezocomposites with high performance for acoustic transducers. a) Optical images of the polished single-crystal piezocomposites (PCs). b) Pictures of the prepared conformally large-area single-crystal piezocomposites. c) Comparison of k_t and d_{33} with the reported single-crystal and ceramic PCs. d) Comparison of the k_t of the reported large-area piezoelectric materials. Reproduced with permission.^[131b] Copyright 2023, American Chemical Society. Shear mode ultrasonic transducers from flexible piezoelectric plla fibers for structural health monitoring. e) Field emission scanning electron microscope (FESEM) micrograph of aligned PLLA fibers. f) Schematic illustration of using an ultrasonic transducer made of PLLA fiber mat for generating and detecting SH0 wave mode in aluminum plate. g) Ultrasonic signal when using PLLA fiber mat as an ultrasonic transmitter. Reproduced with permission.^[157] Copyright 2023, Wiley. 3D Printing and processing of miniaturized transducers with near-pristine piezoelectric ceramics for localized cavitation. h) Schematic of the fabricated miniaturized ultrasound transducer with curved PZT elements. i) Micro-curved stave elements with different curvatures. j) Polarization-electric field (P-E) loop of 3D printed PZT. k) d_{33} and k_t benchmarked with state-of-the-art 3D printed piezoelectric materials. Reproduced under the terms of the Creative Commons License.^[152] Copyright 2023, The Authors. published by Springer Nature Limited.

2.2.2. Piezoelectric Biomaterials

Piezoelectric biomaterials represent a category of functional materials that not only have the capability to convert mechanical deformation into electrical energy and vice versa, but also have the potential to exhibit biocompatibility, flexibility, environmental sustainability, minimal toxicity, and robust mechanical properties, rendering them suitable for the development of sustainable and compliant devices for health and environmental applications.^[134] In recent years, the biodegradable polymers known as poly-L-lactic acid (PLLA) or poly(D-lactic acid) (PDLA) have been investigated as biodevices, including biosensors, bioactuators, and tissue electrical stimulators or ultrasound

stimulators, because they exhibit a distinctive set of material properties, including low density, low processing temperature, notable flexibility, high tensile strength, and a pure shear piezoelectric response that does not necessitate electrical poling.^[135] Ren's group mainly focused on the PLLA as the pulse sensor and energy harvester due to easy fabrication and relatively simple structure.^[136] Whereas, Nguyen's group has shown the prospective uses of PLLA polymer as ultrasound transducers with various dimensions for different biomedical applications, including electromechanical force sensing to record important physiological forces,^[137] highly sensitive biodegradable pressure sensor to monitor vital physiological pressures, and a biodegradable ultrasonic transducer for blood-brain barrier opening.^[134a]

exercise-induced piezoelectric stimulation for the treatment of osteoarthritis,^[138] and skin scaffold electrical stimulator for skin-wound healing^[139] and bone regeneration.^[140] In addition, PLLA can also be fabricated in shear mode for cUSE to perform structural health monitoring. These PLLA-based transducers demonstrate a reliable level of sensitivity in identifying flaws in both liquid and air mediums. Furthermore, it should be noted that the sole shear mode observed in PLLA fibers is derived from their crystal structure, eliminating the need for electrical poling to induce piezoelectric behavior. Theoretical analysis and experimental findings pertaining to both flat and tubular structures have demonstrated the considerable potential of PLLA material (Figure 4e–g). Moreover, the utilization of the PLLA fiber-based shear mode ultrasonic transducers has been found to offer significant advantages for underwater structural health monitoring (SHM) applications. Different from PLLA, chitosan is another biomaterial that can be processed into a very thin and highly compliant flexible film for flexible MEMS and miniaturized devices.^[141] Additional investigations have been conducted on several organic piezoelectric gels^[142] and piezoelectric biomaterials^[143] (i.e., glycine, cellulose, collagen, and silk) to explore their potential use as piezoelectric devices. However, there is currently no available literature reporting their utilization as ultrasound transducers. In the realm of future research, it is crucial to address the main challenge that must be overcome to enhance the utilization of biomaterials. This inquiry involves the enhancement of moderate piezoelectric constants in organic materials, as well as the regulation of the dissolution rate of specific biodegradable piezoelectric polymers to ensure their suitability for prolonged utilization.

2.2.3. 3D Printed Piezoelectrics

In recent years, there has been an increasing tendency towards the utilization of 3D printing technology to produce piezoelectric materials that possess intricate geometries and customized features.^[144] The 3D printing processes commonly employed for piezoelectric materials include stereolithography (SLA), selective laser sintering (SLS), direct ink writing (DIW), digital light processing (DLP), inkjet printing (IJP), and fused deposition modeling (FDM).^[145] In general, the selection of printing methods is contingent upon factors such as resolution specifications, the nature of materials involved, and the need for multi-material fabrication capabilities. The utilization of 3D printing technology enables the precise manipulation of the composition, microstructure, and shape of materials, hence leading to notable improvements in the performance of piezoelectric materials with the advantages of fast molding, high precision, 3D modeling, materials technology, and digital information technology.^[146] The 3D-printed high-performance piezoelectric materials hold substantial potential for a wide range of applications, such as sensors, energy harvesting, and medical devices.^[146,147] Zhou's groups have reported several interesting works on 3D printed ultrasound transducers for biomedical applications,^[148] including BaTiO₃ piezoceramic ($d_{33} = 160 \text{ pC N}^{-1}$ and $k_t = 0.47$) for ultrasonic focusing imaging on the porcine eyeball,^[149] BaTiO₃ with honeycomb structure ($d_{33} = 60 \text{ pC N}^{-1}$ and $k_t = 0.31$) to avoid the dicing-filling method,^[150] and lithium niobate helical-like config-

uration for microparticle manipulation.^[151] For example, the 3D-printed dense piezoelectric elements achieve high piezoelectric properties ($d_{33} = 583 \text{ pC N}^{-1}$ and $k_t = 0.57$) and complex architectures for localized cavitation (Figure 4h–j).^[152] The utilization of 3D printing technology in the production of package components allows for the adjustment of acoustic properties, thereby enabling the adaptation of PZT elements to various transmission media and applications. This enhances the adaptability of the ultrasound transducers manufactured through this process, particularly in the field of medical treatments. In addition, other ceramics, including PZT,^[153] Pb(Ni_{1/3}Nb_{2/3})O₃-PZT,^[154] doped-KNN,^[155] PVDF,^[156] have also been 3D printed for ultrasound transducers. Although the utilization of 3D printing for piezoelectric materials exhibits potential for enhancing their performance and expanding their range of applications, there remain various obstacles and constraints, including the issue of porosity, the high rate of damage incurred throughout the production process, and constrained dimensions and configurations of the piezoelectric components.

2.2.4. Summary and Perspective

Flexible piezoelectric materials have garnered significant attention in recent years due to their potential applications cUSE. However, like any emerging technology, there are several challenges and perspectives that need to be considered for the future development and utilization of flexible piezoelectric materials. First, it is critical to maintain piezoelectric performance and flexibility concomitantly. The challenge lies in developing flexible materials with high piezoelectric coefficients to generate sufficient electrical output for practical applications. Second, it should ensure the long-term reliability and robustness of these materials, especially when subjected to mechanical stress and environmental factors. Third, it deserves to explore a broader range of materials and produce flexible piezoelectric materials in large quantities and with consistent properties, including organic and hybrid materials, to improve flexibility, scalability, and cost-effectiveness. Furthermore, the aspect of miniaturization is a significant factor to consider, particularly in relation to the potential decline in performance resulting from 3D printing of small components or biopolymers with reduced aperture sizes. The issue lies in effectively incorporating these materials into compact, portable, and pliable devices while maintaining optimal functionality. Therefore, it is of great importance for piezoelectric material to exhibit a combination of desirable characteristics, including a high level of piezoelectric performance, exceptional mechanical flexibility, biocompatibility or biodegradability, environmental sustainability, and the ability to be fabricated on a large scale at a reasonable cost. The performance of the flexible composites based cUSE will be discussed in Section 3.2.1.

2.3. Structure and Configurations of Ultrasound Transducers

2.3.1. Structure and Parameters of Transducers

Three-Port Network: The core component of the ultrasound system is the ultrasound transducer. The performance of the

ultrasound transducer is mostly determined by the transducer's design. The essential parts of a transducer are similar, even though the design changes greatly depending on the diverse needs. In medical ultrasound diagnosis, there are two primary categories of ultrasonic transducers: single-element and array transducers (including linear array and phased array). Single-element transducers generate images through mechanical scanning. In contrast, array transducers utilizing electronic scanning are preferred in clinical ultrasound imaging systems due to their numerous benefits, including high frame rate imaging, dynamic focusing capability, real-time flow measurement, and clinical convenience. An ultrasound transducer, as shown in Figure 3c, is usually treated as a three-port network: two acoustic (or mechanical) ports on the front (matching layer) and back (backing layer) sides of the piezoelectric material, and one electrical port coupled to the driving/receiving circuits.^[23b] The background layer, active layer, matching layer, and optional focusing lens are the major structural components, from bottom to top. For electrical shielding and safety, the transducer is housed in a grounded enclosure.

Matching Layer: Piezoelectric materials have an acoustic impedance of 30 MRayl, which is substantially higher than that of biological tissues (1.5 MRayl). Due to the acoustic impedance mismatch, ultrasound is reflected at the interface, and thus the ultrasound wave cannot effectively travel across the interface. As a result, the acoustic matching layer is necessary, which can improve the transducer's sensitivity, bandwidth, and energy transfer efficiency. The matching layer design requires exact acoustic impedance and precise thickness to achieve excellent matching performance. The acoustic impedance of the matching material is tuned by mixing high impedance particles (i.e., metal particles, metal oxides particles) with low impedance polymer (i.e., Epoxy) at a certain ratio.^[23b] Recently, for different requirements of the transducer design, various matching layers have been proposed to improve the bandwidth, including a matching layer for a high-frequency (> 100 MHz) transducer (BW at -6dB = 58.3%),^[158] neural network modeled for 2-2 composites (79.6%),^[159] acoustic metamaterial (silica with epoxy) with broadband gradient impedance matching (107%),^[160] nano tungsten-epoxy based broadband gradient impedance matching (BW = 170%),^[161] transparent matching layer,^[162] five equivalent layers (142%),^[163] and so on.

Backing layer: When an electrical source excites a transducer, it resonates at its natural resonant frequency. For continuous-wave applications, the transducers are air-backed to enable the maximum amount of energy to be radiated forward. Due to the disparity in acoustic impedance between air and piezoelectric material, acoustic energy is reflected in the forward direction at this interface.^[164] Thus, a negligible amount of energy is lost through the rear port. This mismatch, which generates the so-called ringing effect in pulse-echo applications, is extremely undesirable because it increases the pulse duration. To reduce ringing or widen the bandwidth, absorbent backing materials with acoustic impedances comparable to those of the piezoelectric material can be utilized. The backing material should reduce the mismatch in acoustic impedance as well as absorb some of the energy from the rear face's vibration. The energy that enters it is absorbed to the greatest extent possible. It should be emphasized that sensitivity must be sacrificed to suppress

ringing or reduce pulse duration because the backing material absorbs a significant amount of energy.^[165] As a result, sensitivity and pulse duration are usually traded off to increase a transducer's sensitivity by altering the backing layer impedance. Tungsten-loaded epoxy and Esolder 3022 are quite popular for backing material, and the impedance can range from 8 to 20 MRayl.^[23,166]

Acoustic Lens: Acoustic lenses are widely used in focused ultrasound transducers to i) regulate the acoustic field (i.e., focus the ultrasound beam and produce high acoustic intensity) at the focal point, and ii) protect the matching layer because the lens directly contacts the target for medical transducers.^[167] Acoustic field regulation technology, based on piezoelectric ultrasonic transducers, can be bifurcated into active and passive control strategies. Passive control encompasses techniques such as solid curved lenses, acoustic Fresnel lenses, acoustic projectors, liquid acoustic lenses, acoustic metasurfaces, photonic crystals, and acoustic holography.^[168] Conversely, active control primarily involves techniques like piezoelectric arrays, piezoelectric metamaterials, and coded piezoelectric metasurfaces.^[169] For example, the unique advantages of liquid acoustic lenses,^[168d,170] and acoustic projectors,^[171] are their capacity to dynamically modulate the focused acoustic field distribution by altering the volume of injected liquid and the angle of the reflective mirror. The novel acoustic hole-hologram, ensures optimal acoustic beam focusing while providing the transducer with high sensitivity.^[172] Coded piezoelectric metasurfaces,^[173] with their dual function of sound wave generation and modulation, showcase their potential as innovative disruptors in the field of high-frequency acoustic field control.

Critical Parameters: Because the piezoelectric element is essential to the transducer, the majority of the material-related parameters were covered in Section 2.1.1 and are included in Table 1. Table 2 primarily contains transducer-related parameters, such as basic ultrasonic principles, transducer design, transducer evaluation, and certain resolution and doppler parameters. The link between ultrasonic velocity and wavelength is the foundation of transducer design. To accomplish 100% transmission from transducer to object, many equations describing acoustic impedance and matching layer thickness are typically utilized for computation. The three most significant characteristics for evaluating the transducer's acoustic performance are -6 dB bandwidth, insertion loss (sensitivity), and peak-to-peak voltage. With a compromise between bandwidth and sensitivity, the resolution of an ultrasound imaging system is highly dependent on the design of its transducer elements. To generate high resolution images in both the axial and lateral directions, the transducer elements must generate brief acoustic pulses, and the system as a whole must have a high signal-to-noise ratio and adequate focus. Ultrasonic transducer systems have evolved to use linear and two-dimensional arrays in which an image is formed by electronically sweeping a beam. This is in response to the issue of poor resolution outside the focal plane and limited frequency in single-element transducer systems. The sound field, beam diameter, and focal zone of the single element probe determine transducer performance. Spatial resolution, temporal resolution, and contrast resolution in ultrasound imaging are all affected by the pulse excitation as well as the transducer parameters.

2.3.2. Single Element Transducers

Single element transducers are the most prevalent type of transducer, particularly for ultrasonic imaging and diagnostic applications requiring high frequency. Throughout the first few decades, the majority of ultrasonic systems utilized single-element transducers. As depicted in Figure 3c,d, the typical structure of a single-element transducer consists of a stack of one piezoelectric element for energy conversion, multiple matching layers to maximize energy transmission into the loading medium, and one backing layer to provide a rigid support for the fragile piezoelectric element and adjust the bandwidth and sensitivity of the transducers. In general, single-element transducers can be classified as planar or focused for specialized applications.^[23] Because the planar structure limits lateral resolution and sound intensity, focusing is employed to improve lateral resolution and performance in high-resolution imaging applications. Shaping the piezoelectric element or using a lens to create focused transducers is a typical way. The main advantage of a single-element ultrasonic transducer over an array ultrasound transducer is its lower geometrical complexity. As a result, the single-element ultrasound transducer has been investigated at ultrahigh frequencies (300 MHz).

Considering the configuration of the active layer, planar single-element transducers are commonly employed in applications requiring miniature transducers or needle transducers, such as intraoral ultrasonography^[174] and intravascular ultrasound (IVUS) imaging using high working frequencies (20 MHz to over 60 MHz).^[175] Intraoral ultrasonography is based on a high working frequency with a small aperture due to the narrow space around the gingival area, while IVUS imaging is based on side-looking single-element ultrasound transducers mechanically driven by a motor to rotate inside the vessel to form a 360° cross-sectional image.^[176] The focused transducer configuration can improve lateral resolution and performance in high-resolution imaging applications. In some work, the focused lenses were added to achieve focused imaging without a destructive pressing effect on the piezoelectric element.^[177] However, the lower sensitivity due to attenuative losses and the mechanical quality of the lens limited its practical application.^[178] In recent studies, with the development of novel piezoelectric materials and composites, planar single-element transducers have always been fabricated and characterized using standard methods to check the performance of new materials because of their simplest configuration. It should be mentioned that the smaller surface area of piezoelectric materials results in a higher electrical impedance when fabricating needle transducers.^[70b] Therefore, new piezoelectric materials with large clamped permittivity and high piezoelectric properties are advantageous for fabricating needle transducers with high performance. Various single-element transducers with different piezoelectric materials, including ceramics, single crystals, and composites, have been intensively investigated (Table 3).

2.3.3. Array Transducers

Array transducers contain multiple elements. These elements may be rectangular and arranged in a line (referred to as a 1D linear array transducer), square and arranged in rows and columns

(referred to as a 2D array transducer), or arranged in a circle (referred to as a circular array), or ring-shaped and arranged concentrically (referred to as an annular array).^[23b] Figure 3e depicts the schematic diagram of different array transducers. Array transducers are preferred over single-element transducers in clinical applications due to their clinical convenience, increased frame rates, and ability to dynamically focus the beam. Applying repeated voltage pulses to groups of elements is how an array is operated. An image identical to that obtained by mechanically scanning a single transducer is created as the sound beam is moved electronically across the transducer's front side.

In contrast to a linear array, which typically has a pitch of one wavelength, a phased array has a pitch that is less than half that wavelength. A phased array can direct beams with a narrower pitch without creating grating lobes. Additionally, the relatively smaller footprint of the array is advantageous when only a very small contact area is allowed. A linear phased array has an element spacing of $\lambda/2$ and can steer the ultrasonic beam off the axis of the array, whereas a linear array has an element separation of one wavelength in the tissue and focuses along the array axis. A 2D array may focus and scan a symmetrically focused beam throughout a volume to produce a 3D image. It has an element spacing of λ or $\lambda/2$ in both dimensions. Real-time volumetric imaging of complete organs is now therapeutically feasible on high-end ultrasound scanners because of the development of 2D matrix transducer arrays.^[179] Although a matrix probe has demonstrated excellent resolution in 3D imaging, N^2 connections cannot be avoided, where N is the number of elements in each dimension of the 2D array.^[180] Row-column addressed (RCA) probes have the potential to be more affordable to produce, and the use of fewer connections makes setup easier. In order to reduce the number of channels in a completely populated matrix array of dimension $N \times N$ by a factor of $N/2$, the idea of RCA probes with $N + N$ components has been suggested.^[181] Recently, the RCA matrix has been utilized for many applications, mainly volumetric flow imaging.^[179]

2.3.4. Piezoelectric Micromachined Ultrasonic Transducers

As previously noted, such transducers typically consist of a piezoelectric material sandwiched by electrode layers, often with an adhesive layer, and finally coupled by electrical wires. This type of construction, however, has significant restrictions. The anti-resonant frequency of the transducer is proportional to the thickness of the piezoelectric material and the longitudinal velocity of sound in the piezoelectric material's poling direction. Because of the direct dependence of the resonance frequency on layer thickness, transducer design and structure are limited for certain applications.^[104] Due to the complexities of matching layers with precise thickness for high frequency ultrasound transducers, the fabrication difficulties of traditional piezoelectric transducer architectures increase considerably for 1D linear and 2D ultrasound arrays for beam steering and 3D volumetric imaging.^[182]

In recent decades, micromachined ultrasonic transducers (MUTs) have been investigated as an alternative to conventional piezocomposite ultrasonic transducers, primarily due to the advantages that microelectromechanical systems (MEMS) provide in minimizing and eliminating the problems that were

mentioned above.^[183] Sensors that utilize MEMS technology have shown a decrease in noise in data collection, lower power consumption, and can be produced in large batches.^[103,184] One of the most common MUTs being developed and researched today is the piezoelectric micromachined ultrasonic transducer (pMUT). For ultrasound imaging, the acoustic pressure emitted by each PMUT element is reflected by an object and returns to the PMUT array to induce stress in the piezoelectric layers (Figure 3f). Recently, many pMUT have been designed using the RCA connection due to the easy and large-scale fabrication.^[185] Unlike CMUTs, which improve transducer sensitivity by reducing the impacts of parasitic capacitance while allowing for the use of low voltage electronics. In comparison with bulk piezoelectric ultrasound transducers, pMUTs offer advantages such as increased bandwidth, flexible geometries, and a good acoustic match with the medium.^[186] In comparison with capacitive micromachined ultrasonic transducers (cMUT), PMUTs, do not require a high voltage bias and have fewer geometric and design constraints, making integration with low voltage circuits easier. PMUTs also have various advantages, such as larger capacitance, lower electrical impedance, and higher acoustic intensity.

3. Advanced Designs and Technologies for Conformable Ultrasound Electronics

3.1. Current Limitations and Motivation

Most conventional ultrasound probes have been widely used for medical diagnosis and non-destructive testing (NDT), including linear arrays, convex/concave arrays, phased arrays, and 2D matrix arrays. They are notable for being presented in a rigid format, whose size and shape are decided upon at the time of manufacture and fastened to a solid support. In addition, it is not possible to maintain solid interfacial contact and excellent coupling with irregular non-planar surfaces, such as engineering components (vessel/pipe, wind turbine blade, aircraft structures, etc.) or human body parts (human skull, belly, shoulder, etc.). Air gaps or inadequate contacts at these interfaces result in significant acoustic energy reflections and wave distortions, resulting in unreliable test results. Although many applications can be satisfactorily accommodated by these hard probes, they have inherent limits in certain situations and still face fundamental challenges that significantly limit their usability for the next generation of wearable technologies and their applications.^[24] For instance, it is impossible to achieve sufficient contact over soft surfaces in large areas (such as the shoulder or breast) or small joints (such as the finger or wrist joints) because the ultrasound transducer is rigid and planar in contrast to the curvilinear shape of the body parts. Similarly, it is also difficult to let the probe fully contact the irregular surface, or examine the interior walls of a hollow workpiece through a small opening. The defect detection sensitivity is reduced, and the possibility of receiving false signals is increased. Attempts at imaging these body and object parts are highly operator-dependent, requiring manually scanning back and forth at different orientations.^[187] To solve these challenges, the past six years have witnessed the development and impact of wearable electronic devices on a range of areas, of which healthcare is considered to be the most promising due to the long-term, continuous wearability of these devices.

Compared with traditional ultrasound probes, cUSE with different designs exhibited many advantages that meet the requirements of next-generation biomedical devices.^[27,29,33–35,63] The cUSE can i) balance the high ultrasound performance and mechanical stretchability over irregular surfaces of objects or the human body, ii) achieve seamless adhesion for long-term and comfort monitoring, iii) provide expanded detection and an enlarged field of view in a more operator-independent fashion, accumulating more information in a single scan without translating and rotating transducers manually, iv) enhance the signal quality, power transferring, and beam focusing capabilities, v) improve the ultrasound wave penetration, and vi) provide efficient and accurate therapy. With these advantages, the cUSE can be performed safely at home and is easy to use by patients themselves, eliminating the dependence on a trained ultrasound technician. In the next section, five design strategies for cUSE with examples will be summarized and discussed (Figure 5).

3.2. Strategies towards Conformable Ultrasound Electronics

3.2.1. Type I: Flexible Single Element

This form of cUSE has been extensively studied because polymer-based transducers are typically the first option when discussing flexible/wearable piezoelectric devices. The single flexible element may consist of any piezoelectric material, including polymers and flexible composites (Figure 5a). The flexible single element can usually be used to transmit and receive signals for A mode ultrasound measurement or utilize the entire device to generate ultrasound power. Even though some devices employ array configurations, they are still regarded as singular elements. PVDF and PVDF-based copolymers have been fabricated as ultrasound transducers with unique properties for a wide range of medical and biological imaging applications.^[113c,193] PVDF-based flexible sensors have attracted considerable attention due to their advantages of flexibility, wide frequency response, low cost, ease of fabrication, biocompatibility, and lightweight.^[110c] Although the electromechanical properties of PVDF fall short of those of composite ceramic materials in the traditional diagnostic frequency range, it has substantial advantages between 25 and 100 MHz. In the past few decades, PVDF films have been extensively investigated as sensors for physiological signal-measuring systems. Its low acoustic impedance, which mirrors that of the body reasonably well, and its flexible mechanical properties are most notable.

Most ultrasonic sensors were made of PVDF film with silver paint electrodes and polyimide (PI) films with silicone glue for electrical insulation, sensor protection, and water resistance.^[113d,194] Despite the fabrication and monitoring of several ultrasound sensors for diverse organs, including muscle thickness,^[195] skeletal muscle,^[188] diabetic foot care,^[113d] artery monitoring,^[196] and finger printing.^[113a] This particular design exhibited three significant flaws: i) the PI film and silicone adhesive caused internal ultrasound reflections that made it hard to find desired ultrasonic signals near the sensor, ii) the sensor was sensitive to electronic noise because it did not have a way to block out electromagnetic radiation, and iii) the polymers are not suitable to serve as transmitters because of their

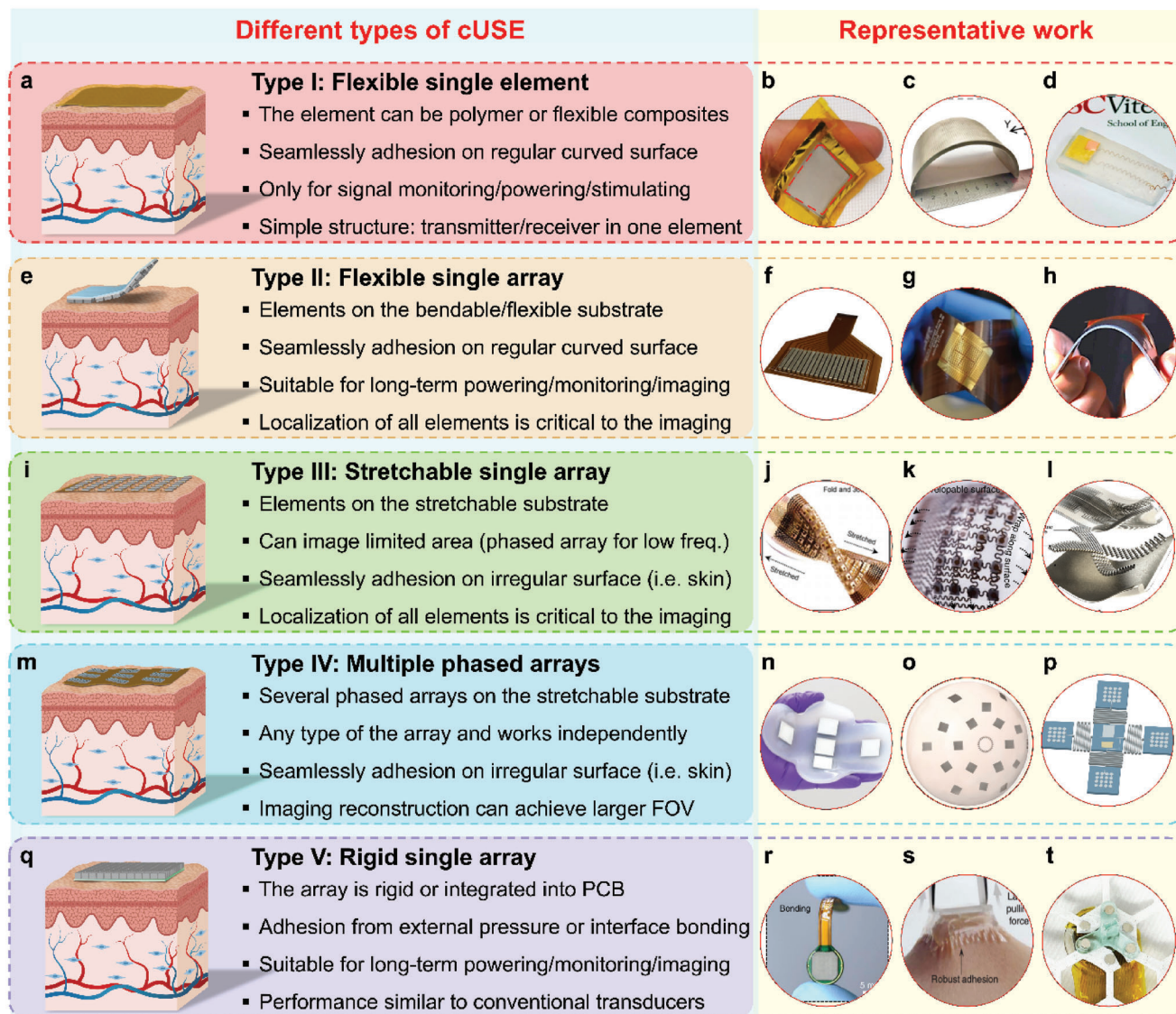


Figure 5. Strategies toward conformable ultrasound electronics. a) Type I: Flexible single element. b) Ultrasound measurement of skeletal muscle contractile parameters using flexible and wearable single-element ultrasonic sensor. Reproduced under the terms of the Creative Commons License.^[188] Copyright 2020, The Authors, Published by MDPI. c) Conformally large-area single-crystal piezocomposites with high performance for acoustic transducers. Reproduced with permission.^[131b] Copyright 2023, American Chemical Society. d) 3D-printing piezoelectric composite with honeycomb structure for ultrasonic devices. Reproduced under the terms of the Creative Commons License.^[189] Copyright 2020, The Authors, Published by MDPI. e) Type II: Flexible single array. f) Continuous monitoring with a permanently installed high-resolution ultrasonic phased array. Reproduced with permission.^[28] Copyright 2023, The Authors, Published by SAGE Publications. g) Flexible ultrasound transceiver array for non-invasive surface-conformable imaging enabled by geometric phase correction. Reproduced under the terms of the Creative Commons License.^[190] Copyright 2022, The Authors, Published by Springer Nature Limited. h) Thin, flexible, and biocompatible medical ultrasound array transducer using a sol-gel composite spray technique.^[191] Copyright 2023, The Japan Society of Applied Physics. i) Type III: Stretchable single array. j) Stretchable ultrasonic transducer arrays for three-dimensional imaging on complex surfaces. Reproduced under the terms of the Creative Commons License.^[27] Copyright 2018, The Authors, Published by American Association for the Advancement of Science. k) Monitoring of the central blood pressure waveform via a conformal ultrasonic device. Reproduced under the terms of the Creative Commons License.^[34] Copyright 2018, The Authors, Published by Springer Nature Limited. l) A wearable cardiac ultrasound imager. Reproduced under the terms of the Creative Commons License.^[45] Copyright 2023, The Authors, Published by Springer Nature Limited. m) Type IV: Multiple phased arrays. n) Conformable phased array ultrasound patch for bladder volume monitoring. Reproduced with permission.^[32] Copyright 2023, Springer Nature Limited. o) Methods and apparatus for imaging with conformable ultrasound patch. Reproduced under the terms of the Creative Commons License.^[192] Copyright 2020, The Authors. p) Bendable pMUT arrays based on silicon-on-insulator (SOI) technology.^[63d] The schematic drawn by authors is to show the design of this work. q) Type I: Rigid single array. r) Flexible ultrasound-induced retinal stimulating piezo-arrays for biomimetic visual prostheses. Reproduced under the terms of the Creative Commons License.^[40] Copyright 2022, The Authors, Published by Springer Nature Limited. s) Bioadhesive ultrasound for long-term continuous imaging of diverse organs. Reproduced under the terms of the Creative Commons License.^[29] Copyright 2022, The Authors, Published by American Association for the Advancement of Science. t) Conformable ultrasound breast patch for deep tissue scanning and imaging. Reproduced under the terms of the Creative Commons License.^[31] Copyright 2023, The Authors, Published by American Association for the Advancement of Science.

low electromechanical coupling coefficients, low dielectric constants, and high dielectric losses.^[197] To solve these challenges, some flexible piezocomposites have been proposed to improve acoustic power and provide short pulse generation, as discussed in Section 2.2.^[130a,198] Potential candidates for single-element transducers will also include some other freshly manufactured piezoelectric composites, such as 0–3 composites,^[199] 1–3 composites (Figure 5c),^[128b,131b] and 3D printed complex structure (Figure 5d).^[189]

3.2.2. Type II: Flexible Single Array

This type of cUSE with a flexible single array is derived from Type I because Type I only utilized a single element that was incapable of achieving B mode ultrasound imaging. The main configuration of Type II is to distribute piezoelectric elements on the bendable/flexible (not stretchable) substrate to achieve good contact on the developed (curved and regular) surface (Figure 5e). For this type, there are fewer reports on PVDF-based flexible arrays because PVDF does not have strong imaging capability.^[200] Therefore, most of the flexible array are based on commercial PZT ceramics or PZT and AlN thin films, including a flexible ultrasound array for structural health monitoring (Figure 5f),^[190] a flexible PZT linear array by the sol-gel composite spray technique (Figure 5h),^[191] a 3D-smart flexible phased array with a profilometer for element localization,^[201] piezoelectric fibers with air gap to achieve flexibility,^[202] flexible 2 × 8 array with copper-clad flexible printed circuit,^[203] affixable thin flexible ultrasound transducer using PZT mounted on the silicon islands for needle guidance,^[204] a ring-annular ultrasound array for use in interventional procedures,^[205] MEMS fabricated flexible 4 × 4 transducer,^[206] rubber encapsulated flexible array for inspecting curved components,^[207] 1–3 composites encapsulated by rubber layer for irregular surface,^[208] flexible transducer for imaging aluminum pipe with interior crack,^[209] bendable pMUT array for brain stimulation,^[210] wearable pMUT array for muscle disorder diagnostics,^[211] bendable array for the image-guided neural therapy,^[187] AlN based flexible pMUT,^[212] PZT with flexible passive rubber imaging on a fractured cortical bovine bone,^[63a] Ag-NWs electrodes for 1–3 bendable composites,^[63b] and ‘belt-type’ conformal transducer array for transcranial brain imaging.^[213] In addition to pMUT, researchers also expanded their studies on cMUT in a flexible configuration,^[214] but continue to emphasize the fabrication method and rarely discuss the imaging application.

The advantages of Type II can be summarized as follows: i) increased image information during a single scan due to the increased coverage; ii) potentially reduce both the expertise required to acquire an image and the variance between users of varying skill levels; iii) conformal images can be created via post-processing. There are also some critical issues to which attention needs to be paid during design and fabrication: i) trade-off between the desirable high aspect ratio of their piezoelectric rods and the flexibility and durability of the piezoelectric polymer matrix, ii) these flexible arrays can only conform to surfaces that can be developed, such as cylindrical surfaces, and not non-developable surfaces, such as spherical surfaces, iii) the element position is critical to the image post-processing, and iv)

when used repeatedly, the flexible conductive interconnections are prone to breakage or debonding because their flexibility is insufficient to handle the complex and time-dynamic motion of the electrodes and the device during measurements.

3.2.3. Type III: Stretchable Single Array

In general, most of the work reported in Types I and II suffered from several limitations. First, the flexible ultrasonic probe should not be considered a heavy-duty tool because constant pressure should be applied to the probe to maintain good adhesion for clear signals. To solve this problem, the flexible probe was usually connected to a holder assembly for operation or pressed by hand to achieve sufficient contact on the irregular surface. Second, it is still difficult to accurately calculate the time delay for curved components, and it is not applicable to use theories of planar time delay laws for array elements distributed on curved surfaces. Third, the flexible device is not stretchable, which can only fully conform to developable surfaces (i.e., cylindrical surfaces) but cannot seamlessly attach to non-developable surfaces (i.e., spherical, or irregular surfaces). Fourth, the current work is mainly dedicated to the design and fabrication of the conformable ultrasound transducer, lacking consideration of the flexible integrated circuit and whole imaging system in a conformable way. As a result, it is highly desirable to develop conformable ultrasound transducer arrays that are operator-independent and provide seamless contact with the curvilinear surfaces. Meanwhile, it is also important to accurately determine the time delay laws and sound field distribution inside the object with curved surfaces, then refine the inspection technique and improve reliability and repeatability.

The key distinction between type III and type II is that type III can accomplish greater coupling with irregular, non-planar surfaces. Based on this perspective, replacing the flexible substrate with a stretchable substrate (e.g., PDMS, Ecoflex) allows for the fabrication of a stretchable single array.^[215] However, to achieve device flexibility while preserving the rigid key components of the transducer (i.e., active elements, backing layer, matching layer), the “island-bridge” structure has been widely used (Figure 5i),^[46b] which consists of thin piezoelectric elements as transducers, single or multilayered serpentine metal traces as electrical interconnects, and low-modulus elastomer membranes as encapsulation materials.^[27] This type of cUSE was first proposed by Zhang and Sheng in 2018,^[216] then have become the most widely used design in the past 6 years. Many researchers have become dedicated to combining ultrasound functionality with this type of design.^[27,33–35,63] The top and bottom stretchable interconnections are usually made of copper (Cu) as a conductive layer and polyimide (PI) as a protective layer. This design utilizes the advantage of stretchability while maintaining the ultrasound performance of each element and has been achieved in various applications, including for Al block imaging (Figure 5j),^[27] blood pressure monitoring (Figure 5k),^[34,217] blood velocity monitoring,^[35] cardiac monitoring (Figure 5l),^[45] treatment on bone injury,^[218] wireless multifunctional implants,^[219] 3D scanning on skull model,^[63e,220] chronic wound healing,^[39] deep brain stimulation,^[42] and many other monitoring.^[33,221]

Similar to Type III, some critical issues have been overcome but still need further investigation: i) the multiple electrode design would greatly increase the difficulty and cost of fabrication, ii) precise and dynamic localization of all elements with advanced imaging algorithms, iii) combination of the transducer with on-board signal pre-conditioning, memory, and wireless data transmission, and iv) replacing the power supply with a flexible lithium-polymer battery of the highest quality.

3.2.4. Type IV: Multiple Phased Arrays

The design idea of the cUSE with multiple phased arrays can be found as early as in C. Daft's introduction^[24] and X. Jiang's further concept description,^[222] then realized for breast patch design^[31] and achieved on bladder imaging with a clinical study by Zhang and Dagdeviren (Figure 5m–o).^[32] This design enabled the wearable integration of ultrasound technology and displayed a spatio-temporally precise image reconstruction technique on a larger field of view (FOV) for monitoring deeper bodily components. Different from the Type III design, which uses hundreds of elements on the stretchable substrate, in this design, adjacent parts are brought closer together to build phased arrays to balance the mechanical stretchability and ultrasound imaging resolution. The aperture of the phased array is designed to produce a higher FOV and cover the space between adjacent arrays. The array can be either a 1D array or a 2D matrix phased array. As a result, the phased array imaging performance is maintained while simultaneously allowing for large surface area coverage and mechanical deformation. The new design demonstrates both local stiffness and global malleability. The partial overlap between images from each phased array helps with the final image reconstruction. This design is also feasible for the bendable pMUT with high element density and reduced fabricated steps. Puer's group proposed pMUT based multiple arrays on the silicon islands, which were connected by the silicon strings (Figure 5p).^[63d] The induced wave generated by a pMUT can be transmitted easier through the substrate to other pMUTs. Based on the suggested methodology, a bendable array is very conformal to the intended structure. Several silicon islands, each carrying a pMUT array and linked together by silicon springs, make up the flexible structure. Very recently, a novel transformable design inspired by the paper-folding mechanism was proposed, which can transform between a 1D linear array and a 2D planar array with the ability to switch between different functions, including 2D/3D imaging and high-intensity focused ultrasound beamforming.^[63f]

For specific applications, such as imaging and monitoring large organs (breast, bladder, fetus, etc.), this design can obtain the images in two orientations (transverse and sagittal planes)^[32] or any orientation (breast)^[31,192] simultaneously, avoiding the requirement for manual rotation. For localizing the position of each array and image reconstruction, we suggested two methods: i) to use the position of the objects in the overlapped area in the ultrasound images to stitch different images, ii) to use separate elements to localize the array positions by ultrasound wave, which is similar to the principles used in the global positioning system (GPS).^[192]

3.2.5. Type V: Rigid Single Array

In recent work for cUSE, this type of design represents a unique path. The configuration is like the first generation of conformable electronics, which employed a belt, band, straps, or holder to wear the functional devices on the human body, because it uses a rigid single array with a high density of elements or integrated rigid components with the PCB. This type of cUSE still requires support for adherence because it cannot be laminated on the skin by itself. Examples of such assistance include tape or adhesive between the device/skin interface, external pressure on the device's back, and other frame or holder pressing on the skin (Figure 5q). However, this kind of adhesion did not hamper patients' mobility or cause any inconvenience or discomfort. The main reason we take this type into account in the cUSE is because it meets the requirements of long-term continuous imaging and monitoring and operates independently.

Zhao's group recently reported that they had made a bioadhesive ultrasound (BAUS) device that stuck well to the skin. It had a small, rigid ultrasonic array and a coupling layer made of a flexible, resilient, bioadhesive hydrogel-elastomer hybrid.^[29] The BAUS device provides 48 hours of continuous imaging of diverse internal organs. The innovation can be attributed to the hydrogel-elastomer hybrid, which paved the way for future long-term monitoring not only for the cUSE, but also for other conformable electronics.^[223] In some organs, it does not require long-term monitoring but requires precise repeatability of array positioning on a large, curved surface over a long time. Very recently, Dagdeviren's group proposed a different design that uses a nature-inspired honeycomb patch to hold the rotated phased array on the breast to achieve tumor imaging.^[31] Breast imaging, unlike heart, bladder, and other organ monitoring, focuses on the precise position of the cyst in the breast rather than requiring continuous imaging during a person's activities. The patch design provides several developments, including i) the ability to move through a path of 15 imaged sections to cover a larger area; ii) mechanical support and stability for the array, with a tracker to achieve images at different angles via rotation; iii) the elimination of the need for an operator to constantly move the array; and iv) great repeatability positions, demonstrating reliable and comparable breast tissue screening for long-term monitoring. This design solved the conventional transducers with small apertures could not achieve continuous imaging and large area scanning at the same time, providing a new, easy-operated strategy for imaging large area surfaces. Besides the single rigid array, the transducer integrated with the electronics to form a miniaturized cUSE is another important type. Material selection, advanced manufacturing processes, and circuit integration are critical to the miniaturized cUSE.^[26c] This design usually targets special or internal organs with a small area, such as ultrasound-induced retinal stimulating,^[40] and miniaturized neural dust mote.^[224]

3.3. Advanced Materials and Technologies for cUSE

Advanced materials and novel technologies are critical for cUSE to achieve superior ultrasound performance and mechanical conformability. For the different types of cUSE discussed in Section 3.2, besides the selection of advanced piezoelectrics,

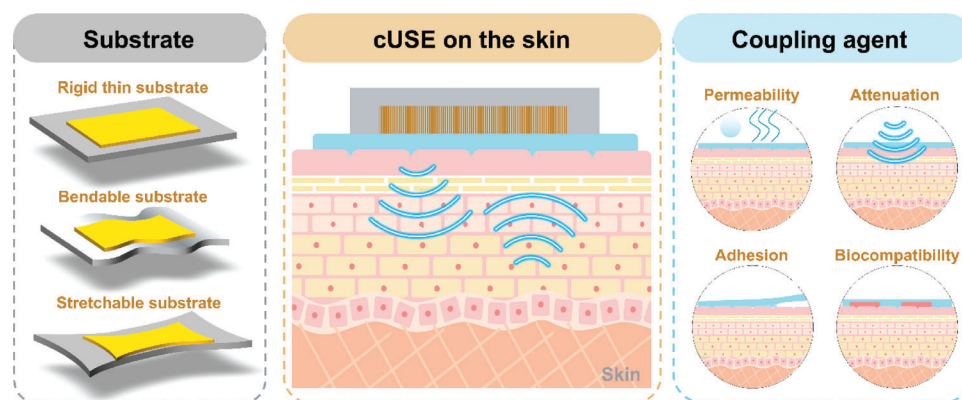


Figure 6. Schematic of various substrates and coupling agents for cUSE.

various novel structure designs, high-tech fabrication, and integrated electronics are also needed to be summarized.

3.3.1. Substrates: from Hard to Soft

Conventional ultrasound transducers were fabricated on rigid substrates such as silicon wafers. Due to the increasing demand for mechanically flexible ultrasonic transducers for wearable biomedical applications, several approaches have been developed to realize flexible or even stretchable ultrasonic transducers (**Figure 6**).^[29,45,220,225] In that sense, substrates also need to become softer and more flexible. The mechanical properties of commonly used substrates are listed in Table 5, and the selection of the substrate will depend on the application of the ultrasonic transducer. In general, substrates for conformable ultrasonic transducers require good thermal stability, biocompatibility, and proper mechanical properties. The mechanical properties of the substrate can also be modified by optimizing the thickness of the substrate, since the bending stiffness of the thin film is a function of Young's modulus and the thickness.^[226] If the transducer will be used for monitoring relatively large organs with low surface curvature, such as the heart, fetus, and bladder, a flexible substrate will be sufficient. Whereas if the transducer will be applied to organs with small features or larger curvatures, such as the skull, elbow, or small organs, ultrasonic transducers should be in a thin and stretchable form.

In terms of device fabrication, it is quite challenging to fabricate high-performance flexible ultrasonic transducers directly onto a flexible substrate since most piezoceramic materials require high-temperature processing (over 700 °C) to increase piezoelectric performances, or mechanical dicing or laser cutting methods to fabricate high-performance piezoelectric composites, which are not compatible with flexible polymeric substrates.^[27,54a,227] Thus, several approaches were developed to fabricate flexible ultrasonic transducers: i) fabricate ultrasonic transducers on the rigid substrate and transfer them to the flexible substrate; and ii) use low-temperature processable piezoelectric materials such as polymer-based or high-performance piezoelectric thin films. Hu et al. reported stretchable ultrasonic transducers and fabricated 1–3 piezoelectric composites on a rigid

glass substrate using the dice-and-fill technique and transferred them onto a stretchable Ecoflex substrate (**Figure 7a,b**).^[27] Furthermore, Liu et al. reported thin PZT film-based flexible ultrasonic transducers on polyimide substrates. They fabricated Pt/PZT/Pt structured ultrasonic transducers on the silicon wafer with silicon dioxide and transferred it onto polyimide films (**Figure 7c**).^[227b] On the other hand, Mastronardi et al. reported flexible piezoelectric transducers based on AlN thin film.^[109b] They directly deposited a transducer with a Mo/AlN/Mo structure on the flexible PI substrate using the sputtering method (**Figure 7d**). As summarized in Table 5, there are various substrates that could be applied to mechanically flexible and stretchable ultrasonic transducers. However, innovation is required in piezoelectric materials such as novel processing methods or low-temperature processable high-performance piezoelectric materials to fabricate flexible ultrasonic transducers with high reliability.

3.3.2. Interconnects and Electrodes

Interconnects and electrodes are critical for whole conformable ultrasound systems because they are the electrical skeleton that physically links the transducers to the electronic hardware and transmits electrical signals from elements to the system. Since most high-performance piezoelectric materials are based on rigid piezoelectric ceramics, most flexible or stretchable ultrasonic transducers are based on an island interconnect structure, in which small islands of transducer arrays are connected by conductive interconnects.^[27,225,228] However, conventional conductive traces such as metal thin films or foils could not be applied to flexible and stretchable ultrasonic transducers due to their brittle nature. Hence, the development and integration of highly flexible, even stretchable, conductive layers with piezoelectric layers are also critical challenges in flexible ultrasonic transducers. In general, there are two types of approaches to developing mechanically robust conduction layers. One is adopting structural modifications, such as serpentine structured conductive layers. In this approach, metal thin films are patterned into serpentine structures (**Figure 7a,b**).^[27] This structural modification minimizes the applied strain on the metal thin film interconnect, hence preventing catastrophic failure of the interconnects.^[225] By

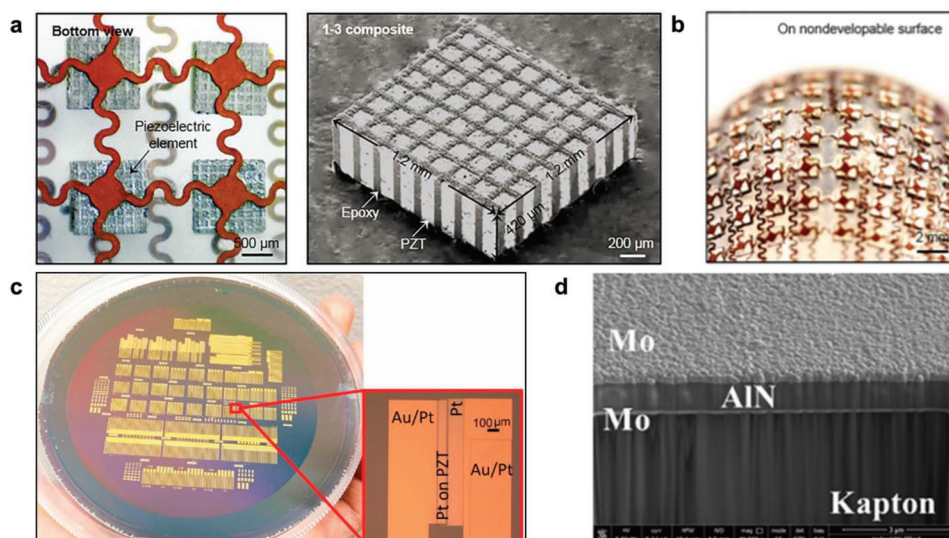


Figure 7. Flexible or stretchable ultrasonic transducers fabricated by various methods. a) A optical microscope image of 1–3 composites mounted on the stretchable Ecoflex substrate and connected by serpentine interconnects (left) and scanning electron microscopy image of 1–3 composite piezoelectric ceramic. b) A stretchable ultrasonic transducer array using diced piezoelectric ceramics mounted on a curved surface. Reproduced with permission from the Creative Commons License.^[27] Copyright 2018, The Authors, Published by American Association for the Advancement of Science. c) A 1D array of thin film ultrasonic transducer fabricated on Si wafer prior to transfer it to the flexible polyimide substrate. Reproduced with permission.^[227b] Copyright 2021, MDPI. d) A cross-section scanning electron microscopy image of a thin film ultrasonic transducer directly deposited on a polyimide substrate. Reproduced with permission.^[109b] Copyright 2014, Elsevier.

designing the interconnects, the maximum stretchability of serpentine traces could go up to 300%.^[229] Serpentine interconnects can be fabricated using conventional photolithography processes or laser cutting.^[220,228,230] Although the metal layer in serpentine design can improve the flexibility of the entire device, metal-type electrodes still suffer from cracking or delamination during mechanical bending or stretching, and it has not been overcome very well, as shown in (Figure 8a,d).^[231]

Hence, researchers also tried to develop intrinsically flexible or stretchable conductive materials. In this approach, various novel nanomaterials such as carbon nanotubes (CNTs), metallic nanowire networks, liquid metals, and conducting polymers such as polyaniline and Poly(3,4-ethylenedioxythiophene) polystyrene sulfonate (PEDOT:PSS) have been adopted for conductive traces and interconnects. However, the conductivity and electromechanical effects of conductive polymers limited their use as electrodes for the transducer. Recently, Kim et al. proposed flexible electrodes, mixing silver nanowires (AgNWs) with PDMS, were deposited on the transducers using a spray coating method, providing sufficient conductivity through the repeated bending tests.^[63b] The AgNW/PDMS electrodes can maintain excellent conductivity in a highly strained state (e.g. > 5000 S cm⁻¹ at 50% tensile strain).^[232] Hu et al. reported stretchable ultrasonic transducers using liquid metal conductive interconnects (Figure 8e,f). They mixed eutectic gallium-indium liquid metal into a poly(styrene-ethylene-butylene-styrene) co-polymer matrix to make a highly stretchable interconnect, and this conducting layer could be stretched up to 750% (Figure 8e).^[45] They could continuously monitor cardiac activity by using ultrasonic transducers with liquid metal interconnects. Although serpentine-shaped metal thin films could produce highly stretchable electrical interconnects, novel intrinsically flexible or stretchable con-

ductive materials could prevent the delamination issue and enable high density ultrasonic transducer arrays.

3.3.3. Device-Skin Interface

When designing the interface between the flexible ultrasonic transducer and skin, two major points need to be considered: i) good mechanical interface and ii) acoustic matching. For wearable electronics that receive physiological signals from the human body, maintaining good conformal contact with the skin is crucial for accurate measurement.^[228,233] To maintain good conformal contact with the skin, the interfacial layer should have a similar Young's modulus and high adhesion strength to the skin.^[29,233] If ultrasonic transducers have poor conformal contact with the skin, an air gap will be formed at the interface, which results in severe noise and scattering of the ultrasonic wave.^[228] Young's modulus of the skin is reported to be 5 kPa to 140 MPa, and it is important to develop a proper matching layer to improve the conformal contact.^[234] In summary, the interface layer should be evaluated by the following criteria: strong adhesion for robust bonding, small attenuation for wave penetration, excellent permeability for moisture evaporation, and good biocompatibility for safe and comfortable monitoring (Figure 6).

In a recent study, researchers proposed that hydrogels meet the suggested requirement to solve the mechanical mismatch between ultrasound transducers and soft skin to achieve a chronically stable and robust device-skin interface.^[47b,235] A new group of hydrogel-based sensor-tissue interfaces exploits hydrogels with both mechanical toughness and tissue-adhesive features to realize strong bonding at the sensor-tissue interface.^[236] By minimizing the mechanical mismatch between the device and the

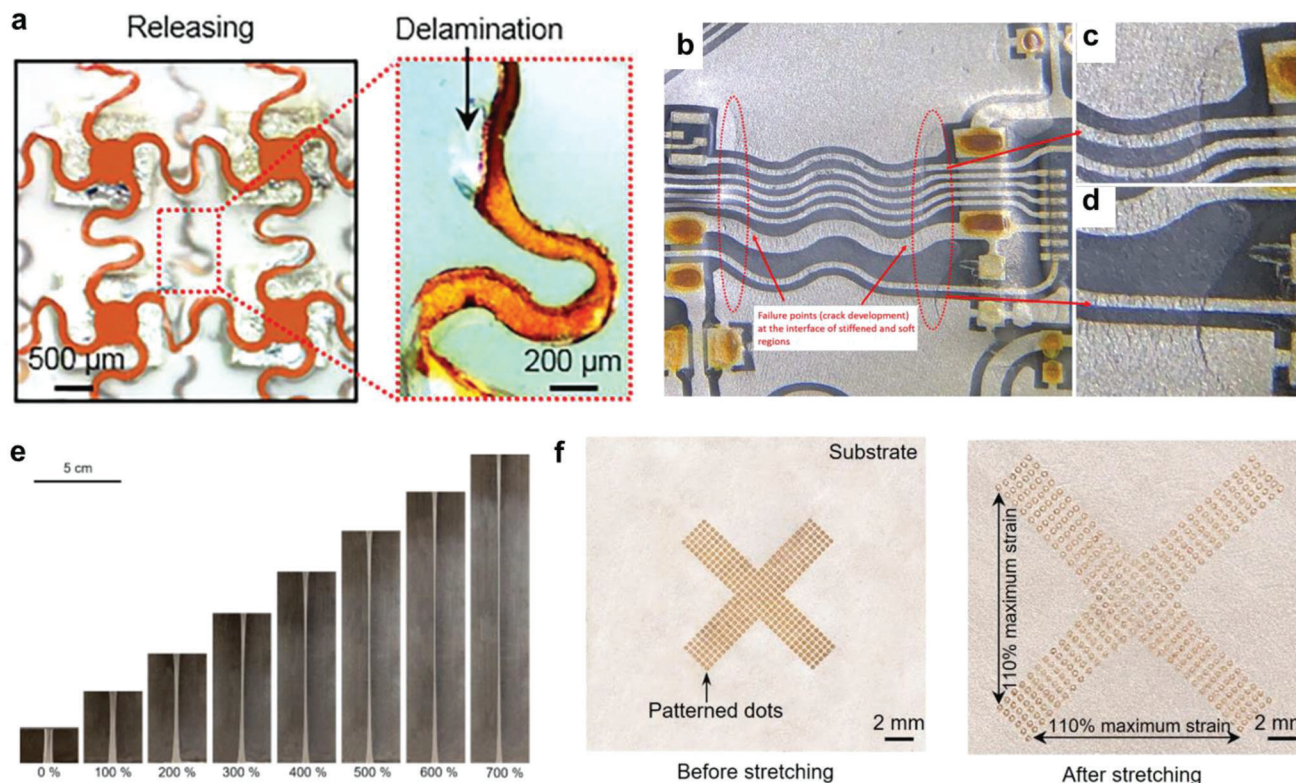


Figure 8. Various electrical conductor materials for flexible and stretchable ultrasonic transducers. a) A photograph of metal thin film-based serpentine interconnect under mechanical stretching and releasing. Delamination has occurred at the interconnect/elastomer interface. Reproduced under the terms of the Creative Commons License.^[27] Copyright 2018, The Authors, Published by American Association for the Advancement of Science. b) An optical microscopy image of serpentine interconnect under stretching with 10% strain. Cracks were observed on the surface of the interconnect, which could be observed in the magnified images (c) and (d). Reproduced under the terms of the Creative Commons License.^[231] Copyright 2021, The Authors, Published by IEEE. e) liquid metal-based stretchable conductive layers under various strains. f) An ultrasonic transducer using liquid metal-based interconnects under mechanical stretching. Reproduced under the terms of the Creative Commons License.^[45] Copyright 2023, The Authors, Published by Springer Nature.

tissues compared with conventional ultrasound probes, hydrogels also eliminate the tiny voids that typically increase interfacial impedance at the device/tissue interface. For example, Wang et al. reported a bioadhesive ultrasound (BAUS) device that consists of a thin and rigid piezoelectric probe array robustly adhered to the skin via a couplant made of a soft, tough, anti-dehydrating, and bioadhesive hydrogel-elastomer hybrid.^[29] This hydrogel matching layer has a Young's modulus value of 100 kPa and an interfacial toughness of 853 J m^{-2} with the skin, which showed good conformal contact with the skin for 48 hours and superior acoustic matching, enabling wearable long-term ultrasound imaging.

3.3.4. Integrated System

The basic working principle of an ultrasound data acquisition system for imaging can be described as following.^[237] The multi-element transducer is stimulated by a high-voltage waveform via a transmit/receiver (T/R) switch. The application of this voltage induces expansion and contraction of the transducer element through the phenomenon of piezoelectric effect, resulting in the generation of an ultrasonic wave. Following the act of firing, the

transmit/receive (T/R) switch undergoes a transition to the receive pathway. The process of ultrasound reflections, known as echos, involves the expansion and compression of the transducer element upon their return to the transducer. This expansion and compression generate a voltage, facilitated by the piezoelectric effect. The voltage is modulated by an analog front end (AFE). The AFE commonly consists of several gain and filtering stages. Frequently, the amplification of a stage exhibits temporal variation upon triggering. To mitigate the detrimental effects of waveform spreading and attenuation, time-gain compensation is employed. The conditioned signal is subsequently converted into digital form through the utilization of an analog-to-digital converter (ADC). The controller is responsible for regulating several aspects of the transmission process, including the voltage levels, waveform shape, and timing between different channels to ensure proper beam focusing. Additionally, it controls the gains and filters on the receiving side and manages the digitized data stream. It may also do additional signal conditioning and receive-side beam focusing as necessary. Additionally, the controller has the capability to perform additional data processing in order to generate B-mode images.

The existing electronics architecture of conventional imaging systems encounters several obstacles for the future

requirement of ultrasound imaging because i) the form factor changing from a traditional bulky probe to portable and patches,^[238] ii) imaging requirements from 2D to 3D with enhanced resolution, and iii) the operator expanded from expert sonographers into more widespread general public users.^[237c] The current electronics architecture of conventional imaging systems, which relies on readily available commercial components, lacks scalability in relation to the newly introduced form factors, particularly in terms of size and power consumption. Furthermore, in regards to channel count, these architectures exhibit limited scalability when applied to 3D imaging. Integrated circuits (ICs) and MEMS technology supported ultrasound-on-chip platforms are of paramount importance in facilitating these advancements.^[239] Recently, many electrical engineers dedicated to this field have proposed advanced systems, such as area- and power-efficient application-specific integrated circuit (ASIC) for a miniaturized 3-D ultrasound system,^[240] a PMUTon-CMOS with a competitive noise efficient factor,^[241] a compact high-voltage transmit circuit,^[242] an analog-front-end circuit,^[243] a PMUT device with the companion ASICs,^[244] and a field-programmable gate array (FPGA)-based portable system.^[245]

As previously indicated, the structures of interest demand some tradeoffs in terms of the quality and strength of the signals that may be acquired when employing a conformable ultrasonic device. Conformable technologies provide a wide range of wearable applications, which necessitate the adaptation of classic ultrasonic acquisition methods to meet the demands.^[3] Current systems have several drawbacks that have limited their application for cUSE, i) present systems lack an integrated, portable, and low-cost imaging system with sufficient resolution to determine the optimal position and focal depth for modulation; ii) the current systems' relative size, weight, and power are prohibitive to widespread deployment; iii) the imaging quality highly relies on the large control systems. It is not easy to combine hard ultrasonic chips with a soft adhesive substrate to achieve stable contact with human skin. Thus, Soumyajit's group proposed several custom-designed bendable prototypes and data acquisition systems to demonstrate its capability in acquiring ultrasound images, including modulating nerve conduction, imaging to monitor the target,^[63c] image-guided neural therapy,^[187] and cardiovascular diseases.^[246] However, it is still highly desirable for a fully integrated system to be integrated into an entire conformable device. Very recently, Sheng's group described the development of a fully integrated autonomous wearable ultrasonic-system-on-patch (USoP) (Figure 9a–d).^[30] For signal preconditioning and wireless data transfer, a tiny, flexible control circuit is devised to communicate with an ultrasound transducer array. Machine learning is employed to track shifting tissue targets and aid in data interpretation. This work offered continuous deep tissue signal decoding and imaging. It also pushes the cUSE to a new high level that combines a stretchable array, a soft system, long-term monitoring for clinical studies, and machine learning analysis in one work, expanding a new dimension for the existing cUSE. Meanwhile, Feng's group proposed another type of soft system for acoustic energy transfer and communication (Figure 9e–i).^[36] Compared to imaging, the system requirements of the non-imaging application is much simpler and easier to achieve mechanical conformability. It should be mentioned that they developed a universal soft implantable platform for both the

transmit system and the receiver patch, which is another great milestone in the development of cUSE.

4. Applications of Conformable Ultrasound Electronics

Conformable ultrasound electronics can expand the use of ultrasonic sensors and actuators in a variety of circumstances. Numerous groups have proposed and developed numerous biomedical and healthcare applications in recent years.^[27,33–35,63] Conformal ultrasound transducers can support ultrasound applications in diagnostics and healthcare, ranging from intravascular imaging to encompass the catheter tip to large area imaging and deep stimulation with variable focal length. Prior research focused primarily on five distinct aspects: components/tissue imaging, health monitoring, energy harvesting and power supply, organ/tissue electrical stimulation, and treatment. (1) Imaging is one of the most common nondestructive diagnostic and biomedical engineering applications of ultrasound. Utilizing large area conformal ultrasound transducers to produce detailed 2D or 3D overview images of large portions of objects and the human body was the focus of the present research (Table 6). (2) Vital body functions, such as blood flow and pressure sensing, wound healing, and cardiac monitoring, can be observed in real-time through the use of ultrasound body patches for health monitoring. (3) Energy harvesting and power supply for next-generation bioimplantable systems utilize wireless and acoustic energy transfer. (4) Ultrasound-based electrical stimulation has recently become a popular area of study because it has the potential to combine noninvasiveness with high spatial selectivity. Highly desirable is the next-generation, pleasant ultrasound patch for neural interfacing. (5) Therapy is typically the last step of ultrasound body patches, which can reduce the patient's burden by enabling them to move freely during treatment, such as pain relief, skincare, odor control, and hyperthermia treatment. This section summarizes and discusses five applications of conformable ultrasound transducers, including device configuration, signal acquisition, and result analysis. Other prospective applications for future development are suggested.

4.1. Imaging on the Complex Surface

The most important application of ultrasonic transducers is to image objects for NDT (inspecting components for subsurface defects) and biomedical diagnostics (imaging deep tissue/organ). The majority of ultrasonic brightness-mode (B-mode) images are reconstructed using beamformers that rely on the delay-and-sum (DAS) technique.^[27,247] In the setting of DAS, processing of high frequency signals relies on the determination of time-of-flight (ToF) from the sending element to the receiving element as it traverses the imaging point. In order to accurately determine the ToF value, it is imperative to have access to relevant data pertaining to the geometry of the element array. In the event that DAS beamforming is executed with an incorrectly assumed element array geometry, the resulting reconstructed image will exhibit a lack of focus and distortion.^[248] The phased array with various imaging algorithms such as plane wave imaging (PWI),

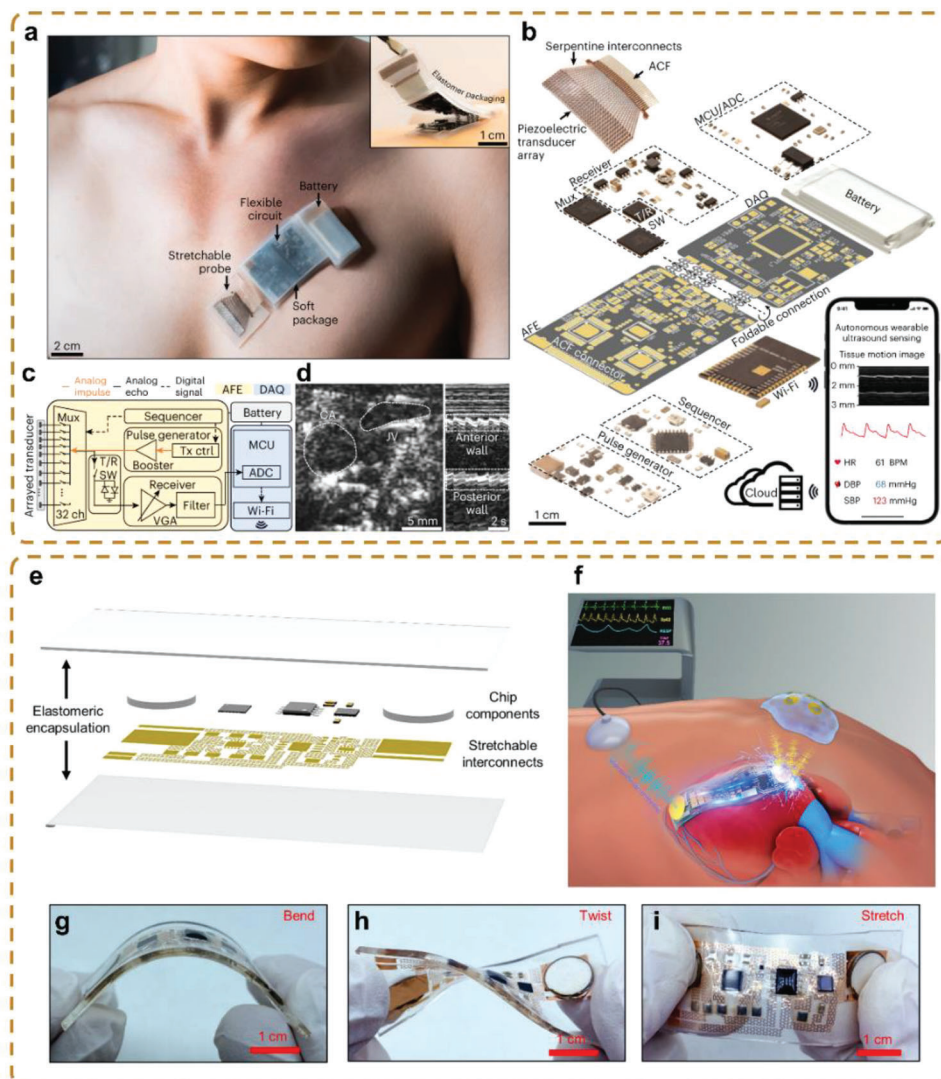


Figure 9. The integrated wearable ultrasound systems. A fully integrated wearable ultrasound system to monitor deep tissues in moving subjects: a) A photograph of the encapsulated USoP laminated on the chest for measuring cardiac activity via the parasternal window. The inset shows a folded circuit. b) Design of the USoP, including a stretchable ultrasonic probe, a flexible control circuit, and a battery. The ultrasonic probe consists of a piezoelectric transducer array, serpentine interconnects, and an ACF (upper left). c) Block diagram of the USoP showing the flow of analog impulse, analog echo, and digital signals. d) B-mode imaging of the carotid artery (CA) and jugular vein (JV), while the subject is performing the Valsalva maneuver to dilate the JV (left). M-mode imaging of the pulsation pattern of CA walls (right). Reproduced with permission.^[30] Copyright 2023, Springer-Nature. A flexible, stretchable system for simultaneous acoustic energy transfer and communication: e) Exploded schematics of the device structure. f) Illustration showing the AECD function—wireless charging and communication based on ultrasound. g) Image of the device in the bent configuration. h) Image of the device in the twisted configuration. i) Image of the device in the stretched configuration. Reproduced under the terms of the Creative Commons License.^[36] Copyright 2021, The Authors, Published by American Association for the Advancement of Science.

synthetic aperture focusing technique (SAFT), and total focusing method (TFM), possesses the advantageous capability to provide beam steering at various angles and focalization at any desired location, hence enabling comprehensive scanning even in situations where detecting areas are limited in accessibility.^[28] The time delay law governing the formation of dynamic beams is a basic principle that underlies both theoretical investigations and actual implementations of phased array technology. Conventional rigid probes are particularly advantageous for in situ inspection as they offer the greatest inspection coverage from a single de-

tected location. However, it is often necessary to perform imaging on rigid components or human body parts with curved surfaces, and this can cause complications that lead to a reduction in defect detection sensitivity and an increased chance of false information. Despite the numerous advantages, it remains a challenge for conventional rigid probes to image human body parts with irregular surfaces due to several drawbacks, such as high operator dependence, measurement variability and inability to cover curved surfaces, poor physical connection, and degrading ultrasonic signals by distortion and loss of sound energy. In addition,

Table 6. The comparison of cUSE for deep tissues and organs imaging.

Work	Type of cUSE	Array in a patch	Elements and materials	Form Factor	Freq. [MHz]	Pitch [mm]	Max. Depth [mm]	Axial Res. [mm]	Targets
Wang et al. (2018) ^[34]	Type III	2D array	5 × 4 of 1–3 PZT/Epoxy	Stretchable	7.5	2.5/2.0	40 in tissue	0.5	Blood pressure
Oliveira et al. (2019) ^[63a]	Type III	1D linear array	48 elements of PZT	Flexible	2.25	0.6	–	–	Bone phantom
Kim et al. (2019) ^[63b]	Type II	Single patch	1–3 PZT/PDMS composites	Bendable	1.7	–	90 in water	–	–
Pashaei et al. (2020) ^[63c]	Type II	1D linear array	64 elements of PZT	Flexible	4.0	0.2	20 in tissue	0.3	Nerve imaging
Sadeghpour et al. (2020) ^[63d]	Type II	6 of 2D arrays	3 × 3 pMUT array	Bendable	0.42	0.49	–	–	–
Wang et al. (2021) ^[33]	Type III	2D phased array	12 × 12 of 1–3 PZT/Epoxy	Stretchable	2.0	0.8	140 in tissue	2.5	Blood
Wang et al. (2021) ^[35]	Type III	2D array	3 × 3 of 1–3 PZT/Epoxy	Stretchable	5.0	2.0	25 in tissue	–	Blood velocity
Liu et al. (2021) ^[63e]	Type III	2D array	6 × 6 of PZT	Stretchable	1.92	4.5	–	–	Skull phantom
Zhang et al. (2022) ^[63f]	Type IV	5 of 1D array	1–3 PZT/Epoxy composites	Foldable	1.01	–	60 in tissue	–	–
Wang et al. (2022) ^[29]	Type V	1D array	1–3 PZT/Epoxy composites	Wearable	3.0	0.5 (λ)	180 in phantom	0.77	Various organs
Hu et al. (2023) ^[45]	Type III	Orthogonal array	1–3 PZT/Epoxy composites	Stretchable	3.0	0.4 (0.78 λ)	110 in phantom	0.8	Heart
Hu et al. (2023) ^[221]	Type III	2D array	16 × 16 of PZT	Stretchable	2.8	0.8 (1.5 λ)	40 in tissue	0.5	Tissue biomechanics
Zhang et al. (2023) ^[32]	Type IV	5 of phased arrays	64 elements of Sm/La-PMN-PT	Stretchable	3.5	0.22 (0.56 λ)	160 in tissue	0.6	Bladder imaging
Du et al. (2023) ^[31]	Type V	1D array	64 element of Yb/Bi-PIN-PMN-PT	Wearable	7.0	0.125 (0.56 λ)	80 in tissue	0.2	Breast imaging

the interface curvature can cause ultrasonic beam self-focusing or divergence and sound energy concentration or dispersion during wave propagation. In recent decades, with the development of transducer fabrication technologies, conformable ultrasound transducers have become a wonderful alternative to inspecting the parts/body with complex surfaces.

The configuration and fabrication of various cUSE have been discussed in Section 3, In this section, we only discussed the conformable ultrasound transducers that have generated ultrasound imaging for NDT and biomedical diagnostics. Casula et al. proposed 2D and 3D flexible phased array transducers, which were mechanically assembled with springs to couple the irregular surfaces directly and improve the contact inspection of pipes and complex geometry components.^[201] The radiating surface consisted of mechanically assembled independent piezoelectric elements, and a profilometer, embedded in the transducer, measured local distortion. The computed form is used by an algorithm to compute the adapted delay legislation in real-time to compensate for 2D and 3D profile distortions. The flexible array transducers ultimately can inspect the defects in different irregular components (i.e., butt weld, nozzle, and elbow). Lane et al. proposed a low-profile flexible linear array probe to inspect curved components with a sinusoidal profile using the total focusing method, which combined a fiber optic shape sensing device to measure the position of the elements along the array.^[207] Similarly, Nakahata et al. used a flexible array transducer to obtain images of flaws in cylinder specimens, cubic specimens, and specimens with complicated surface.^[208] To improve the resolu-

tion, the author used scattering amplitude extracted from raw signal data and introduced a numerical apodization technique to suppress the influence of side lobes. It should be noted that the current design is designed with specific application variables in mind and is not suitable for all applications and use cases. Besides the configuration of flexible patches, the design and validation of body-conformal active ultrasound patches with system leveled integrated imaging and modulation modalities have also been proposed. Pashaei et al. presented a mechanically-flexible linear 64-element array of piezoelectric transducers with a resonance frequency of 5 MHz for nerve localization.^[63c] A strain sensor integrated on the probe provides patient-specific feedback information on array curvature for real-time optimization of focusing and image processing. The flexible array that generated the image on an artificial vein phantom (water-filled tube embedded in gelatine) and the accuracy of the image were also confirmed by the Verasonics Vantage research ultrasound system. Although some artifacts can be observed in the image, the results showed promising functionality of the flexible probe for imaging and target localization.

As discussed in Section 3.2.3, based on these considerations, some groups proposed new structures or new theoretical frameworks for conformable ultrasound arrays. To overcome the bottleneck, advanced transducers that combine excellent ultrasonic performance with desirable mechanical properties were proposed by Xu's group with a stretchable form factor that can conform to and detect non-planar complex surfaces.^[27] The probe consists of a 10 × 10 array of piezoelectric transducers that

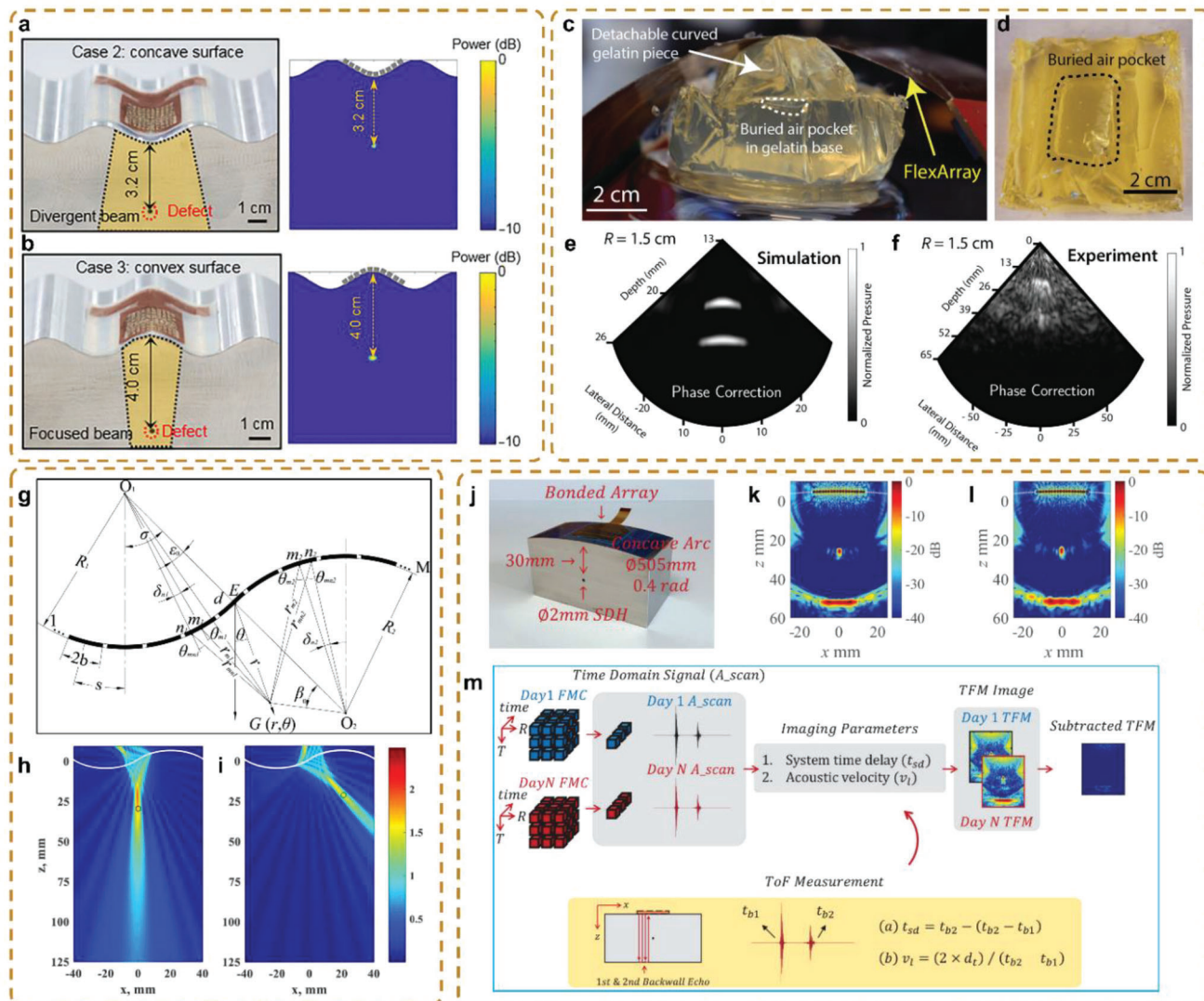


Figure 10. The beamforming of cUSE on complex surfaces. Stretchable ultrasonic transducer arrays for three-dimensional imaging on complex surfaces: a) concave surfaces and b) convex surfaces showing the good conformability of the device on these surfaces and acquired 2D images using delay multiply and sum algorithms. Reproduced under the terms of the Creative Commons License.^[27] Copyright 2018, The Authors, Published by American Association for the Advancement of Science. Flexible ultrasound transceiver array for non-invasive surface-conformable imaging enabled by geometric phase correction: c) Photograph of the cast gelatin phantom used to collect B-mode images at arbitrary curvatures. d) Plan-view photograph of the air pocket-containing gelatin mold. e) Simulated B-mode image when the radius of curvature is 1.5 cm and phase correction is implemented. f) Experimental B-mode image of an air pocket in gelatin captured with the FlexArray when the radius of curvature is 1.5 cm. Reproduced under the terms of the Creative Commons License.^[190] Copyright 2022, The Authors, Published by Springer Nature Limited. Beam generating and sound field modeling of flexible phased arrays for inspecting complex geometric components: g) Schematic diagram for calculating the time delays of single concave/convex components with beam steering and focusing. h, i) Sound field distribution of the concave/convex specimen without or with the time delays. The circles represent the desired focal points. Reproduced with permission.^[249] Copyright 2019, Elsevier. Continuous monitoring with a permanently installed high-resolution ultrasonic phased array: j) the prepared sample block with a curved top surface where a developed flexible ultrasonic array is bonded. k) the TFM image after data acquisition using the MicroPulse array controller system. l) the TFM image after data acquisition using the low-cost multiplexed array controller. m) Diagram of the data compensation strategy. Reproduced under the terms of the Creative Commons License.^[28] Copyright 2023, The Authors, Published by SAGE Publications.

exploit an “island-bridge” layout with multilayer electrodes, encapsulated by thin and compliant silicone elastomers. The stretchable probe shows excellent electromechanical coupling, minimal cross-talk, and more than 50% stretchability. Its performance was demonstrated by reconstructing defects in 3D space with high spatial resolution through flat, concave, and convex

surfaces (Figure 10a,b). The unique device design, combined with the advanced delay multiply and sum imaging algorithms, enables accurate, artifact-free, full-field, and nondestructive examinations underneath general complex surfaces. Very recently, Zheng et al. studied the beam steering and focusing of flexible phased arrays for inspecting complex geometric components

(Figure 10g–i). The authors derived the time delay laws and the sound field analytic expressions for beam steering and focusing on the curved components with a constant radius (concave, convex, concave/convex).^[249] Sun et al. presented the design concept on both the flexible array and controller system for a permanently installable ultrasonic array for high-resolution long-term localized monitoring of industrial structures (Figure 10j–m).^[28]

4.2. Continuous Imaging on Various Organs

Continuous imaging of large and deep tissues and organs is very important to offer clinicians a peek inside the body to monitor health or diagnose disease. However, the conventional ultrasound probes that are mounted on rigid substrates with thick device structures require time-consuming manual operation during measurements, preventing them from being seamlessly integrated with the human body for continuous and long-term monitoring. Even though some cUSE (i.e., Type I and II) have been proposed to seamlessly attach to the irregular surface of objects to achieve good images, they still suffer from three main limitations: i) uncertain imaging quality during body movement because of the short continuous imaging stability; ii) limited freedom of monitoring due to wire connections between the device and the back-end processing system; and iii) limited covering area of deep organs due to the small area of the device. Researchers proposed various methods to solve both challenges and approved their strategy in the clinical study on the imaging of large and deep tissues and organs.

To solve the first limitation, firmly bonding the cUSE to the skin to minimize the influence of body movement is critical. Wang et al. clearly mentioned the similar opinion that Type I and Type II are to make the devices thin and stretchable, which cannot solve this limitation. They proposed a different biointegration paradigm, using a soft, durable, and bioadhesive couplant to securely attach thin, rigid devices to the body (Figure 11a–c),^[29] which avoided the issue of the device on the skin shifting in position relative to the target tissue. To solve the second problem, the fully integrated USoP opened the possibility of long-term monitoring during body movement (Figure 9a–d),^[30] which enables the continuous monitoring of physiological signals from tissues as deep as 164 mm and continuously monitors physiological signals on mobile subjects for up to 12 hours.

The third challenge is not easy to solve because there are many large and curved organs, such as the breast, shoulder, knee, and belly, that cannot be easily and fully monitored in a single shot. The human breast poses a unique challenge in the large-area, deep tissue imaging area because of its geometry and deformability, which are highly variable not only between subjects but also at various times and ages within a given subject.^[250] Breast imaging focuses on the precise location of the cyst in the breast rather than requiring continuous imaging throughout a person's activities, in contrast to heart, bladder, and other organ monitoring. Very recently, Dagdeviren's group proposed a different design that uses a nature inspired honeycomb patch to hold the rotated phased array on the breast to achieve tumor imaging.^[31] Breast imaging, unlike heart, bladder, and other organ monitoring, focuses on the precise position of the cyst in the breast rather than requiring continuous imaging during a person's activities.

Even though handheld ultrasonography (HHUS) and automated breast ultrasound (ABUS) are the most appropriate ultrasound breast imaging methods right now, there are still technical gaps that need to be filled before ultrasound can be used as a reliable method for breast screening, such as: (i) HHUS relies heavily on the skill and training of the technician to manually scan the whole breast by applying strong pressure, and (ii) ABUS can scan the whole breast at once but still has poor skin contact and a stationary setting. For this reason, Du et al. proposed a first-of-its-kind on-body ultrasound technology with a nature-inspired design that offers noninvasive, real-time, continuous monitoring of curved breast tissue, a wide field of view, and an easy-to-use interface (Figure 11d–f). The patch provided high-performance image production with i) deep image depth (≈ 80 mm), ii) sufficient contrast sensitivity (≈ 3 dB at 30 mm depth), iii) desired axial/lateral resolution (0.25/1.0 mm), and (iv) a larger field of view for breast tissue imaging, which is cross-validated with a commercial ultrasound probe in a clinical study (Figure 11g–h). In a subsequent work from Dagdeviren's group, Zhang et al. used bladder volume monitoring as an example and successfully demonstrated the advantages of Type IV using multiple phased arrays to obtain both high resolution and deep detection (Figure 11i–l). Compared to the conventional probe, this patch not only avoids the requirement for manual rotation to obtain the images in two orientations (transverse and sagittal planes),^[32] but also shows comparable results with a commercial, bulky ultrasound machine, even without using the ultrasound gel. Both of these works provide novel strategies to achieve the goals of large area imaging and high resolution.

4.3. Long-Term Cardiac and Haemodynamics Monitoring

Blood supply is critical for tissue survival, and the presence of pulse is one of the fundamental signs of life. The blood pressure waveform and blood flow alterations contain valuable information about specific dynamic cardiovascular activities, and continuous, real-time monitoring of their variation has immense clinical value for the diagnosis and prognosis of cardiovascular diseases.^[251] The major challenge using conventional clinical ultrasonic probes to measure the arterial diameter or blood flow is the motion artifact. The blood motion in the underlying tissues leads to inaccurate and inconsistent measurements. Although some flexible devices were proposed, such as ultrathin inorganic piezoelectric array sensors,^[16b,54a,252] they still suffer from drawbacks such as insufficient penetration depth and variable accuracy, making them not suitable for continuous or long-term measurement.

The ultrasound wall-tracking technique provides high penetration capability and real-time measuring capability for blood pressure. To avoid invasive measurement and further improve device conformability and measurement accuracy, Huang et al. proposed a lightweight, wearable, and flexible ultrasonic sensor made of piezoelectric PVDF film to measure the diameter change of the brachial artery while minimizing errors due to motion artifacts.^[253] A conventional clinical ultrasound probe was used to perform a diameter measurement of the brachial artery of a subject alongside the proposed flexible ultrasound sensor to serve as a comparison. Both results demonstrated the capability to

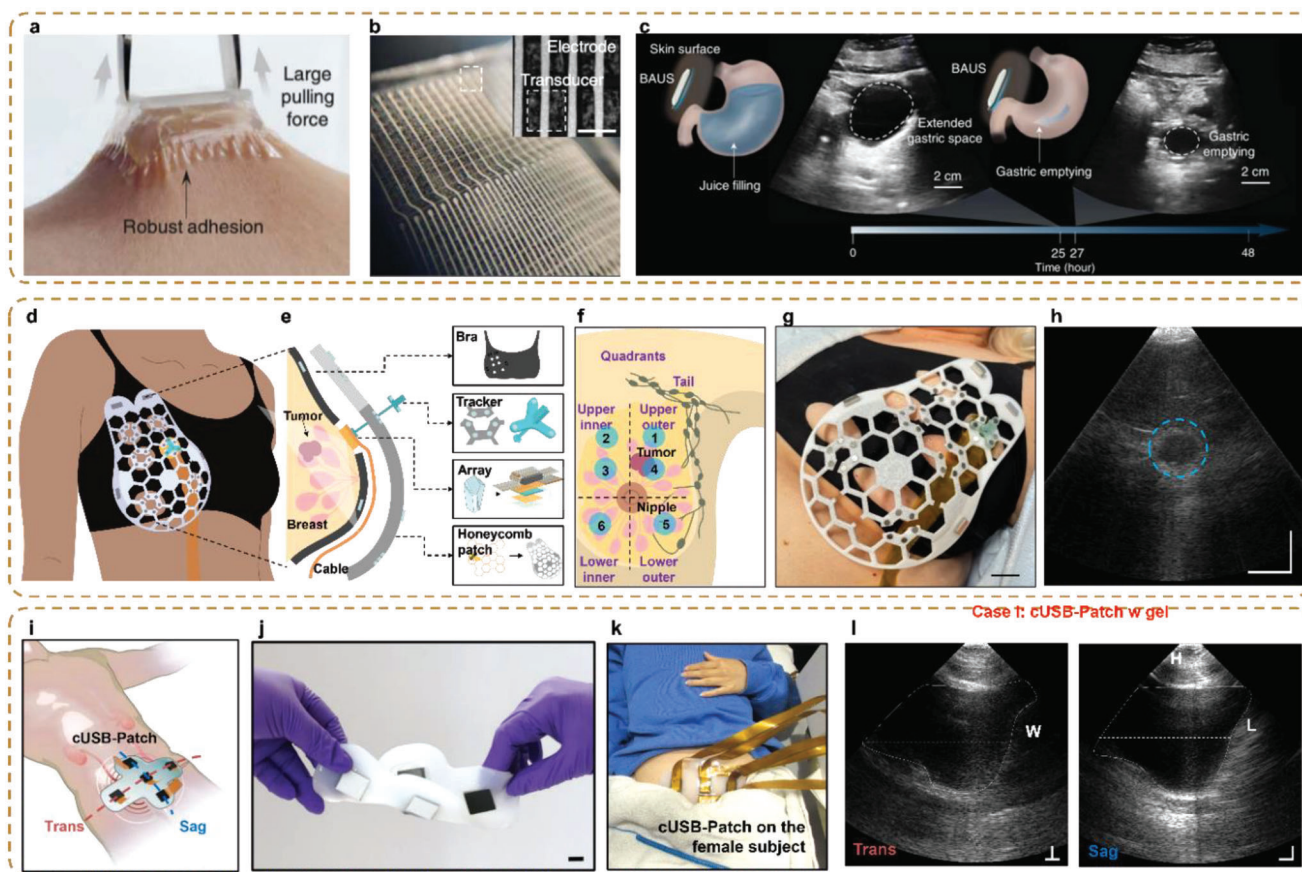


Figure 11. The cUSE for large organs imaging. Bioadhesive ultrasound for long-term continuous imaging of diverse organs: a) The BAUS device adhered on the skin can withstand high pulling forces. b) Optical microscopic image of a BAUS probe with 3D-printed top and bottom circuits. c) The BAUS imaging shows the dynamics of the stomach. The gastric antral cross-sectional area gradually decreases after the subject drinks 450 ml of juice. Reproduced with permission.^[29] Copyright 2022, American Association for the Advancement of Science. Conformable ultrasound breast patch for deep tissue scanning and imaging: d) Schematic of a cUSBr-Patch on the body. e) Exploded view of the cUSBr-Patch to illustrate its four main components: a soft fabric bra to serve as a familiar intermediary layer, a honeycomb patch as the outside layer to provide structure and guidance of the 1D array, the tracker to hold and rotate the 1D array, and the single crystal based 1D phased array. f) Schematic of breast quadrants and the positions of circular regions that align with the patch openings and circular holes in the bra. g) The photo of the cUSBr-Patch on the left breast of a female subject. h) Ultrasound images at Position 4. The blue dashed circle indicates the hypoechoic lesion. Reproduced under the terms of the Creative Commons License.^[31] Copyright 2023, The Authors, Published by the American Association for the Advancement of Science. Conformable phased array ultrasound patch for bladder volume monitoring: i) Schematic of the cUSBr-Patch on the human's lower abdomen for bladder imaging. To avoid the requirement for manual rotation, the cUSBr-Patch can obtain the images in two orientations simultaneously. j) the image of the cUSBr-Patch under twisting. k) The cUSBr-Patch, which is connected to the multiplexer box, was applied to the female subject during the clinical study. l) The results on female Subject. The ultrasound images of full bladders for Case I: the cUSBr-Patch with gel and without gel. Reproduced with permission.^[32] Copyright 2023, Springer Nature Limited.

capture the diameter variation of the brachial artery over the cardiac cycle. The clinical ultrasound probe provided easier identification of the arterial boundaries but suffered from errors associated with motion artifacts. Comparatively, the flexible ultrasonic measurement system had difficulties identifying the posterior boundary of the brachial artery due to the weaker signal strength of the transmitted ultrasound. To ensure conformal intimate contact with the curvilinear and time-dynamic skin surface, Wang et al. have demonstrated a new class of conformal and stretchable ultrasonic devices that offer non-invasive, accurate, and continuous monitoring of vital signs from well below the human skin, adding a new dimension to the sensing range of conventional stretchable electronics.^[34] The system exploits strategic material integration and advanced microfabrication techniques to achieve both state-of-the-art functions and suitable mechan-

ical compliance (can be stretched with strains up to 60%) that allows intimate coupling with the human skin (Figure 12a–d). This device can be used to capture a series of key features in the central blood vessels such as the carotid artery and jugular vein with reliable performance and has strong clinical implications. However, the flexible ultrasonic sensor demonstrated the capability of measuring changes in brachial artery diameter with fewer motion artifacts. Improvement of ultrasonic performance, such as signal strength and signal-to-noise ratio, of the flexible sensor is a future research subject for more reliable and reproducible measurements. After that, Sheng's group reported several work on the Type III of the cUSE for long-term cardiac and haemodynamic monitoring,^[33,254] and finally innovated a wearable ultrasonic device for continuous, real-time and direct cardiac function assessment (Figure 12h–i).^[45] This technology enables dynamic,

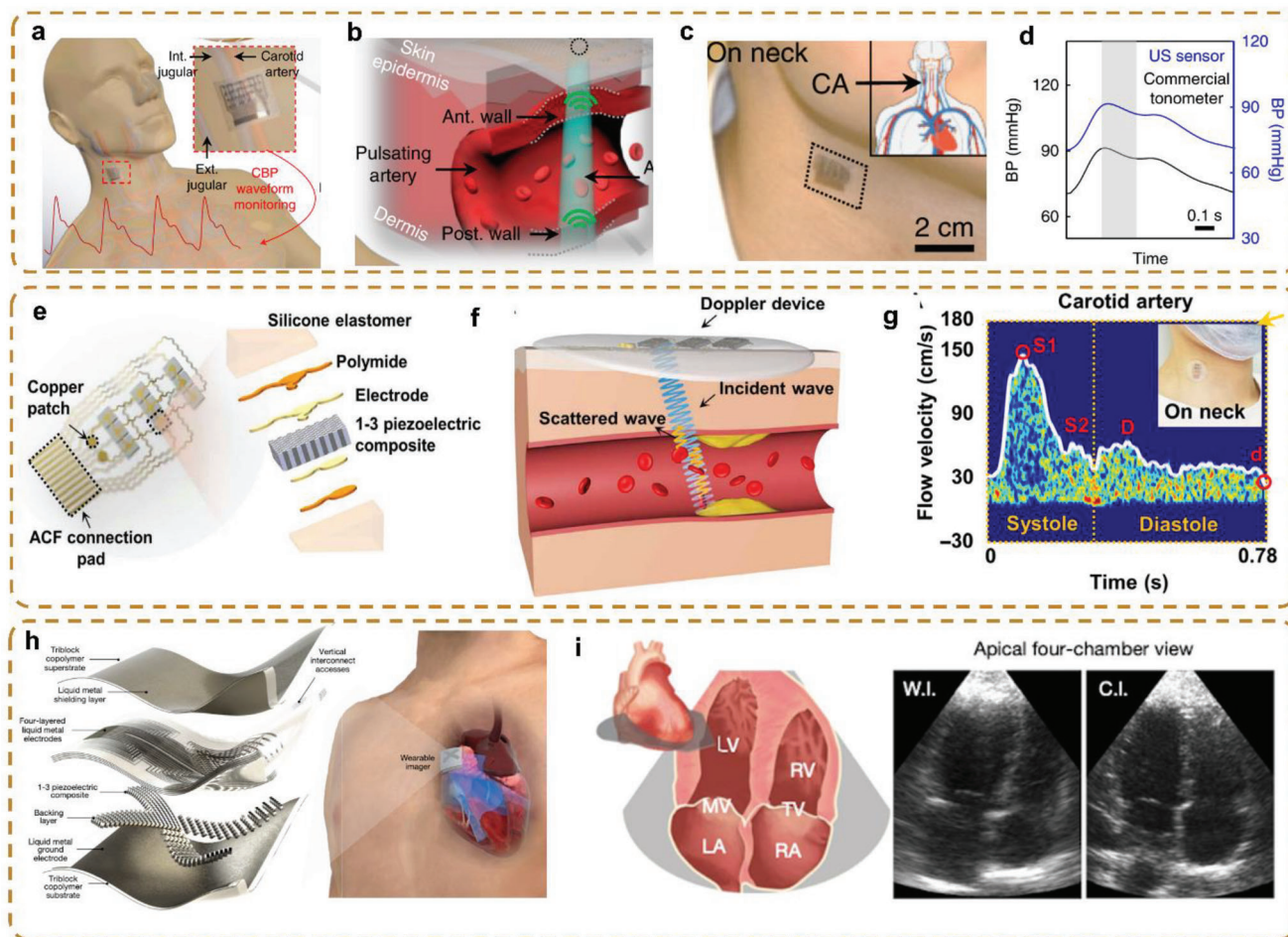


Figure 12. Long-term cardiac and haemodynamics monitoring. Monitoring of the central blood pressure waveform via a conformal ultrasonic device. a) Schematics of the stretchable ultrasonic device. When mounted on the human neck, the device enables monitoring of central blood pressure by capturing the pulsating vessel diameter of the carotid artery, internal jugular vein (int. jugular), and external jugular vein (ext. jugular) using the pulse-echo method, as illustrated in (b). c) BP measurements from the central to peripheral arteries and d) validation using a commercial tonometer. Reproduced with permission.^[34] Copyright 2018, Springer Nature Limited. Flexible Doppler ultrasound device for the monitoring of blood flow velocity. e) Schematics (left) and exploded view (right) of the device structure. f) Schematic of the Doppler ultrasonic device. The device continuously transmits ultrasound waves and receives echoes from a moving scatterer (such as red blood cells). g) Typical carotid blood flow spectra during a cardiac cycle (left) and several cycles (right). Feature points are marked in the left image. Insets: An image showing the device mounted on the neck. Reproduced under the terms of the Creative Commons License.^[35] Copyright 2021, The Authors, Published by American Association for the Advancement of Science. A wearable ultrasonic device for continuous, real-time and direct cardiac function assessment. h) Schematics showing the exploded view of the wearable imager, with key components labelled (left) and its working principle (right), i) Schematics and B-mode images of cardiac anatomies from the wearable and commercial imagers. The wearable imager was placed in the parasternal position for imaging in the parasternal long-axis and short-axis views and relocated at the apical position for imaging in the apical four-chamber and two-chamber views. Reproduced with permission.^[45] Copyright 2023, Springer Nature Limited.

accurate, wearable monitoring of cardiac performance in a variety of environments.

The Doppler ultrasound technique is usually utilized in the clinical setting to evaluate and estimate the blood flow, especially for transcranial examinations and fetal heart rate monitoring.^[227a,255] To overcome the challenge of inaccurate recordings due to compression by traditional ultrasound probes, Song et al. proposed a wearable wireless neckband ultrasound Doppler system that features a single-element ultrasound transducer on each side of the neckband for continuous acquisition of blood flow dynamics from carotid arteries.^[256] As a result, the developed wireless neckband Doppler system can potentially be

used as a monitoring tool for symptomatic or asymptomatic patients with cerebrovascular and/or cardiovascular diseases. However, the position of the ultrasound transducer needs to be manually adjusted before the common carotid arteries can be correctly located to perform measurements, which may present operational challenges that need to be overcome in point-of-care settings. Due to these reasons, a cUSE for precise monitoring the blood flow became a very interesting topic that has been intensively studied. Cannata et al. developed a flexible and implantable PVDF copolymer thin film device that can be wrapped around a blood vessel and accurately measure blood flow.^[257] The device is fabricated using diffraction-grating transducers, which produce

a beam at an angle to the surface, therefore creating a Doppler signal that would not be generated with a conventional transducer. The system feasibility was further demonstrated with an *in vivo* experiment on the rabbit infrarenal aorta, during which the flow sensor was able to continuously operate during the 5-hour experiment with the measured peak blood velocity within 1.7% of the measurement obtained using a duplex ultrasound system. For fetal heart rate (fHR) monitoring, the rigid probe often requires repositioning when there is a period of signal loss because of the inevitable change in the relative fetal heart location (fHL) caused by fetal movement or displacement of the transducer, which complicates the clinical workflow. To resolve this issue, Hammelmann et al. proposed a flexible transducer array composed of PZT discs embedded in PDMS that enables measuring the fHR independently of the fHL.^[215b] The system utilizes a method to improve ultrasound transducer positioning by estimating the fHL relative to the transducer, and the flexible substrate enables a more conformal contact between the device and maternal abdomen so that repositioning can be minimized. However, it is noted that the exact size and shape of the flexible array must be further optimized, and more transducer elements are needed to measure the fHR for all possible fHL within the uterus. In addition, the curvature of the array affects the received Doppler power substantially and would need to be accounted for improved power efficiency. For future work, additional modalities would need to be integrated into the current systems to avoid calibration or manual adjustment. Novel strategies to integrate other functions, such as signal processing and wireless communications, or flexible optoacoustic blood ‘stethoscope’^[258] in a lightweight and stretchable format would greatly enhance system functionality and wearability for the next generation of cardiovascular monitoring devices.

4.4. Tissue Properties Monitoring

The physical properties of muscle tissues, such as thickness, length, density, and stiffness, can provide valuable information for clinical diagnosis and evaluation. Continuous monitoring of these parameters during physical activity allows for applications such as monitoring of muscle strain and fatigue, diagnosis of neuromuscular disorders, and evaluation of efficiency and effectiveness of physical training and rehabilitation.^[259] A variety of techniques, such as electromyography, mechanomyography, electrocardiography, and magnetic resonance imaging, were employed to assess the physical properties of muscle tissues.^[260] However, these techniques suffer from drawbacks such as invasiveness, indirect measurement, or high cost. Compared to these techniques, conventional ultrasound imaging offers advantages such as non-invasiveness, high temporal resolution, and low cost. The operational mechanism of the assessment of tissue properties using ultrasound monitoring is to predicate upon the production, transmission, reflection, and identification of sound waves of high frequencies on the targeted tissue or material.^[261] The propagation of waves within a given medium is contingent upon the velocity, which is influenced by the material’s density and elasticity. Various tissues have distinct acoustic characteristics that influence the velocity of wave propagation. An illustration of this concept can be observed in the relationship between tissue

density and the velocity of sound waves, as well as the influence of tissue elasticity on its ability to undergo deformation when subjected to stress.^[262] Elastography employs ultrasound technology to evaluate the stiffness of tissues, a characteristic that can potentially serve as an indicator of pathological conditions.^[263]

Compared to conventional bulky probes, a flexible ultrasound device that provides conformal contact without affecting the muscle contraction dynamics is desired for obtaining more accurate measurements of muscle tissues. The currently compatible muscle tissue devices were based mainly on Type I, which used PVDF film as an active layer to transmit and get muscle signals at various body locations.^[113d,264] AlMohimeed et al. developed a wearable and flexible ultrasonic sensor based on PVDF polymer film that enables continuous monitoring of skeletal muscle contraction.^[194] The PVDF sheet was encapsulated by a polyimide layer along with silicone adhesive, with the overall system weighing less than a gram and being less than 200 μm thick. It was found that the generated ultrasound wave was able to penetrate at least 23 mm into the lower leg of a human subject, and the measured muscle tissue thickness variations were in accordance with the isometric muscle contraction performed, demonstrating the feasibility of using the flexible PVDF-based ultrasound sensor for accurate muscle tissue monitoring without restricting movements of the underlying tissue. They also used the device to estimate wrist motion to determine whether the relationship between wrist motion and muscle thickness may be a potential indicator of muscle-tendon health.^[195a] To further overcome the intrinsic drawback of the relatively weak transmitting acoustic signal strength of PVDF polymer films, AlMohimeed et al. proposed a double-layer PVDF sensor in hopes of improving the signal-to-noise ratio of the ultrasound signal reflected back from deep tissue.^[265] The two antiparallel-polarized PVDF layers were bonded using a low-viscosity epoxy and connected in parallel electrically and in series acoustically. Compared to a single-layer PVDF sensor of equivalent thickness, the developed double-layer wearable ultrasound sensor achieved 1.7 times greater signal amplitude and was capable of capturing contractions of the biceps muscles in the upper arm. In addition, cardiac tissue motion could be monitored with the device by performing M-mode measurements, whose results corresponded well with the cardiac cycles obtained from simultaneously acquired ECG signals. As a result, with further development of incorporating multiple sensors and validating with different muscle tissues, the double-layer PVDF ultrasonic sensor holds great promise in allowing long-term continuous monitoring of thicker and deeper tissue motion with higher signal strength and accuracy. AlMohimeed et al. further extended their work to not only monitor muscle tissue thickness changes but also extract functional parameters that are considered useful tools to assess the muscle contractile properties during contractions. One study continuously monitored the skeletal muscle contraction, which showed that the muscle did not relax at the electrical muscle stimulator frequency of 16 Hz under the experimental conditions employed, exhibiting tetanic contraction.^[195b] The device in another work was capable of recording isometric contractions of gastrocnemius (GC) muscles in the lower leg of a human subject and extracting parameters such as maximum thickness changes, contraction time, sustain time, half-relaxation time, and contraction velocity, which aid in the assessment of muscle contractile

properties.^[266] Very recently, Jiang's group proposed a stretchable array with 4×4 elements in the PDMS that exhibits high flexibility and wearability.^[267] The average values for the central frequency, -6 dB bandwidth, and electrical impedance in water for the elements were found to be 10.59 MHz, 37.69%, and 78.41 Ω , respectively. The efficacy of the suggested transducer in detecting muscle activity was shown through in vitro tests and first in vivo experiments. The visualization of muscle displacement was achieved through the utilization of muscle movement imaging.

4.5. Ultrasound Energy Harvesting and Wireless Power Supply

Energy harvesting is a process by which electrical energy is derived from ambient energy such as kinetic energy, thermal gradient, and incident light to power autonomous electronic circuits and systems.^[268] Among various energy sources, piezoelectric energy harvesting systems, which are based on vibrational motion and mechanical pressure, have become incredibly attractive candidates for self-powered electronics and standalone systems.^[269] Piezoelectric energy harvesting devices, which can obtain energy from human activities (wearable electronics for walking, running, jogging, talking, etc.), were intensively studied recently for biomedical applications because their theoretically infinite lifetime makes them a promising alternative to replacing batteries.^[14a,46b,54a,270] Compared to wearable electronics outside the body, the surgeries to periodically replace the batteries in implantable devices can often lead to prolonged hospitalization and increased health risks, such as high morbidity or mortality for patients.^[271] As a result, various miniature energy harvesting devices have been developed in hopes of providing a stable and longer-term energy source for implantable devices.^[272]

One of the major limitations of implantable devices is power management.^[273] For now, batteries have been mainly used to power implantable devices, which require additional surgery to charge or replace batteries. Hence, wireless power transfer or energy harvesting could be a strong power management method for implantable devices. Except for directly scavenging biomechanical energy from internal organ motions, energy delivery through ultrasound energy transfer is another promising technique to enable more reliable and miniaturized implantable energy harvesters, which has recently attracted much attention as an energy harvesting technology candidate for next generation bio-implantable systems.^[274] On the one hand, energy harvesting devices integrated in artificial retinas, pacemakers, cardioverter defibrillators, and neural stimulators harvest energy from internal organ movements to support the working system internally. On the other hand, energy can also be transmitted from external sources utilizing stable and adaptable power. Ultrasonic energy harvesters generally utilize piezoelectric transducers to convert mechanical vibrations induced by acoustic waves into electrical power, in order to achieve a desirable power level for in vivo applications.^[275] The piezoelectric ultrasonic energy harvester (PUEH) with wireless charging technology can energize implanted devices due to its advantages in safety, higher efficiencies at longer distances, and smaller device size. Compared to internal energy harvesters, external energy harvesters provide the benefits of adaptability and stability of power output with fewer

restrictions regarding location of implantation, organ shape, and patient body size.

Various structures were reported about the wireless power probe (transmitter from outside the body) and on-board bio-implantable devices (receiver from inside the body). **Figure 13** is a schematic of ultrasound energy harvesting and wireless power supply between transmitters outside the human body and implantable devices as receivers. The most widely used ultrasound power probes are commercially bulky probes with a rigid housing to impose a fixed/clamped condition about the circumference of the plate.^[278] Another type is the diaphragm, such as pMUT, which uses a circular piezoelectric disk fixed to the back side of a larger circular non-piezoelectric shim.^[278a] The on-board bio-implantable devices can be fabricated into various configurations according to the target organ/tissue, including single element (i.e., neural dust system^[224,279]), rigid array,^[277,280] and cUSE.^[36,276] In some work, additional biomedical devices were involved for sensing, actuation, and stimulation, which obtained power/energy from the PUEH.^[281]

Conventional PUEH exhibits two drawbacks that limit its use in self-powered implantable biomedical devices. First, conventional bulky and plate configurations exhibit high theoretical acoustic power output, but provide incongruent contact with corrugated and curved surfaces and thus cannot be applied to general complex surfaces such as organs. Second, the output power of piezoelectric ultrasound transducers fluctuates with transferred distance due to standing waves.^[276,277] Thus, as the applications expand, there is a need for the energy harvesters to be conformable to provide better contact to not be limited to applications associated with non-curved organs. In addition, innovative strategies need to be explored to minimize the effect of standing waves on any distance fluctuation during the energy transfer process so that PUEHs can be utilized to power next-generation biomedical microsystems where transfer through relatively thick barriers is necessary.^[276] In recent years, many flexible/comfortable PUEH for bio-implantable sensors have been reported for both electrical power transmitters (transducers outside the body) and receivers (implantable sensors), as shown in **Figure 14**. From the transmitter side, the second strategy was to use diaphragm architecture, which can achieve conformal contact with the non-planar surfaces of tissues and organs, generating more power than plate architecture and lowering sensitivity to changes in implantation depth and absorption power losses for sub-millimeter size devices.^[276,278a,284] In the future, the third strategy using a flexible/wearable power patch will be proposed to achieve an entire conformable ultrasound system (**Figure 14f–h**).^[36]

From the receiver side, the main strategy is to develop organic piezoelectric films or polymer substrates embedded with piezoelectric ceramic nanoparticles. Selvarajan et al. reported a biodegradable PUEH using 0–3 composites (BaTiO₃ nanoparticles in poly (L-lactic-co-glycolic) acid polymer matrix) to utilize both ultrasonic powering and energy harvesting schemes from low frequency acoustic waves.^[283] The output performance, biocompatibility, and tunable biodegradation of the proposed transducer demonstrate its potential as a biodegradable power source for transient implantable devices. However, those materials either possess inferior electromechanical coupling factors and permittivity, or these properties become compromised when the

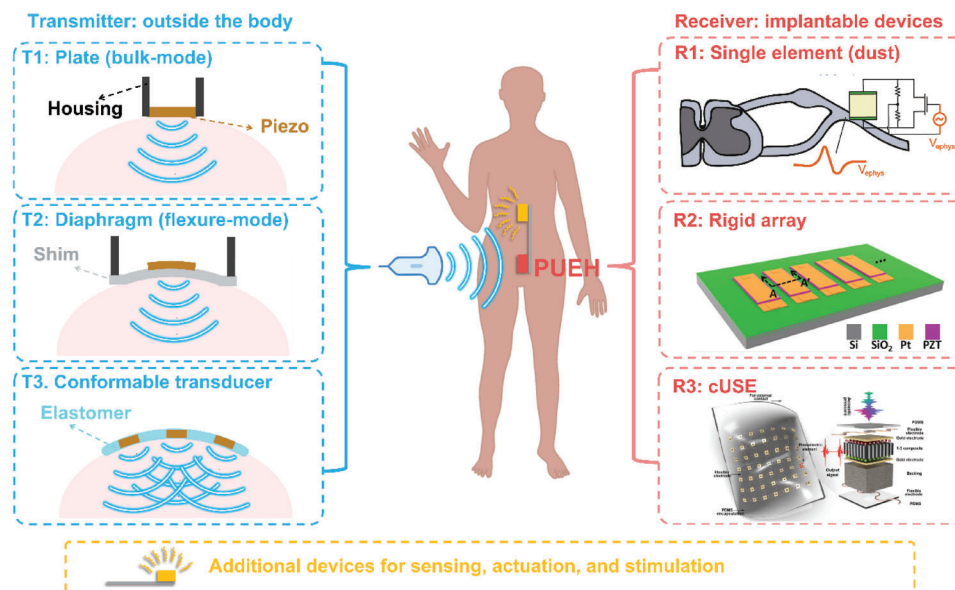


Figure 13. Schematic of ultrasound energy harvesting and wireless power supply between transmitters outside the human body and implantable devices as receivers. The structure of transmitters includes three types: the bulk-mode piezoelectric plate, the flexure-mode unimorph piezoelectric diaphragm, and the proposed conformable ultrasound transducers. The configuration of receivers includes three types. Receiver 1: the single element (i.e., neural dust), Reproduced with permission.^[224] Copyright 2016, Elsevier. Receiver 2: the rigid array (i.e., microfabricated array), Reproduced with permission.^[276] Copyright 2016, Springer Nature Limited. Receiver 3: stretchable transducer (Type III of cUSE).^[277] Copyright 2019, Elsevier, Reproduced with permission.

piezoelectric material is embedded in a polymer substrate. Thus, various efforts have been made for the third strategy, which was embedding miniaturized bulky piezoelectric material in a flexible substrate. Jiang et al. proposed and fabricated a flexible PUEH that provides seamless contact to complex surfaces by integrating an array of piezoelectric active elements of 1–3 composite with multilayered wavy, flexible electrodes in PDMS (Figure 14a–c).^[277] Through an ultrasound energy source, the system can produce continuous power output that can be stored in capacitors and used to light up commercial LEDs on planar surfaces while maintaining excellent output performance on curved surfaces. Furthermore, its excellent power transfer performance was demonstrated by low attenuation in *in vitro* tests of transmitting power through pork tissue of different thicknesses. Compared to the previously reported ultrasonic energy harvesters, the flexible 7 × 7 PUEH array delivered higher output performance and demonstrates great potential for applications in the next generation of wireless powering bioimplantable microdevices (Figure 14d–e). To overcome the performance bottleneck when a piezoelectric material is embedded in a polymer substrate and enhance conformability of the overall system, Jiang et al. also reported a millimeter-scale flexible ultrasound patch to power electrical stimulation of the neurons in retina as a means of restoring vision for people with neurodegenerative diseases (Figure 14i–k).^[282] The flexible patch can be well-attached on complex surfaces and is able to produce adjustable electrical output with a maximum output power of 45 mW cm⁻². Its application in retinal stimulation was verified in an *ex vivo* experiment with the device implanted into an excised porcine eyeball, producing current and current density above the average thresholds, thus demonstrating great potential in utilizing ultrasound-driven

wireless energy transfer for medical electrical stimulation and broader applications for charge bio-implantable devices.

For future work, there are several important approaches for investigation. First, the power transfer performance of PUEHs can fluctuate significantly when changing the distance between the transmitter and receiver. Because of the manual implantation surgical process and inherent differences in the patient's body, distance fluctuation between the external power source and implanted energy harvesting device is unavoidable and has a great impact on coupling efficiency and power delivery. As a result, the frequency at which the ultrasonic transducer operates needs to be adjusted to achieve maximum power transfer efficiency for any given distance, requiring the transducer bandwidth to be wide.^[276,278b] It is desirable to propose a device that has the ability to harvest energy even from small ultrasound intensities, adjust the acoustic energy transfer frequency within the transducer bandwidth, and be adopted as the power source for various implantable biomedical systems. Second, new understanding should be obtained from the combination of PUEH with other mechanical energy harvesting implantable devices. Third, Transient implantable medical devices utilizing biodegradable electronics can be used for diagnostic and therapeutic purposes for a predetermined period of time and then biodegrade (Figure 14o–q).^[283] Fourth, the selection of the ultrasound transmitter has a great impact on the results, and the integration of resonance frequency adjustment circuitry on the transmitter side will also enable higher system efficiency. Further development in novel piezoelectric materials with higher electromechanical coupling performance with miniaturized device dimensions while maintaining flexibility and clever design of electrical connection layers that result in higher compliance will also further improve

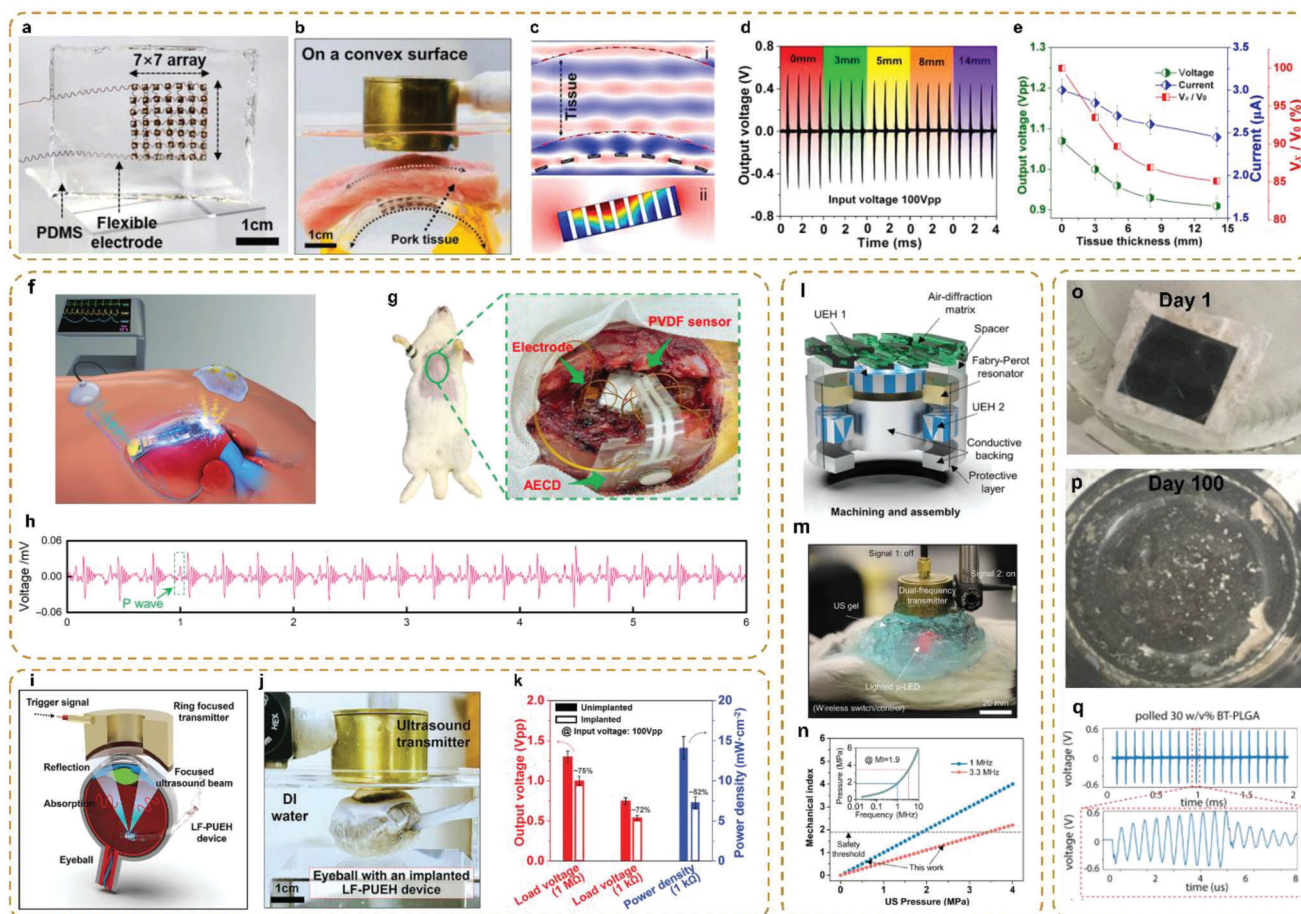


Figure 14. The schematic of the ultrasound-based energy harvesting and power transfer. Flexible piezoelectric ultrasonic energy harvester array for bio-implantable wireless generator: a-e) optical images of the flexible device with 7×7 array. Convex surface where pork tissue inserted between the transmitter and the PUEH device to mimic the implanted situation. Reproduced with permission.^[277] Copyright 2019 Elsevier Ltd. A flexible, stretchable system for simultaneous acoustic energy transfer and communication: f) Illustration showing the AECD function—wireless charging and communication based on ultrasound. g) Image of the device in the bent configuration. h) Image of the device in the twisted configuration. i–k) Ultrasound-induced wireless energy harvesting for potential retinal electrical stimulation application. Reproduced under the terms of the Creative Commons License.^[36] Copyright 2021, The Authors, Published by American Association for the Advancement of Science. Reproduced with permission.^[282] Copyright 2019, Wiley-VCH. l–n) Multichannel piezo-ultrasound implant with hybrid waterborne acoustic metastructure for selective wireless energy transfer at megahertz frequencies. Reproduced with permission.^[37] Copyright 2021, Wiley-VCH. o–q) Ultrasound powering of BT-PLGA transducer: degradation (0.1 M PBS, pH 7.4, and 37 °C) for 100 days, experimental setup for ultrasonic powering and the piezoelectric output voltages of polled 30 w/v% BT-PLGA transducers (the zoomed in view shows the pulse train). Reproduced with permission.^[283] Copyright 2020, IEEE.

the outlook of utilizing PUEHs as the energy source to power biomedical implantable systems.

4.6. Neural Stimulation and Activity Monitoring

Long term neural activity monitoring and neuromodulation have been promising tools for the treatment of various brain diseases such as depression, epilepsy, and Parkinson's disease.^[285] Electrical stimulation, optical stimulation, deep brain stimulation, and transcranial magnetic stimulation are some of the brain stimulation techniques that have been developed and used.^[286] However, these stimulation methods often suffer from drawbacks such as invasiveness, poor spatial resolution, or low penetration depth.^[210] A promising approach for wireless and non-invasive

neural stimulation is represented by the exploitation of piezoelectric based devices with various sources of mechanical stimulation, including vibration, acoustic sounds, and ultrasounds.^[287] In contrast, ultrasound waves can penetrate deep into solid structures such as bones and soft tissues with low transmission loss and have been demonstrated to safely and reversibly modulate the central nervous system, making it a promising method for neuromodulation.^[288] Ultrasonic neuromodulation, or ultrasonic neurostimulation, is a technique that utilizes focused ultrasound waves to target and activate specific areas of the nervous system in a non-invasive manner.^[289] Although definitive conclusions have yet to be reached, various hypotheses and explanations have been put forth in attempts to explain this phenomenon. i) Mechanical Effects: Ultrasound waves induce a mechanical force on biological tissues. The exertion of this force has

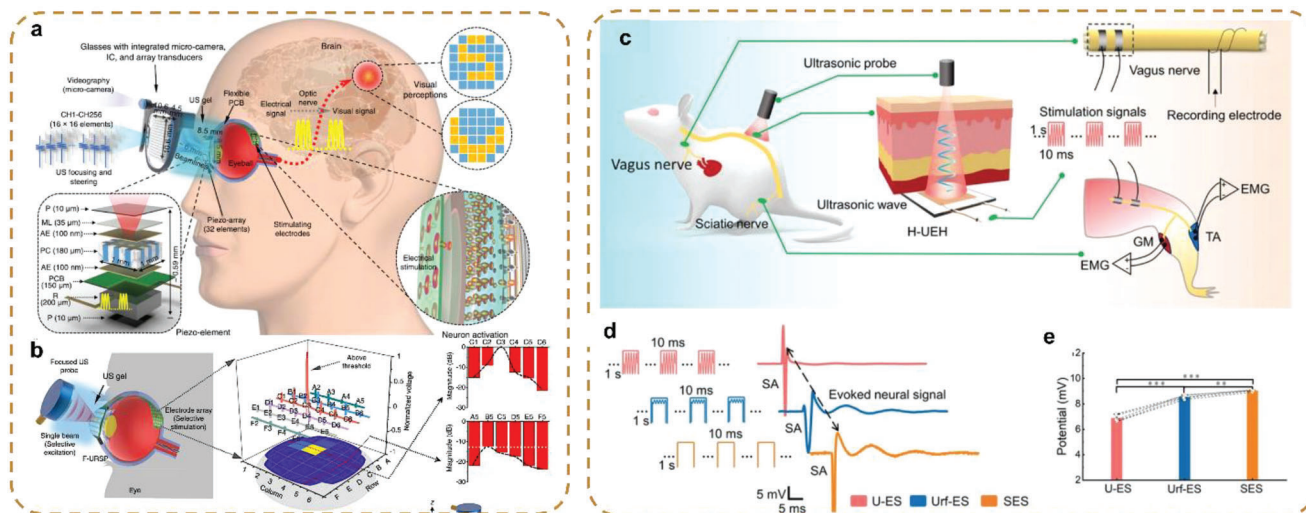


Figure 15. Conformable ultrasound device for nerve stimulation. a) Schematic diagram showing one working model of the F-URSP, in which a focused US probe was used for selective excitation of the piezo-array. b) Under the excitation of a single focused probe, the output voltage magnitude of each element in the array. c) Line profile data showing the signal-to-noise ratio of the output voltage magnitude for two typical positions—one on a row with excitation elements (horizontal line) and one off the excitation (vertical line)—showing unambiguous differences. Reproduced under the terms of the Creative Commons License.^[40] Copyright 2022, The Authors, Published by Springer Nature Limited. Hybrid-piezoelectret-based highly efficient ultrasonic energy harvester for implantable electronics: c) Schematic diagram showing the H-UEH driven by US for peripheral nerve stimulation on a rat model (vagus nerve, and sciatic nerve). d) Representative evoked CNAPs recorded on vagus stimulated by U-ES, Urf-ES, and D-ES. e) Average CNAPs of the vagus in response to different stimulations methods. Reproduced with permission.^[41] Copyright 2022, Wiley-VCH.

the potential to induce mechanical deformation or movement of neurons. ii) Thermal Effects: Ultrasound-Induced Heating refers to the changes or alterations that occur in a system as a result of variations in temperature. There is a potential for localized heating to induce changes in the temperature-sensitive characteristics of neurons, hence influencing their excitability. iii) Acoustic Cavitation: The application of ultrasound waves has the ability to initiate the creation of minuscule bubbles, known as cavitation, within biological tissues. The aforementioned bubbles have the ability to undergo oscillation, collapse, and thus release energy. iv) The phenomenon of electrostriction can result in the generation of electric fields within tissues due to the fast pressure changes caused by ultrasonic waves. The interaction between electric fields and the electrically excitable membranes of neurons has the potential to influence their activity.^[290]

However, the spatial resolution of ultrasound stimulation in small animals for in vivo experiments is still limited by the large size of a bulky transducer element and the fact that only a single element is employed.^[289b,291] To overcome these challenges, novel fabrication methods have been employed to enable a more compact design that allows the integration of the transducer elements into a flexible substrate to attach to the curved surface. Lee et al. proposed a flexible PZT based pMUT array for studying brain stimulation by ultrasound.^[210] It was verified that the PZT layer maintained its high piezoelectric property after the thinning process, and the sound pressure generated by the overall system (44 mW cm^{-2} at 80 V and 4 mm distance) is sufficient for low-intensity ultrasound brain stimulation. In addition, the flexible pMUT array has a radius of curvature less than 5 mm and can withstand compressive and tensile stretching, demonstrating the capability of the device to wrap around a mouse skull. As a result, this novel, flexible pMUT array shows great promise

for applications in ultrasound brain stimulation. Furthermore, Lee et al. developed an in vitro, although not flexible, MEMS ultrasound neurostimulation system that performs accurate localized ultrasonic neuromodulation at the cellular level.^[286c,292] The system integrates a PDMS-based cell culture chamber with PZT pMUT arrays consisting of sub-mm membranes to study the mechanisms of ultrasonic neuromodulation. It was found that the number of responding neuronal cells is proportional to the acoustic intensity of the applied ultrasound, and only the cells surrounding the working transducer would respond to the ultrasound stimulation, demonstrating the capability of the pMUT array to generate sufficient power for neurostimulation and perform localized modulation of neural circuits with high spatial resolution. Despite not being flexible or conformable, this system serves as a powerful tool to investigate the effect and underlying mechanisms of ultrasound stimulation on neurons and brain circuits. Jiang et al. reported a flexible ultrasound-induced retinal stimulating piezo-array that may provide a different wireless artificial retinal prosthesis method for triggering visual perceptions in blind people (Figure 15a,b).^[40] A flexible printed circuit board houses a two-dimensional piezo array with 32 stimulating electrodes for pixels. Programmable ultrasound beamlines can be used to dynamically apply spatially reconfigurable electronic patterns to piezo elements that can be independently and ultrasonically actuated.

Furthermore, ultrasonic neuromodulation is usually combined with other ultrasound technologies, such as wireless power transfer and imaging guided.^[293] Piech et al. developed a wireless, wearable ultrasound system that features an implantable sensor mote and an external ultrasound interrogation device that supports real-time backscatter processing for neuromodulation experiments in animal models.^[294] The implantable sensor module

consists of an array of diced PZT elements on a flexible PCB substrate and communicates with the external interrogator module with a generic digital encoding scheme customarily developed for transmitting neural information. To mimic an *in vivo* environment, ultrasound coupling gel was used as a tissue phantom because its acoustic impedance is like that of target biological tissues. The system's performance was then validated by modulating the backscatter sensor mote, extracting the backscatter modulation in real-time and transmitting that data to a remote client over Bluetooth. However, further validation involving signals more representative of neural activity and *in-vivo* experiments with animal models are needed for further demonstration of applicability in real-time neural activity monitoring. Wang et al. proposed a hybrid, highly effective, simply constructed, and biocompatible ultrasonic energy harvester that can function both as a neuroprosthetic for peripheral nerve stimulation and as a power source for implantable bioelectronics without being constrained by the implant scenario (Figure 15c–e).^[41] Pashaei et al. reported the design and validation of flexible and body-conformal patches for closed-loop image-guided acoustic neuromodulation, along with a comprehensive system design and machine learning algorithm.^[63c] One flexible linear array (64 elements, 5 MHz) was fabricated for nerve localization, and the other array (8 elements, 1.3 MHz) integrated on the wearable probe was used for low intensity focused ultrasound neuromodulation. A sensitivity of 80 kPa V⁻¹ with 3 MHz bandwidth for the modulation and 20 kPa V⁻¹ with 6 MHz bandwidth for the imaging array were obtained from the flexible prototype. For future attempts, the ultrasound transducers for neural activity monitoring and stimulation can follow the strategies discussed in Section 4.5. Both wearable and implantable devices can be fabricated in a conformable configuration to make these ultrasound systems more biocompatible and reliable.

4.7. Wound Healing and Tissue Repair

Chronic non-healing wounds can result in physical pain and inflammation, and they have emerged as one of the most significant healthcare problems.^[295] The majority of wound care methods used today, such as applying bandages or gauze to the wound sites, are passive treatments that infrequently encourage the growth of endogenous cells. Compared to electrical stimulation (ES) treatment and vibration treatment,^[296] ultrasound treatment is one of the wireless energy harvesting methods that delivers energy in the form of mechanical waves to the wound bed. It involves the use of high-frequency sound waves to stimulate tissue repair and regeneration. There are two primary types of ultrasound therapy used for wound healing: low-intensity pulsed ultrasound (LIPUS) and high-intensity focused ultrasound (HIFU). LIU has been shown to stimulate various cellular processes involved in wound healing. It may enhance the production of growth factors, increase collagen deposition, and improve angiogenesis (the formation of new blood vessels), all of which are crucial for wound repair.^[297] HIFU generates heat when focused on a specific area. This localized heating generated by the ultrasound power can stimulate tissue repair and regeneration by increasing blood flow, promoting tissue relaxation, and accelerating various biochemical reactions that aid in

wound healing.^[298] As a result, ultrasound therapy has enormous promise for wound healing. Furthermore, because recent reports indicate that the electrical output of a transducer can be well programmed with adjustable pulse characteristics, the *in situ* piezoelectric stimulation generated by ultrasound irradiation can be accomplished in a more controllable manner.^[41,299]

Recently, most studies on the ultrasound treatment have mainly focused on the implantation part (receivers), including nanowires/nanofibers, thin films,^[299] fluorinated ethylene propylene,^[41] P(VDF-TrFE) based composites,^[300] 3D scaffolds,^[301] and TENG.^[38] A biodegradable high-performance 3D piezoelectric scaffold with US-driven wireless ES capability, and demonstrated its successful application for the repair of spinal cord injuries in a rat model (Figure 16a–d). Meng et al. reported that a bioadhesive triboelectric nanogenerator (BA-TENG) is a first-aid solution for rapid and robust wound closure and ultrasound-driven accelerated wound healing (Figure 16e–g).^[38] This biocompatible BA-TENG has a flexible TENG top layer and a bioadhesive bottom layer, providing excellent electricity supply and robust sutureless sealing on wet tissues. The BA-TENG generated 1.50 V and 24.20 μ A using ultrasound underwater and closed flaws quickly (5 s) with high interfacial toughness (150 J/m²) in the *ex vivo* porcine colon organ models and hemostasis in the rat bleeding liver incision model, lowering blood loss by 82%. The BA-TENG seals skin injuries instantaneously and generates a strong electric field (E-field) of 0.86 kV·m⁻¹ stimulated by ultrasound to speed skin wound healing in rats. E-field-accelerated cell migration and proliferation explain these effects *in vitro*. TENG adhesives can also be used for wound treatment, nerve stimulation and regeneration, and implanted device battery charging.

However, most of the previous work still used conventional ultrasound transducers as the power source. Due to restrictions in use and unpredictable treatment outcomes caused by conventional ultrasonic probes' inability to adhere to the wound surface, they are not frequently employed. There is limited research on creating a flexible ultrasonic patch for efficiently healing chronic wounds. Very recently, Feng's group proposed a patch that was made of discretized, linearly ordered pieces of piezoelectric ceramic in a flexible circuit substrate (Figure 16h–k).^[39] In order to prevent wound infection and ensure that ultrasound may penetrate, a thin hydrogel patch is employed as both an encapsulating and coupling layer. The ultrasonic patch can perfectly fit the treatment region because it is gentle and lightweight. The target treatment area is controlled when the patch is bent because the sound beams are concentrated in the center of the bending circle. Some type II diabetic rats are used in ultrasound therapy research. According to immunohistochemical (IHC) findings, ultrasonics promote Rac1 activation in both the dermal and epidermal layers, which speeds up wound healing. According to treatment outcomes, ultrasound-treated wounds heal more quickly than non-treated wounds. There is a 40% reduction in the healing time.

4.8. Transdermal Drug Delivery

Ultrasound is a novel and interesting theranostic modality that may be employed with great spatial precision to detect drug

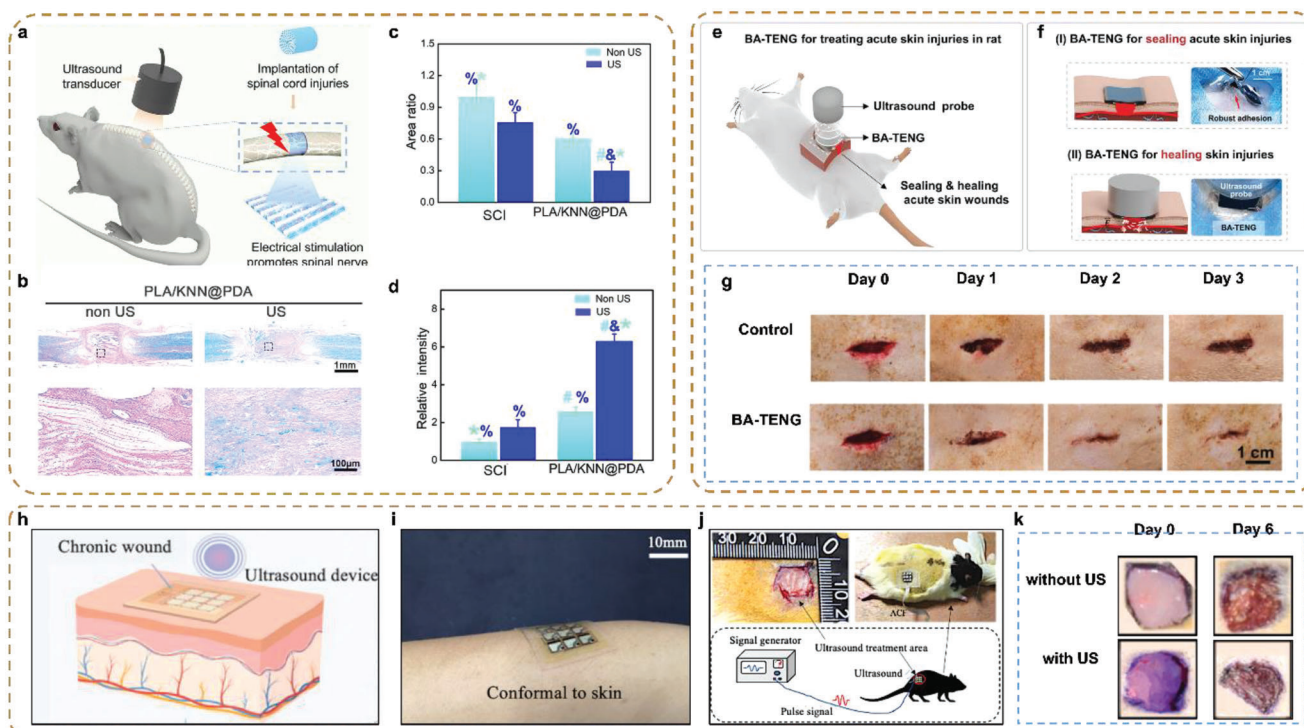


Figure 16. cUSE for Wound management and tissue repair. Ultrasound-powered wireless ES based on a biodegradable high-performance 3D piezoelectric scaffold promotes neural regeneration in spinal cord injuries: a) LFB staining of myelin sheaths on the longitudinal sections of the spinal cords collected at week 8. b) The lesion site area, and the cavity area were quantified according to the HE staining. c-d) Quantitative analysis of the LFB staining with data normalized against the SCI control group. Reproduced with permission.^[301] Copyright 2022, American Chemical Society. An ultrasound-driven bioadhesive triboelectric nanogenerator for instant wound sealing and electrically accelerated healing in emergencies: e) Schematic of the BA-TENG in sealing and ultrasound-driven electrically healing rat skin injuries. f) I) The BA-TENG can adhere to rat skin injury tightly for immediate wound sealing. Scale bar (1 cm). II) Ultrasound to generate the BA-TENG to produce electricity for wound healing. g) Comparison of 3-day wound healing images in the untreated (control), suture, bioadhesive PAV only, and BA-TENG treated groups. Reproduced with permission.^[38] Copyright 2021, Wiley-VCH. Flexible ultrasonic patch for accelerating chronic wound healing: h) Schematic of ultrasound accelerates wound healing by activating Rac1. i) The flexible ultrasonic patch can completely conform to the skin. j) Schematic diagram of wound treatment with the flexible ultrasonic patch. k) The photographs of the healing state, displaying the wounded surfaces for the four experimental groups treated with a functional ultrasonic patch for 6 days. Reproduced with permission.^[39] Copyright 2021, Wiley-VCH.

carriers, trigger drug release, and increase drug deposition.^[302] Sonophoresis involves low-frequency sonophoresis (LFS) (20–100 kHz), intermediate frequency sonophoresis (IFS) (100 kHz to 1 MHz), or high-frequency sonophoresis (HFS) (over 1 MHz).^[303] Based on sonophoresis, an idea for a wearable electronic patch for transdermal drug delivery must overcome a number of challenges: i) seamless conformal adhesion is essential because the propagation effectiveness is significantly decreased by the air between the ultrasonic emission probe and the skin, ii) it is critical to cover a large skin area and still have sufficient power or intensity for drug delivery, iii) independent operation can guarantee long-term use because the process of drug delivery usually takes tens of minutes.^[304] As we discussed in Section 3, it is very difficult for the handheld probe to meet these requirements. To solve this issue, some groups tried their best to overcome the technical challenges of the function of sonophoresis on large-area and complex surfaces of human faces.

Li et al. proposed a stretchable electronic facial mask (SEFM) for sonophoresis, enabling the promotion of the delivery effect of a drug mask (Figure 17a–d).^[43] This work invented the design of a single-side structure for piezoelectric components to

achieve low bending stiffness and high bendability to conform to the human face, and organic–inorganic composite structure to enhance the ductility and robustness of the bridge interconnections. This study shows that the SEFM has great facial healthcare potential. The SEFM can increase skin moisture content on human faces by 20%, which indirectly validates the effect of accelerating the transport of HA once more. The thorough results of this investigation demonstrate the enormous potential for use of the developed SEFM in facial healthcare applications. Very recently, our group first demonstrated a conformable ultrasound patch (cUSP) using intermediate-frequency sonophoresis (IFS) for effective and operator-independent transdermal delivery of cosmeceuticals outside of a clinical setting.^[44] The device is made up of a 2×2 array of piezoceramic (PZT-5H) disc transducers placed in a soft elastomer (PDMS) (Figure 17e), which can create 1 mm-deep and 0.8 cm^2 -area cavitation pockets and can serve as a drug reservoir for prolonged cavitation (Figure 17f). With a 10-minute ultrasound application, the cUSP exhibited a 26.2-fold enhancement in niacinamide transport in a porcine model in vitro (Figure 17g), demonstrating the device's suitability for short-exposure, targeted

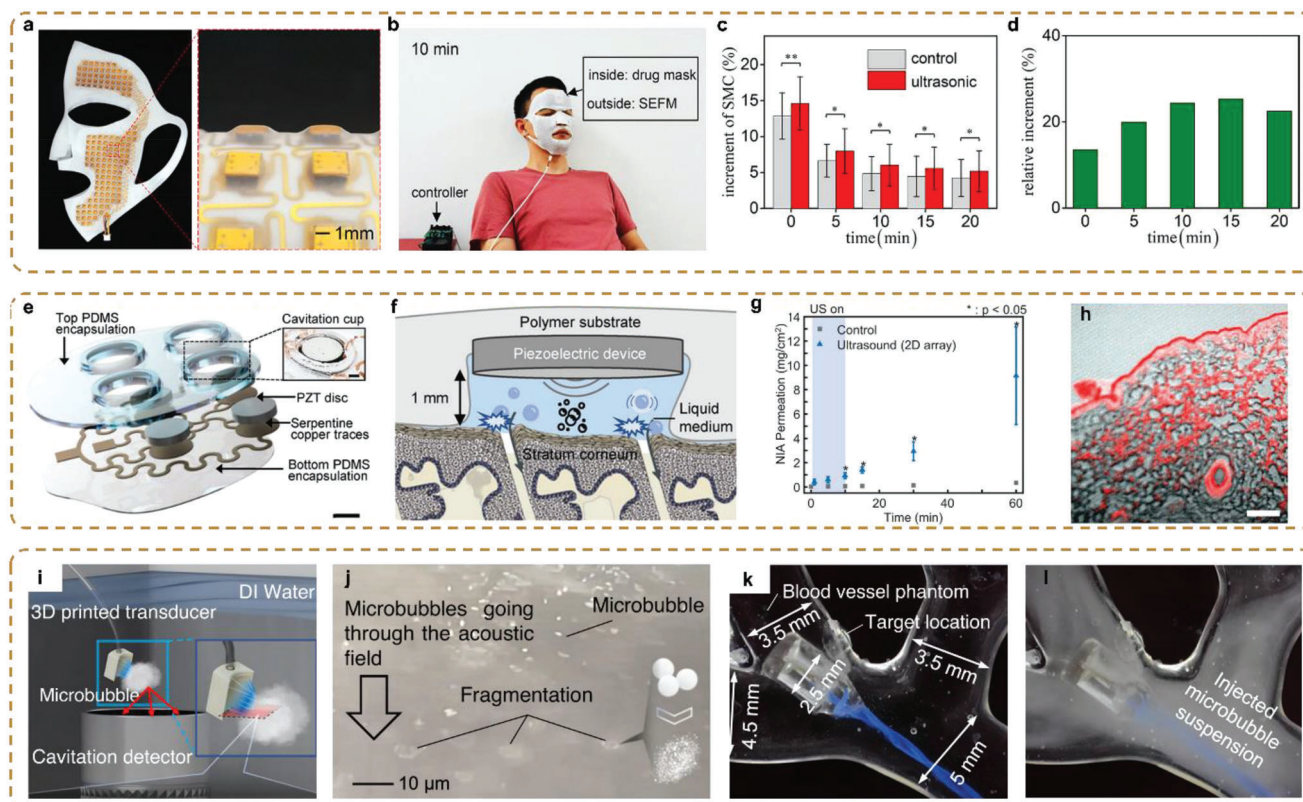


Figure 17. cUSE for drug delivery. Stretchable electronic facial masks for sonophoresis. a) A stretchable electronic facial mask for sonophoresis and island-bridge mesh circuit for the facial mask. b) A user wearing the mask on top of a drug mask for transdermal drug delivery. c) A statistical comparison between control and the ultrasonic group for time-dependent skin moisture content (SMC). d) Relative increment of the mean value of the skin moisture content between the ultrasonic group and the control group. Reproduced with permission.^[43] Copyright 2022, American Chemical Society. A conformable ultrasound patch (cUSP) for cavitation-enhanced transdermal cosmeceutical delivery. e) Exploded view of the cUSP array. f) Schematic illustration of the cUSP on skin. g) Amount of NIA permeated with application of ultrasound versus control for the cUSP array. h) Multiphoton confocal microscopy images showing RhB penetration into a vertical section of a porcine skin sample for 10 min ultrasound treatment. Reproduced with permission.^[44] Copyright 2023, Wiley-VCH. 3D Printing and processing of miniaturized transducers for localized cavitation: i) Schematic of the experiment on capturing the cavitation signal in a microbubble suspension. j) Zoom-in view of microbubble fragmentation. k, l) Ultrasound-induced microbubble fragmentation via our 3D printed miniaturized ultrasound transducer in a 3D printed blood vessel phantom. Reproduced under the terms of the Creative Commons License.^[152] Copyright 2023, The Authors. published by Springer Nature Limited.

sonophoresis for patients and consumers suffering from skin conditions and premature skin aging. In addition, this work exhibited the full range of modeling and experiment-based bimodal characterization approaches, fabrication processes, and in vitro testing results of a ground-breaking prototype of a wearable IFS patch.

In addition to the stretchable ultrasonic patch, numerous novel types of transducers have also been proposed very recently, such as fiber based transducer,^[305] electret,^[306] and 3D printed transducer.^[152] Miniaturized ultrasound transducers with microscale focusing features have been printed by Zheng's group.^[152] These transducers are capable of generating high and localized acoustic pressure in blood vessels with diameters as small as 2.5 mm. This makes it possible to trigger localized cavitation, improve drug delivery, and ultrasonically modulate cellular activity (Figure 17j–l). The blood vessel phantom received a 5 mg/ml microbubble suspension. The transducer was pulsed to generate acoustic pressure. Microbubble fragmentation and acoustic radiation generated a translucent patch in the focal area.

4.9. Ultrasound Therapy

Ultrasound has advanced not just as a diagnostic imaging technique but also as a therapeutic technique that deposits energy in tissue to produce a variety of biological effects.^[307] Ultrasound technology has been extensively applied in the medical field as a therapeutic tool for applications such as biomodulation, orthopedics, treatment of muscle spasms and joint contractures, and acceleration of rehabilitation after bone injury.^[308] The acoustic energy is delivered locally to enhance cellular metabolism, modulate tissue properties, or apply mechanical stimulus.^[307a,308a] The ultrasound wave has a longer wavelength and attenuates to a lesser degree compared to similar therapies that use electromagnetic waves, such as light therapy, which allows it to penetrate deeper into the body for more effective treatment.^[307a,309] Ultrasound devices used for therapeutic purposes are classified into two categories: high-intensity focused ultrasound (HIFU) and low-intensity pulsed ultrasound (LIPU).^[310] HIFU has been used for kidney stone lithotripsy with ultrasonic diagnostic technology and noninvasive tumor therapy, while LIPU has been used

for stimulating chondrocyte proliferation and healing of bone injuries and soft tissue. However, both HIFU and LIPU systems available commercially still suffer from a lack of flexibility and portability, making them unsuitable and inconvenient for long-term treatment and daily usage. It is highly desirable to design and implement low-power, small-size, and completely wearable systems.

To solve these problems, the recently developed therapeutic ultrasound devices are portable and wearable, but not comfortable. The sustained acoustic medicine (SAM) devices can be self-administered and feature ultrasonic patches applied directly over and proximal to the soft tissue injury location. They have been used to treat conditions such as trapezius muscle spasm, shoulder pain from rotator cuff tendinopathy, knee osteoarthritis, and tendon pain in the elbow, knee, or ankle with great success.^[309] The design and validation of a unique wearable conformal ultrasonic array with built-in imaging and modulation capabilities are innovated.^[187] For imaging, a unique 64-element linear PZT array with a 5 MHz resonance frequency was employed. The wearable probe also features an eight-element linear array with bigger PZT elements for effective power transfer, allowing for image-guided brain modulation. The resulting pressure field was estimated at various depths using full-wave models. This study's focus is on vagus nerve modulation utilizing low-intensity focused ultrasound, hence, the appropriate focal depth (10–20 mm) was taken into account for both imaging and modulation array designs. Liu et al. reported a flexible pMUT array with a sandwich structure that exhibits excellent flexibility (maximum tensile stretch of 25%) and acoustic performance for potential adjuvant treatment of bone injury.^[311] The sound pressure level decreased less than 2% when a fatty pork tissue of 3 cm thickness was placed in between the flexible pMUT and hydrophone, indicating good ultrasound penetration that ensures energy transmission to the skeletal tissue. Thus, with its excellent flexibility and acoustic performance through tissue, the flexible pMUT holds great potential for applications in the adjuvant treatment of bone injuries. Very recently, Tian et al. proposed a two-step flexible ultrasound strategy to enhance tumor radiotherapy using a metal-phenolic network nanoplatform and stimulation by the LIPU.^[312] The results indicate that LIPU is a safe approach for successfully modulating hypoxia levels. The two-step method based on PP18-Pt NPs can successfully limit breast cancer tumor development while also activating the body's antitumor immune response. Future advancements in downsizing and fabrication techniques might make it possible for components to be integrated into a single package and fit better to the skin's surface. Incorporating personalized therapy profiles with various frequencies and intensities depending on individual treatment responses might also enhance the system and hasten healing and recovery.

4.10. Hybrid Electronics for Multiple Signals Decoding

Ultrasound technology has been integrated with flexible electronics and other advanced technologies to create innovative medical devices and applications.^[26c] With the development of cUSE, many hybrid options, coupled with other skin-compliant and flexible electronics, have been proposed.

cUSE with Triboelectric Nanogenerators: Recently, it was shown that transcutaneously implanted triboelectric nanogenerators (TENG) could efficiently harvest energy from the ultrasonic transducers placed on the skin (Figure 13), from stimulation to therapy.^[313] Triboelectric generators can generate electrical voltage and current by charge transfer at the interface of different materials.^[314] We could harvest electrical energies from various mechanical movements such as vibration, sliding, and friction. Hinchet et al. used a thin membrane of perfluoroalkoxy, as shown in Figure 18a,b, which vibrates under the acoustic pressure generated from ultrasonic transducers.^[315] The researchers showed a triboelectric generator could generate electrical voltage and current even when implanted under the porcine skin (Figure 18c,d). Such results opened up the possibility of wireless power transfer using ultrasonic transducers and triboelectric nanogenerators. Furthermore, Chen et al. reported micromachined triboelectric nanogenerators that could wirelessly receive energy from an ultrasonic transducer 30 mm away from the triboelectric nanogenerator (Figure 18e–g).^[280] Additionally, they showed the potential application of this technology in signal communication. The electrical signal generation period from the triboelectric nanogenerator is proportional to the operation time of the ultrasonic transducer. These results strongly indicate that ultrasonic transducers can also be applied to wireless energy and signal transmission for implantable devices.

cUSE with Photoacoustic Imaging: The combination of ultrasound and photoacoustic imaging has led to a powerful hybrid imaging technique that strengthens imaging and provides detailed structural and functional information about tissues and organs.^[316] The hybrid device allows for a more comprehensive view of tissue properties and offers enhanced contrast for certain features. This enables multimodal imaging, which can help clinicians make more accurate diagnoses and guide interventions.^[317] Recently, several flexible arrays with photoacoustic functions were proposed, including an A-line photoacoustic signal from the flexible transducer array,^[318] a flexible array transducer for photoacoustic-guided interventions,^[319] a PVDF-based transparent flexible transducer for a photoacoustic imaging system,^[320] and a flexible array transducer for photoacoustic-guided surgery.^[321] For example, Jiang et al. proposed a hybrid-induced energy transfer strategy using photoacoustic and piezo-ultrasound technology in a 3D twining wireless implant for stable powering and high-resolution signal communication.^[219a] The research by Sheng's group demonstrated the use of a photoacoustic patch to perform 3D mapping of hemoglobin within tissues located at significant depths, in contrast to this implantable one. The photoacoustic patch presented in this study incorporates an assemblage of ultrasonic transducers and vertical-cavity surface-emitting laser (VCSEL) diodes on a flexible substrate that conforms to the skin. The device has the capability to acquire 3D images of hemoglobin with a notable spatial resolution. Additionally, it enables the precise and prompt mapping of core temperatures in three dimensions, exhibiting excellent accuracy.^[254] In brief, the integration of ultrasound and photoacoustic imaging has significantly broadened the scope of medical imaging techniques. This technology provides a versatile instrument that may be utilized in both clinical and scientific settings, offering vital insights into the structure and function of many tissues and organs.

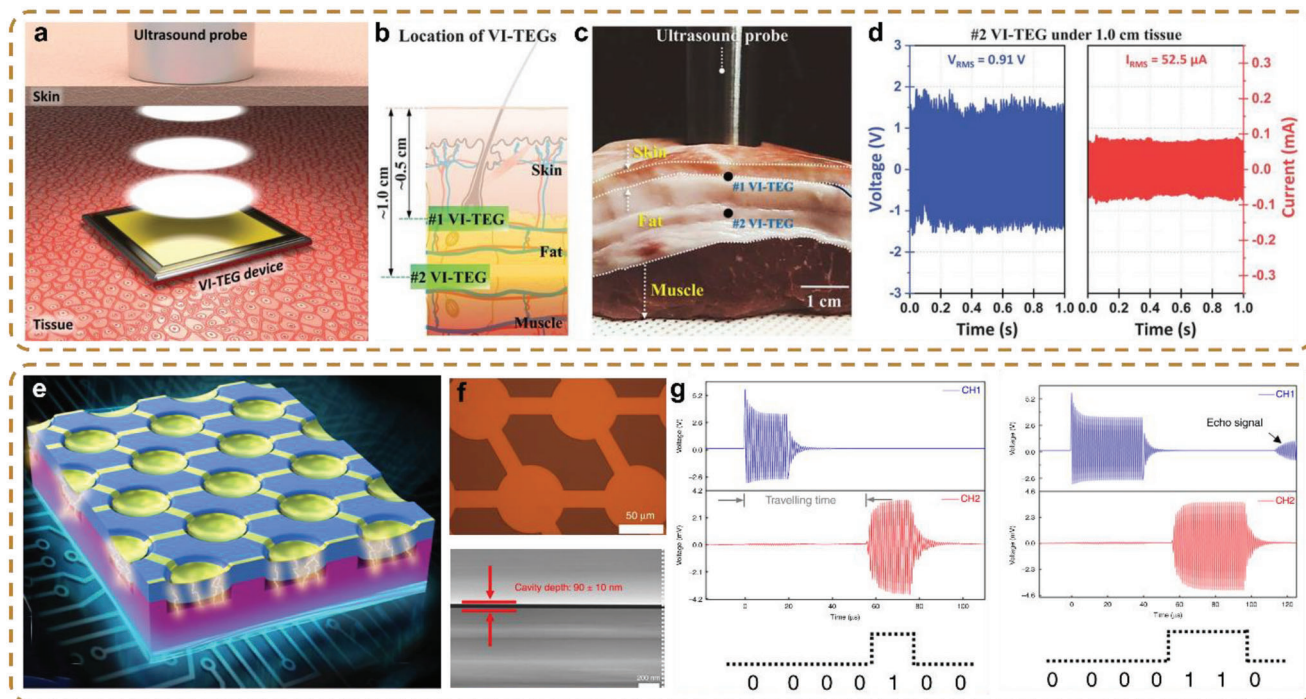


Figure 18. Wireless power and signals transmission using ultrasound transducer and triboelectric nanogenerator. a) Schematic description of wireless power transmission from ultrasound transducer on the skin to implanted triboelectric nanogenerator. b) Schematic shows the location of the implanted VI-TEG. c) Experimental setup of wireless power transfer through porcine skin. d) Electrical voltage (left panel) and current (right panel) output from triboelectric nanogenerator under the ultrasonic wave. Reproduced under the terms of the Creative Commons License.^[315] Copyright 2019, The Authors, Published by the American Association for the Advancement of Science. Micro triboelectric ultrasonic device for acoustic energy transfer and signal communication. e) Representative diagram of the micro triboelectric ultrasonic device (μ TUD). f) Optical microscopy (top) and scanning electron microscopy (bottom) image of micromachined triboelectric nanogenerator. g) Experimental results of wireless signal transmission from ultrasonic transducer (top panel) to triboelectric nanogenerator (bottom panel). Reproduced under the terms of the Creative Commons License.^[280] Copyright 2020, The Authors, Published by Springer Nature.

All-in-One cUSE: There has been an increased focus on all-in-one devices or multiplexed sensor systems. These systems encompass a combination of physical sensors, physical–chemical sensors, and chemical sensors. Their purpose is to assess a wide range of signals and several biomarkers simultaneously.^[322] Recently, ultrasound technology has been involved in these multiplexed sensor systems due to its unique functionality.^[323] Wang’s research team developed a novel skin-worn device that enables the simultaneous monitoring of blood pressure and heart rate using ultrasonic transducers, as well as the measurement of numerous biomarkers through the use of electrochemical sensors.^[324] The device recorded physiological responses related to food consumption and physical activity, specifically focusing on the formation of glucose following digestion, the utilization of glucose through glycolysis, and the compensatory increases in blood pressure and heart rate to counteract oxygen deprivation and lactate production.^[325] In addition, a soft robotic perception system with remote object positioning and multimodal cognition capability is developed by integrating an ultrasonic sensor with flexible triboelectric sensors,^[326] and a flexible optoacoustic blood ‘stethoscope’ for noninvasive, multiparametric, and continuous cardiovascular monitoring.^[258] In conclusion, the utilization of an ultrasound all-in-one patch represents a novel avenue of research. The incorporation of several sensors for the purpose of decoding biosignals would greatly enhance its applicability in var-

ious domains, such as monitoring the health of pregnant women and their fetuses, monitoring the health and wellness of elderly individuals, and facilitating digital monitoring of the entire body in challenging environments.

5. Concluding Remarks and Future Perspectives

In the past six years, cUSE has been intensively studied and has become a popular research topic, ushering in a period of prosperity for the ultrasound research field and opening a new door for conformable electronics. In this review, we presented a comprehensive understanding of piezoelectrics, critical parameters of ultrasound transducers, distinct types of cUSE, advanced technologies towards cUSE, and various applications in healthcare. First, we evaluated the various piezoelectric materials for ultrasound transducers, emphasized the essential parameters for selecting piezoelectrics, and introduced novel materials. Second, we illustrated five distinct categories of cUSE and discussed advanced design and technologies for cUSE, such as soft substrates, stretchable electrodes, device-skin interfaces, and integrated systems. In addition, we reviewed the recent advancements in the development of cUSE and the representative research conducted on the various applications, including soft tissue imaging, long-term monitoring, bio-signal decoding, energy harvesting, power transferring, drug delivery, wound healing, and therapy.

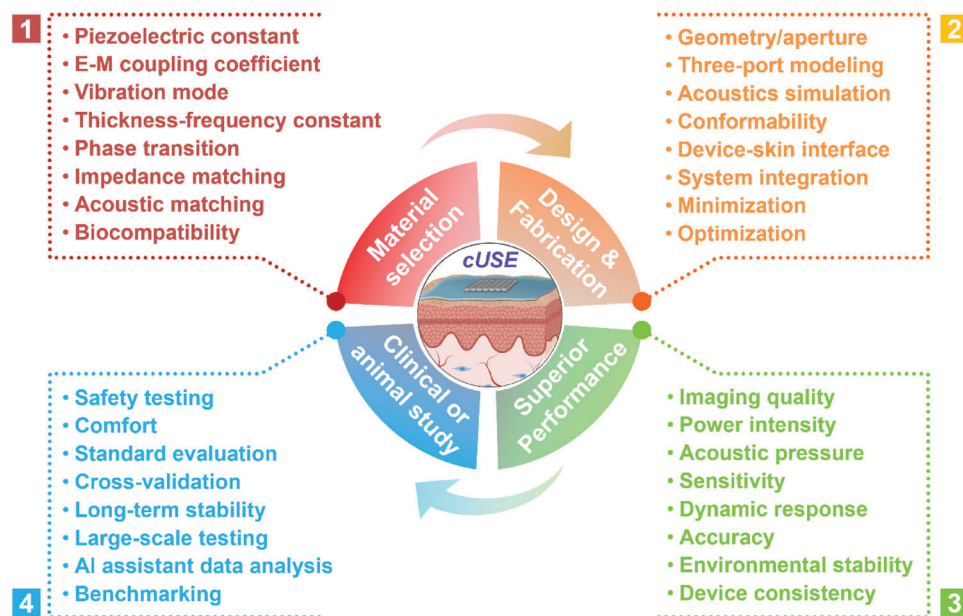


Figure 19. The research flow of the investigation on cUSE.

5.1. Summary and Research Flow

In this section, we would like to first give a summary and recommendation for the investigation into cUSE, particularly for the researchers who are just beginning to focus on this field. The inherent complexity and diversity of ubiquitous ultrasound bioelectronics stem from their interdisciplinary nature. The development of such devices requires intensive and in-depth collaboration among researchers and practitioners from all relevant fields, including materials, chemistry, physics, mechanics, algorithms, software, electrical engineering, signal processing, and clinical medicine, among others.

A comprehensive cUSE is expected to meet four criteria, which can be summed up in a single sentence: i) conformable electronics with ii) an integrated data acquisition system, exhibiting iii) superior ultrasound performance for iv) personalized healthcare. The general research flow is illustrated in Figure 19, which is also implemented for other piezoelectric electronics or conformable electronics. The application determines the entire research endeavor, including the choice of materials and the creation of the devices. High-resolution imaging applications, power transmission applications, stimulation applications, and therapy applications all have unique requirements for device dimensions, form factors, and acoustic performance (such as depth, bandwidth, acoustic pressure, quality factor, etc.). The device design also needs to be aware of mechanical, biotechnical, and biomedical details of the target tissue or organs (Figure 20), ranging from deep organs (such as the bladder and heart) to shallow epidermal (such as the skin, fingerprint, and eye), from large surfaces (such as the breast and knee) to tiny regions (such as the eye, blood vessel, and neuro). The correct components can be chosen with ease if researchers have a thorough understanding of the piezoelectrics' features and characteristics. Bulky crystals and ceramics perform better for applications requiring high power or low frequency than composites and polymers. Composites typ-

ically exhibit better k_t and low Z for high-resolution imaging in order to improve acoustic matching and increase bandwidth. The configuration of the device can select from the five types of cUSE discussed in Section 3.2 and make modifications in accordance with their own needs. The various simulation techniques can be a powerful aid in predicting outcomes and designing devices. Stability, consistency, and acoustic performance are all influenced by the fabrication processes. During the back-and-forth phase of fabrication-characterization, researchers might be having trouble fine-tuning the design parameters and fabrication methods. The efficiency during the fabrication-characterization phase will be improved by the performance evaluation of in vitro phantoms. For animal studies and human clinical studies, besides the performance of the cUSE, researchers also need to have an in-depth understanding and a detailed study plan on the following aspects, such as safety issues, cross-validation, long-term stability, evaluations, and so on.

5.2. Challenges

For the future research suggestion, as depicted in Figure 19, the aim is to propose novel mechanically conformable electronics with fully integrated systems to exhibit superior ultrasound performance for precise diagnosis and therapy in healthcare. Several challenges need to be addressed to propose the next generation of cUSE.

The Best Piezoelectrics vs The Suitable Ones: The choice of piezoelectric material plays a vital role in the performance of ultrasound transducers.^[23b] Most conformable ultrasound devices use commercial lead zirconate titanate (PZT).^[27,33–35,63] The traditional PZT ceramic usually shows low piezoelectric properties, especially k_t (<0.55), and d_{33} (<600), which have strong influence on the acoustic performance of the transducer, including bandwidth, insert loss, sensitivity, etc. Piezoelectric polymers

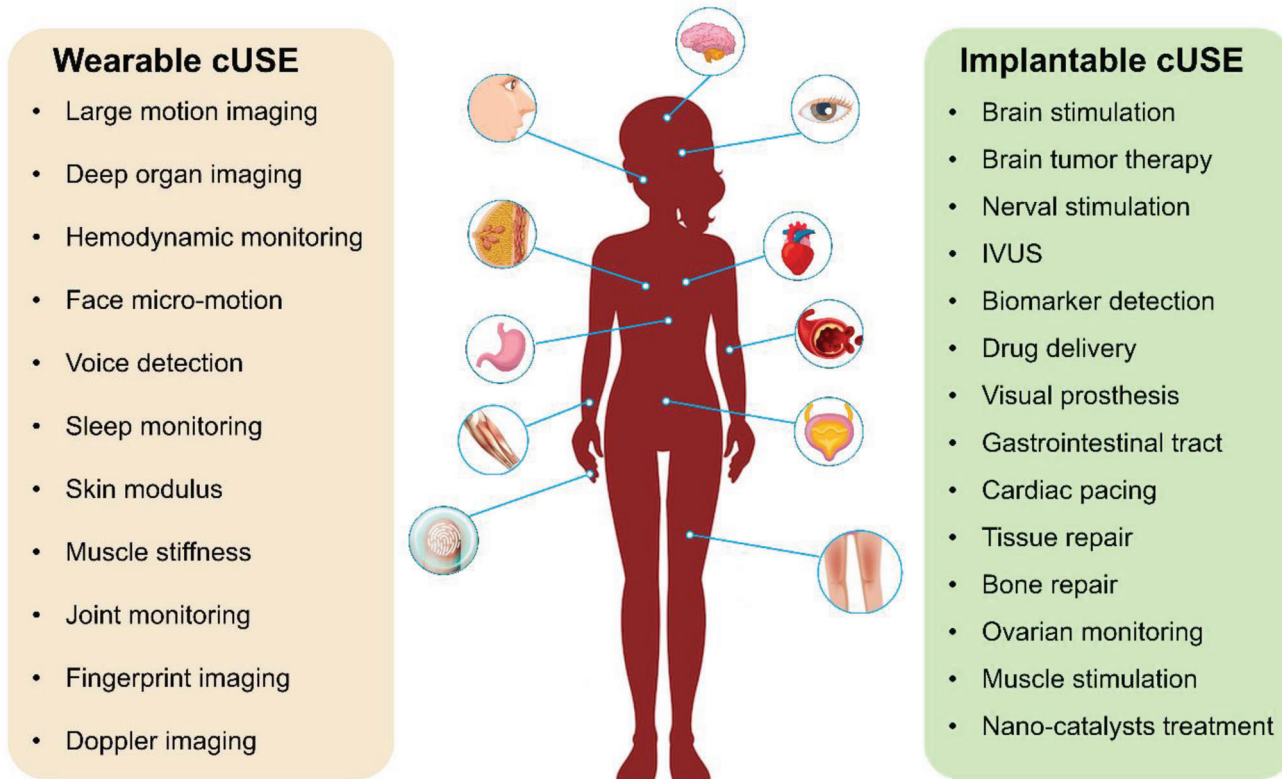


Figure 20. Wearable and implantable cUSE for various applications on different tissue/organs. Some images of organs were designed by Freepik.com.

often have low acoustic impedance and great inherent flexibility, making them ideal for constructing wide bandwidth cUSE without the use of additional matching layers. Their low electromechanical coupling coefficient and relative dielectric permittivity, on the other hand, would limit their use in flexible array ultrasound transducers. Due to their ease of production, rigid piezoelectric films such as PZT and ZnO films are frequently placed on flexible substrates to serve as active materials for single cUSE. Nonetheless, the rigid piezoelectric films' electromechanical coupling and piezoelectric characteristics are lower than those of bulk rigid piezoelectric materials, limiting the sensitivity of the cUSE. However, to avoid losing flexibility and increasing process complexity, cUSE based on stiff piezoelectric films has been designed without backing layers and matching layers, which may narrow the bandwidth and decrease the transducers' quality factor. Furthermore, some piezoelectric crystals exhibit ultrahigh piezoelectric performance, but they still have some limitations, such as being very brittle, having a high acoustic impedance, and having thermal instability. Piezocomposites can modify the properties of rigid piezoelectric materials and piezoelectric polymers that can be employed as active materials in cUSE. However, there are issues with piezocomposites, such as restricted flexibility, insufficient polarization, and expensive production procedures. Therefore, the selection of piezoelectrics is to choose the suitable one, not the best one, according to the device design and application requirements. In recent years, some novel piezoelectrics have been synthesized and produced owing to novel preparation technologies and amazing methods. These piezoelectrics

not only have exceptional piezoelectric capabilities, but also show promise as candidates for ultrasound transducers; some of these have been fabricated for the cUSE. The hot research covers four main directions based on varied manufacturing and design purposes: transparent crystals, flexible composites,^[128b,133] Additive manufacturing for unique 3D structures,^[147,152,153b] biodegradable polymers,^[157,305] and some predicted materials.^[327] The new generation of lead-free, high-performance piezoelectrics that also meet flexibility, lightweight, and environmental criteria is highly desirable.

Dynamic Conformability vs Precise Localization: Examples of soft ultrasonic devices that have already been studied in the literature frequently use targets with predetermined forms and curvatures, which make it possible to correctly calculate the relative placement of each piece on the surface. This enables accurate beamforming and makes it possible to readily determine the direction of the ultrasonic pulse.^[27] However, these artificially controlled conditions are insufficient models for applications on the human skin. The human skin surface is dynamic, which causes the skin curvature to undergo continuous and unpredictable changes, making accurate determination of each element's location on the skin difficult relying solely on existing methods.^[328] The capacity to conduct independent imaging without the need for manual scanning or turning the imaging equipment across different angles is one of the most important goals of proposing wearable and conformable ultrasound technologies. On the other hand, most previous systems captured a relatively small sensing area, imaging only the region directly beneath the instrument, re-

stricting application because large sections of soft tissues and organs could not be studied in full. Although a stretchable phased array is offered in one example to electronically regulate beam focusing and steering, preserving stretchability comes at the cost of a large pitch (greater than half wavelength), thereby restricting imaging to low frequencies (typ. < 2 MHz), poor spatial resolutions due to both low frequencies and low numbers of elements, and the narrow imaging angles characteristic to linear arrays. The narrow imaging angle is especially exacerbated for stretchable arrays that attempt to operate at higher frequencies. In future work, researchers should balance stretchability and exact localization, as both are crucial to imaging quality and precise diagnosis and therapy.

Simplify the Fabrication Processes vs Scalable Manufacturing: cUSE are primarily based on traditional ultrasound transducer manufacturing and combined with other novel technologies, including micromachining manufacturing, additive manufacturing, all of which require complicated fabrication processes for the piezoelectric active layer, electrode connections, soft substrates, and circuit integration.^[26d] With more fabrication technologies involved, there is a higher risk of instability in mechanical robustness and performance reliability after long periods of deformation. In addition, in future work, fabrication procedures should be simplified in order to improve the stability and repeatability of flexible ultrasound transducers during real time processing.

5.3. Outlook

Standard Evaluation: Although there have been hundreds of relevant studies on cUSE, it is still not easy to compare different reported works (i.e., resolution using different element numbers and working frequencies, power transfer capability, or imaging resolution by various algorithms) due to various working mechanisms, design methods, testing conditions, and application scenarios. Sometimes commercial probes can be used for cross-validation, but it is still unfair to compare the performance of cSUE with a well-established system with no identical device structure. Therefore, assessing the potential commercialization of cUSE technologies is an urgent priority for both consumers and companies.

System-Level Miniaturization and Integration: The majority of cUSE is still in the proof-of-concept phase and is coupled to complex supporting components. Designing a wearable ultrasound patch involves integrating complex ultrasound components into a compact and lightweight form factor. Ensuring that all necessary components, such as transducers and electronics, fit into a small, conformable patch without compromising image quality can be a challenge. In addition, the integrated system should not restrict human activity, so the device should be small enough to impart only a minimal mechanical load to the skin, or it should be soft enough to conform to the skin surface. Creating a user-friendly interface that allows medical professionals to control and interpret the device's output is important. The patch should be designed with ease of use in mind to facilitate its integration into medical workflows.

Cloud Computing and Big Data: Recently, machine learning has led to revolutionary breakthroughs in various image processing tasks and big data analysis for flexible electronics^[329] and

cUSE.^[45,247,330] Because cUSE can gather tons of ultrasound images and data when combined with machine learning and other algorithms in a very short time, cloud computing and big data is highly desirable. Based on this, enormous amounts of data would be analyzed and computed on cloud platforms, which might yield more precise information. Furthermore, smooth communication, precise analysis, and fast feedback are critical for remote smart medical care that would be greatly assisted in the future with high-efficient data analysis in the cloud. This is profoundly important for enhancing the convenience and quality of our daily lives.

Finally, we hope that this review will act as an overview of recent advancements in conformable ultrasound electronics and a guide for many fields to better design piezoelectrics and transducers for novel biomedical engineering applications. We believe this comprehensive review will inspire individuals to dedicate themselves to this field, propose novel conformable devices, enrich the toolbox for clinical researchers, and achieve the ultimate goal of noninvasive, continuous, wireless, precise, reliable, personalized, target-specific, and predictive monitoring of physiological signals and deep tissues for advanced and intelligent healthcare.

Acknowledgements

This work was supported by the National Science Foundation CAREER: Conformable Piezoelectrics for Soft Tissue Imaging (Grant No. 2044688), 3M Non-Tenured Faculty Award, and MIT Media Lab Consortium funding. W.D. was supported by the National Science Foundation Graduate Research Fellowship Program under Grant No. 2141064. Any opinions, findings, and conclusions or recommendations expressed in this material are those of the author(s) and do not necessarily reflect the views of the National Science Foundation.

Conflict of Interest

The authors declare no conflict of interest.

Keywords

biomedical applications, conformable electronics, piezoelectric materials, ultrasound transducers

Received: July 31, 2023
Revised: September 19, 2023
Published online:

- [1] H. Wu, W. Gao, Z. Yin, *Adv. Healthcare Mater.* **2017**, *6*, 1700017.
- [2] X. Wang, Z. Liu, T. Zhang, *Small* **2017**, *13*, 1602790.
- [3] a) F. Tasnim, A. Sadraei, B. Datta, M. Khan, K. Y. Choi, A. Sahasrabudhe, T. A. Vega Gálvez, I. Wicaksono, O. Rosello, C. Nunez-Lopez, C. Dagdeviren, *Phytopharmacology* **2018**, *20*, 589; b) S. V. Fernandez, D. Sadat, F. Tasnim, D. Acosta, L. Schwendeman, S. Shahsavari, C. Dagdeviren, *foresight* **2022**, *24*, 75.
- [4] C. Dagdeviren, F. Javid, P. Joe, T. von Erlach, T. Bensenl, Z. Wei, S. Saxton, C. Cleveland, L. Booth, S. McDonnell, J. Collins, A. Hayward, R. Langer, G. Traverso, *Nat. Biomed. Eng.* **2017**, *1*, 807.

- [5] T. Sun, F. Tasnim, R. T. McIntosh, N. Amiri, D. Solav, M. T. Anbarani, D. Sadat, L. Zhang, Y. Gu, M. A. Karami, C. Dagdeviren, *Nat. Biomed. Eng.* **2020**, *4*, 954.
- [6] I. Wicaksono, C. I. Tucker, T. Sun, C. A. Guerrero, C. Liu, W. M. Woo, E. J. Pence, C. Dagdeviren, *npj Flexible Electron.* **2020**, *4*, 5.
- [7] W. Zhang, L. You, X. Meng, B. Wang, D. Lin, *Micromachines* **2021**, *12*, 1308.
- [8] C. Zhang, M. O. G. Nayeem, Z. Wang, X. Pu, C. Dagdeviren, Z. L. Wang, X. Zhang, R. Liu, *Prog. Mater. Sci.* **2023**, *138*, 101156.
- [9] Z. Huang, Y. Hao, Y. Li, H. Hu, C. Wang, A. Nomoto, T. Pan, Y. Gu, Y. Chen, T. Zhang, W. Li, Y. Lei, N. Kim, C. Wang, L. Zhang, J. W. Ward, A. Maralani, X. Li, M. F. Durstock, A. Pisano, Y. Lin, S. Xu, *Nat. Electron.* **2018**, *1*, 473.
- [10] C. M. Boutry, L. Beker, Y. Kaizawa, C. Vassos, H. Tran, A. C. Hinckley, R. Pfattner, S. Niu, J. Li, J. Claverie, Z. Wang, J. Chang, P. M. Fox, Z. Bao, *Nat. Biomed. Eng.* **2019**, *3*, 47.
- [11] G. Schwartz, B. C. K. Tee, J. Mei, A. L. Appleton, D. H. Kim, H. Wang, Z. Bao, *Nat. Commun.* **2013**, *4*, 1859.
- [12] J. Kim, M. Lee, H. J. Shim, R. Ghaffari, H. R. Cho, D. Son, Y. H. Jung, M. Soh, C. Choi, S. Jung, K. Chu, D. Jeon, S.-T. Lee, J. H. Kim, S. H. Choi, T. Hyeon, D.-H. Kim, *Nat. Commun.* **2014**, *5*, 5747.
- [13] S. Hong, Y. Gu, J. K. Seo, J. Wang, P. Liu, Y. S. Meng, S. Xu, R. Chen, *Sci. Adv.* **2019**, *5*, eaaw0536.
- [14] a) C. Dagdeviren, P. Joe, O. L. Tuzman, K.-I. Park, K. J. Lee, Y. Shi, Y. Huang, J. A. Rogers, *Extreme Mech Lett.* **2016**, *9*, 269; b) C. Dagdeviren, Z. Li, Z. L. Wang, *Annu. Rev. Biomed. Eng.* **2017**, *19*, 85.
- [15] C. Dagdeviren, Y. Shi, P. Joe, R. Ghaffari, G. Balooch, K. Usgaonkar, O. Gur, P. L. Tran, J. R. Crosby, M. Meyer, Y. Su, R. Chad Webb, A. S. Tedesco, M. J. Slepian, Y. Huang, J. A. Rogers, *Nat. Mater.* **2015**, *14*, 728.
- [16] a) L. Persano, C. Dagdeviren, Y. Su, Y. Zhang, S. Girardo, D. Pisignano, Y. Huang, J. A. Rogers, *Nat. Commun.* **2013**, *4*, 1633; b) C. Dagdeviren, Y. Su, P. Joe, R. Yona, Y. Liu, Y.-S. Kim, Y. Huang, A. R. Damadoran, J. Xia, L. W. Martin, Y. Huang, J. A. Rogers, *Nat. Commun.* **2014**, *5*, 4496.
- [17] J. R. Windmiller, J. Wang, *Electroanalysis* **2013**, *25*, 29.
- [18] X. Huang, Y. Liu, H. Cheng, W.-J. Shin, J. A. Fan, Z. Liu, C.-J. Lu, G.-W. Kong, K. Chen, D. Patnaik, S.-H. Lee, S. Hage-Ali, Y. Huang, J. A. Rogers, *Adv. Funct. Mater.* **2014**, *24*, 3846.
- [19] a) H. J. Chung, M. S. Sulkin, J. S. Kim, C. Goudeseune, H. Y. Chao, J. W. Song, S. Y. Yang, Y. Y. Hsu, R. Ghaffari, I. R. Efimov, J. A. Rogers, *Adv. Healthcare Mater.* **2014**, *3*, 59; b) M. T. Ghoneim, A. Nguyen, N. Dereje, J. Huang, G. C. Moore, P. J. Murzynowski, C. Dagdeviren, *Chem. Rev.* **2019**, *119*, 5248.
- [20] W. Gao, S. Emaminejad, H. Y. Y. Nyein, S. Challa, K. Chen, A. Peck, H. M. Fahad, H. Ota, H. Shiraki, D. Kiriya, D.-H. Lien, G. A. Brooks, R. W. Davis, A. Javey, *Nature* **2016**, *529*, 509.
- [21] G. S. Jeong, D.-H. Baek, H. C. Jung, J. H. Song, J. H. Moon, S. W. Hong, I. Y. Kim, S.-H. Lee, *Nat. Commun.* **2012**, *3*, 977.
- [22] A. Barone, in *Akustik II /Acoustics II* (Eds.: R. W. Leonard, A. Barone, R. Truell, C. Elbaum, B. E. Noltingk), Springer Berlin Heidelberg, Berlin, Heidelberg **1962**, pp. 74–152.
- [23] a) Q. Zhou, S. Lau, D. Wu, K. Kirk Shung, *Prog. Mater. Sci.* **2011**, *56*, 139; b) Q. Zhou, K. H. Lam, H. Zheng, W. Qiu, K. K. Shung, *Prog. Mater. Sci.* **2014**, *66*, 87.
- [24] C. M. W. Daft, in *2010 IEEE International Ultrasonics Symposium*, **2010**, pp. 798–808.
- [25] R. S. Singh, M. O. Culjat, S. P. Vampola, K. Williams, Z. D. Taylor, H. Lee, W. S. Grundfest, E. R. Brown, in *2007 IEEE Ultrasonics Symposium Proceedings*, **2007**, pp. 1824–1827.
- [26] a) M. Lin, H. Hu, S. Zhou, S. Xu, *Nat. Rev. Mater.* **2022**, *7*, 850; b) J. Li, Y. Ma, T. Zhang, K. K. Shung, B. Zhu, *BME Front.* **2022**, *2022*, 9764501; c) L. Jiang, J. Wu, *Prog. Mater. Sci.* **2023**, *136*, 101110; d) D. Ren, Y. Yin, C. Li, R. Chen, J. Shi, *Micromachines* **2023**, *14*, 126; e) L. Jiang, Y. Yang, Y. Chen, Q. Zhou, *Nano Energy* **2020**, *77*, 105131.
- [27] H. Hu, X. Zhu, C. Wang, L. Zhang, X. Li, S. Lee, Z. Huang, R. Chen, Z. Chen, C. Wang, Y. Gu, Y. Chen, Y. Lei, T. Zhang, N. Kim, Y. Guo, Y. Teng, W. Zhou, Y. Li, A. Nomoto, S. Sternini, Q. Zhou, M. Pharr, F. L. di Scalea, S. Xu, *Sci. Adv.* **2018**, *4*, eaar3979.
- [28] X. Sun, A. J. Croxford, B. W. Drinkwater, *Structural Health Monitoring* **2023**, *22*, 3451.
- [29] C. Wang, X. Chen, L. Wang, M. Makihata, H.-C. Liu, T. Zhou, X. Zhao, *Science* **2022**, *377*, 517.
- [30] M. Lin, Z. Zhang, X. Gao, Y. Bian, R. S. Wu, G. Park, Z. Lou, Z. Zhang, X. Xu, X. Chen, A. Kang, X. Yang, W. Yue, L. Yin, C. Wang, B. Qi, S. Zhou, H. Hu, H. Huang, M. Li, Y. Gu, J. Mu, A. Yang, A. Yaghi, Y. Chen, Y. Lei, C. Lu, R. Wang, J. Wang, S. Xiang, et al., *Nat. Biotechnol.* **2023**.
- [31] W. Du, L. Zhang, E. Suh, D. Lin, C. Marcus, L. Ozkan, A. Ahuja, S. Fernandez, I. I. Shuvo, D. Sadat, W. Liu, F. Li, A. P. Chandrakasan, T. Ozmen, C. Dagdeviren, *Sci. Adv.* **2023**, *9*, eadh5325.
- [32] L. Zhang, C. Marcus, D. Lin, D. Mejjorado, S. S. Jr, T. Pierce, V. Kumar, S. Fernandez, D. Hunt, Q. Li, I. Shuvo, D. Sadat, W. Du, H. Edenbaum, L. Jin, W. Liu, Y. Eldar, F. Li, A. Chandrakasan, A. Samir, C. Dagdeviren, *Nat. Electron.* **2023**, <https://doi.org/10.1038/s41928-023-01068-x>.
- [33] C. Wang, B. Qi, M. Lin, Z. Zhang, M. Makihata, B. Liu, S. Zhou, Y.-h. Huang, H. Hu, Y. Gu, Y. Chen, Y. Lei, T. Lee, S. Chien, K.-I. Jang, E. B. Kistler, S. Xu, *Nat. Biomed. Eng.* **2021**, *5*, 749.
- [34] C. Wang, X. Li, H. Hu, L. Zhang, Z. Huang, M. Lin, Z. Zhang, Z. Yin, B. Huang, H. Gong, S. Bhaskaran, Y. Gu, M. Makihata, Y. Guo, Y. Lei, Y. Chen, C. Wang, Y. Li, T. Zhang, Z. Chen, A. P. Pisano, L. Zhang, Q. Zhou, S. Xu, *Nat. Biomed. Eng.* **2018**, *2*, 687.
- [35] F. Wang, P. Jin, Y. Feng, J. Fu, P. Wang, X. Liu, Y. Zhang, Y. Ma, Y. Yang, A. Yang, X. Feng, *Sci. Adv.* **2021**, *7*, eabi9283.
- [36] P. Jin, J. Fu, F. Wang, Y. Zhang, P. Wang, X. Liu, Y. Jiao, H. Li, Y. Chen, Y. Ma, X. Feng, *Sci. Adv.* **2021**, *7*, eabg2507.
- [37] L. Jiang, G. Lu, Y. Yang, Y. Xu, F. Qi, J. Li, B. Zhu, Y. Chen, *Adv. Mater.* **2021**, *33*, 2104251.
- [38] X. Meng, X. Xiao, S. Jeon, D. Kim, B.-J. Park, Y.-J. Kim, N. Rubab, S. Kim, S.-W. Kim, *Adv. Mater.* **2023**, *35*, 2209054.
- [39] W. Lyu, Y. Ma, S. Chen, H. Li, P. Wang, Y. Chen, X. Feng, *Adv. Healthcare Mater.* **2021**, *10*, 2100785.
- [40] L. Jiang, G. Lu, Y. Zeng, Y. Sun, H. Kang, J. Burford, C. Gong, M. S. Humayun, Y. Chen, Q. Zhou, *Nat. Commun.* **2022**, *13*, 3853.
- [41] X. Wan, P. Chen, Z. Xu, X. Mo, H. Jin, W. Yang, S. Wang, J. Duan, B. Hu, Z. Luo, L. Huang, J. Zhou, *Adv. Funct. Mater.* **2022**, *32*, 2200589.
- [42] T. Zhang, H. Liang, Z. Wang, C. Qiu, Y. B. Peng, X. Zhu, J. Li, X. Ge, J. Xu, X. Huang, J. Tong, J. Ou-Yang, X. Yang, F. Li, B. Zhu, *Sci. Adv.* **2022**, *8*, eabk0159.
- [43] S. Li, J. Xu, R. Li, Y. Wang, M. Zhang, J. Li, S. Yin, G. Liu, L. Zhang, B. Li, Q. Gu, Y. Su, *ACS Nano* **2022**, *16*, 5961.
- [44] C.-C. Yu, A. Shah, N. Amiri, C. Marcus, M. O. G. Nayeem, A. K. Bhayadia, A. Karami, C. Dagdeviren, *Adv. Mater.* **2023**, *35*, 2300066.
- [45] H. Hu, H. Huang, M. Li, X. Gao, L. Yin, R. Qi, R. S. Wu, X. Chen, Y. Ma, K. Shi, C. Li, T. M. Maus, B. Huang, C. Lu, M. Lin, S. Zhou, Z. Lou, Y. Gu, Y. Chen, Y. Lei, X. Wang, R. Wang, W. Yue, X. Yang, Y. Bian, J. Mu, G. Park, S. Xiang, S. Cai, P. W. Corey, et al., *Nature* **2023**, *613*, 667.
- [46] a) C. Wang, C. Wang, Z. Huang, S. Xu, *Adv. Mater.* **2018**, *30*, 1801368; b) S. V. Fernandez, F. Cai, S. Chen, E. Suh, J. Tjepelt, R. McIntosh, C. Marcus, D. Acosta, D. Mejjorado, C. Dagdeviren, *ACS Biomater. Sci. Eng.* **2023**, *9*, 2070; c) S. V. Fernandez, D. Sadat, F. Tasnim, D. Acosta, L. Schwendeman, S. Shahsavari, C. Dagdeviren, *Phytopharmacology* **2022**, *24*, 75.

- [47] a) X. Meng, Z. Zhang, D. Lin, W. Liu, S. Zhou, S. Ge, Y. Su, C. Peng, L. Zhang, *J. Adv. Ceram.* **2021**, *10*, 991; b) Y. Du, W. Du, D. Lin, M. Ai, S. Li, L. Zhang, *Micromachines* **2023**, *14*, 167.
- [48] Y. Zhuang, J. Li, Q. Hu, S. Han, W. Liu, C. Peng, Z. Li, L. Zhang, X. Wei, Z. Xu, *Compos. Sci. Technol.* **2020**, *200*, 108386.
- [49] M. T. Chorsi, E. J. Curry, H. T. Chorsi, R. Das, J. Baroody, P. K. Purohit, H. Ilies, T. D. Nguyen, *Adv. Mater.* **2019**, *31*, 1802084.
- [50] a) J. Briscoe, S. Dunn, *Nano Energy* **2015**, *14*, 15; b) F. Narita, M. Fox, *Adv. Eng. Mater.* **2018**, *20*, 1700743; c) Z. Yang, S. Zhou, J. Zu, D. Inman, *Joule* **2018**, *2*, 642.
- [51] L. Jiaqing, T. Guo, Y. Weiqing, D. Weili, *Recent Progress in Flexible Piezoelectric Devices Toward Human-Machine Interactions* **2022**, *2*, 22.
- [52] N. Amiri, F. Tasnim, M. Tavakkoli Anbarani, C. Dagdeviren, M. A. Karami, *Smart Mater. Struct.* **2021**, *30*, 085017.
- [53] Y. Guan, L. Tu, K. Ren, X. Kang, Y. Tian, W. Deng, P. Yu, C. Ning, R. Fu, G. Tan, L. Zhou, *ACS Appl. Mater. Interfaces* **2023**, *15*, 1736.
- [54] a) C. Dagdeviren, B. D. Yang, Y. Su, P. L. Tran, P. Joe, E. Anderson, J. Xia, V. Doraiswamy, B. Dehdashti, X. Feng, B. Lu, R. Poston, Z. Khalpey, R. Ghaffari, Y. Huang, M. J. Slepian, J. A. Rogers, *Proc. Natl. Acad. Sci. USA* **2014**, *111*, 1927; b) M. O. G. Nayeem, S. Lee, H. Jin, N. Matsuhisa, H. Jinno, A. Miyamoto, T. Yokota, T. Someya, *Proc. Natl. Acad. Sci. USA* **2020**, *117*, 7063.
- [55] S. Chun, J.-S. Kim, Y. Yoo, Y. Choi, S. J. Jung, D. Jang, G. Lee, K.-I. Song, K. S. Nam, I. Youn, D. Son, C. Pang, Y. Jeong, H. Jung, Y.-J. Kim, B.-D. Choi, J. Kim, S.-P. Kim, W. Park, S. Park, *Nat. Electron.* **2021**, *4*, 429.
- [56] S. Zhang, F. Li, *J. Appl. Phys.* **2012**, *111*, 031301.
- [57] a) S. Zhang, F. Li, X. Jiang, J. Kim, J. Luo, X. Geng, *Prog. Mater. Sci.* **2015**, *68*, 1; b) T. Zheng, J. Wu, D. Xiao, J. Zhu, *Prog. Mater. Sci.* **2018**, *98*, 552; c) X. Gao, J. Yang, J. Wu, X. Xin, Z. Li, X. Yuan, X. Shen, S. Dong, *Adv. Mater. Technol.* **2020**, *5*, 1900716; d) H. Jin, X. Gao, K. Ren, J. Liu, L. Qiao, M. Liu, W. Chen, Y. He, S. Dong, Z. Xu, F. Li, *IEEE Trans. Ultrason. Ferroelectr. Freq. Control.* **2022**, *69*, 3057.
- [58] a) A. V. Hippel, *Dielectric Materials and Applications*, Technology Press of MIT, Cambridge, MA **1954**; b) K. C. Kao, *Dielectric Phenomena in Solids*, Elsevier Academic Press, San Diego, CA **2004**.
- [59] S. Jiang, L. Jin, H. Hou, L. Zhang, in *Polymer-Based Multifunctional Nanocomposites and Their Applications* (Eds.: K. Song, C. Liu, J. Z. Guo), Elsevier, Higher Education Press, Amsterdam **2019**, pp. 201–243.
- [60] C. J. Dias, D. K. Das-Gupta, *Ferroelectric Polymer and Ceramic-Polymer Composites*, Trans Tech Publications Ltd, Switzerland, **1994**.
- [61] J. H. Lee, S. Zhang, Y. Bar-Cohen, S. Sherrit, *Sensors* **2014**, *14*, 14256.
- [62] L. Jin, V. Porokhonsky, D. Damjanovic, *Appl. Phys. Lett.* **2010**, *96*, 242902.
- [63] a) T. F. de Oliveira, C. N. Pai, M. Y. Matuda, J. C. Adamowski, F. Buiochi, *Rev. Bras. Eng. Biomed.* **2019**, *35*, 27; b) T. Kim, Z. Cui, W. Chang, H. Kim, Y. Zhu, X. Jiang, *IEEE Trans Ind Electron* **2019**, *67*, 6955; c) V. Pashaei, P. Dehghanzadeh, G. Enwia, M. Bayat, S. J. A. Majerus, S. Mandal, *IEEE Trans Biomed Circuits Syst* **2020**, *14*, 305; d) S. Sadeghpour, B. Lips, M. Kraft, R. Puers, *J. Microelectromech. Syst.* **2020**, *29*, 378; e) W. Liu, W. Chen, C. Zhu, D. Wu, *Micro and Nano Engineering* **2021**, *13*, 100096; f) Q. Zhang, T. Ma, C. Wang, X. Liu, Y. Li, Y. Chang, J. Liu, J. Huang, Y. Xiao, T. Pan, H. Zheng, *IEEE Trans Ind Electron* **2022**, *69*, 3078.
- [64] T. R. Shrout, S. J. Zhang, *J. Electroceram.* **2007**, *19*, 113.
- [65] S. Trolier-McKinstry, S. Zhang, A. J. Bell, X. Tan, *Annu. Rev. Mater. Res.* **2018**, *48*, 191.
- [66] L. Zhang, Z. Xu, Y. Feng, Y. Hu, X. Yao, *Ceram. Int.* **2008**, *34*, 709.
- [67] D. Lin, Z. Li, F. Li, Z. Xu, X. Yao, *J. Alloys Compd.* **2010**, *489*, 115.
- [68] K. K. Shung, J. M. Cannata, Q. F. Zhou, *J. Electroceram.* **2007**, *19*, 141.
- [69] a) F. Li, D. Lin, Z. Chen, Z. Cheng, J. Wang, C. Li, Z. Xu, Q. Huang, X. Liao, L.-Q. Chen, T. R. Shrout, S. Zhang, *Nat. Mater.* **2018**, *17*, 349; b) C. Li, B. Xu, D. Lin, S. Zhang, L. Bellaiche, T. R. Shrout, F. Li, *Phys. Rev. B* **2020**, *101*, 140102.
- [70] a) Z. Zhang, M. Su, F. Li, R. Liu, R. Cai, G. Li, Q. Jiang, H. Zhong, T. R. Shrout, S. Zhang, H. Zheng, W. Qiu, *IEEE Trans. Ultrason. Ferroelectr. Freq. Control.* **2020**, *67*, 2085; b) Z. Zhang, F. Li, R. Chen, T. Zhang, X. Cao, S. Zhang, T. R. Shrout, H. Zheng, K. K. Shung, M. S. Humayun, W. Qiu, Q. Zhou, *IEEE Trans. Ultrason. Ferroelectr. Freq. Control.* **2018**, *65*, 223.
- [71] a) E. Buixaderas, D. Nuzhnyy, J. Petzelt, L. Jin, D. Damjanovic, *Phys. Rev. B* **2011**, *84*, 184302; b) E. Buixaderas, I. Gregora, M. Savinov, J. Hlinka, L. Jin, D. Damjanovic, B. Malic, *Phys. Rev. B* **2015**, *91*, 014104.
- [72] a) Y. Yamashita, T. Karaki, H. Y. Lee, H. Wan, H. P. Kim, X. Jiang, *IEEE Trans. Ultrason. Ferroelectr. Freq. Control.* **2022**, *69*, 3048; b) D. Damjanovic, N. Klein, J. I. N. Li, V. Porokhonsky, *Funct. Mater. Lett.* **2010**, *03*, 5.
- [73] a) Z. Zhang, J. Xu, L. Yang, S. Liu, J. Xiao, X. Li, X. a. Wang, H. Luo, *Sens. Actuators, A* **2018**, *283*, 273; b) C.-M. Wong, Y. Chen, H. Luo, J. Dai, K.-H. Lam, H. L.-w. Chan, *Ultrasonics* **2017**, *73*, 181.
- [74] a) F. Li, M. J. Cabral, B. Xu, Z. Cheng, E. C. Dickey, J. M. LeBeau, J. Wang, J. Luo, S. Taylor, W. Hackenberger, L. Bellaiche, Z. Xu, L.-Q. Chen, T. R. Shrout, S. Zhang, *Science* **2019**, *364*, 264; b) Q. Li, Y. Liu, J. Liu, K. Song, H. Guo, F. Li, Z. Xu, *Adv. Funct. Mater.* **2022**, *32*, 2201719; c) Y. Liu, Q. Li, L. Qiao, Z. Xu, F. Li, *Adv. Sci.* **2022**, *9*, 2204631; d) L. Yang, H. Huang, Z. Xi, L. Zheng, S. Xu, G. Tian, Y. Zhai, F. Guo, L. Kong, Y. Wang, W. Lü, L. Yuan, M. Zhao, H. Zheng, G. Liu, *Nat. Commun.* **2022**, *13*, 2444.
- [75] a) C. Luo, H. Wan, W.-Y. Chang, Y. Yamashita, A. R. Paterson, J. Jones, X. Jiang, *Appl. Phys. Lett.* **2019**, *115*, 192904; b) J. Liu, C. Qiu, L. Qiao, K. Song, H. Guo, Z. Xu, F. Li, *J. Appl. Phys.* **2020**, *128*, 094104; c) A. D. Ushakov, Q. Hu, X. Liu, Z. Xu, X. Wei, V. Y. Shur, *Appl. Phys. Lett.* **2021**, *118*, 232901.
- [76] C. Qiu, B. Wang, N. Zhang, S. Zhang, J. Liu, D. Walker, Y. Wang, H. Tian, T. R. Shrout, Z. Xu, L.-Q. Chen, F. Li, *Nature* **2020**, *577*, 350.
- [77] a) J. Lin, Y. Wang, R. Xiong, B. Sa, C. Shi, J. Zhai, Z. Fang, K. Zhu, F. Yan, H. Tian, G. Ge, G. Li, H. Bai, P. Wang, Y. Zhang, X. Wu, *Acta Mater.* **2022**, *235*, 118061; b) H. Chen, S. Mirg, M. Osman, S. Agrawal, J. Cai, R. Biskowitz, J. Minotto, S. R. Kothapalli, *IEEE Sens. Lett.* **2021**, *5*, 1; c) F. Zheng, X. Tian, Z. Fang, J. Lin, Y. Lu, W. Gao, R. Xin, D. Fu, Y. Qi, Z. Ma, W. Ye, Y. Qin, X. Wang, Y. Zhang, *ACS Appl. Mater. Interfaces* **2023**, *15*, 7053; d) P. Yan, Y. Qin, Z. Xu, F. Han, Y. Wang, Z. Wen, Y. Zhang, S. Zhang, *ACS Appl. Mater. Interfaces* **2021**, *13*, 54210.
- [78] X. Gao, L. Qiao, C. Qiu, T. Wang, L. Zhang, J. Liu, S. Yang, H. Jin, B. Xin, S. Zhang, S. Dong, Z. Xu, F. Li, *Appl. Phys. Lett.* **2022**, *120*, 032902.
- [79] a) Y.-Q. Lu, Y.-X. Li, *J. Adv. Dielectr.* **2011**, *01*, 269; b) D. Xiao, *J. Adv. Dielectr.* **2011**, *01*, 33.
- [80] J. Hao, W. Li, J. Zhai, H. Chen, *Materials Science and Engineering: R: Reports* **2019**, *135*, 1.
- [81] a) J. Gao, D. Xue, W. Liu, C. Zhou, X. Ren, *Actuators* **2017**, *6*, 24; b) L. Jin, W. Luo, L. Hou, Y. Tian, Q. Hu, L. Wang, L. Zhang, X. Lu, H. Du, X. Wei, Y. Yan, G. Liu, *J. Eur. Ceram. Soc.* **2019**, *39*, 295.
- [82] a) K. Wang, J.-F. Li, *J. Adv. Ceram.* **2012**, *1*, 24; b) H.-C. Thong, C. Zhao, Z. Zhou, C.-F. Wu, Y.-X. Liu, Z.-Z. Du, J.-F. Li, W. Gong, K. Wang, *Mater. Today* **2019**, *29*, 37; c) J. Wu, D. Xiao, J. Zhu, *J. Mater. Sci.: Mater. Electron.* **2015**, *26*, 9297; d) L. Zhang, R. Jing, Y. Huang, Q. Hu, D. O. Alikin, V. Y. Shur, D. Wang, X. Wei, L. Zhang, G. Liu, L. Jin, *J. Eur. Ceram. Soc.* **2022**, *42*, 944.
- [83] a) N. D. Quan, L. Huu Bac, D. V. Thiet, V. N. Hung, D. D. Dung, *Adv. Mater. Sci. Eng.* **2014**, *2014*, 365391; b) X. Zhou, G. Xue, H. Luo, C. R. Bowen, D. Zhang, *Prog. Mater. Sci.* **2021**, *122*, 100836; c) R. Jing, L. Zhang, Q. Hu, D. O. Alikin, V. Y. Shur, X. Wei, L. Zhang, G. Liu, H. Zhang, L. Jin, *Journal of Materomics* **2022**, *8*, 335.

- [84] a) J. Wu, *J. Appl. Phys.* **2020**, 127, 190901; b) Y. Huang, L. Zhang, R. Jing, Y. Yang, V. Shur, X. Wei, L. Jin, *J. Mater. Sci. Technol.* **2024**, 169, 172.
- [85] a) L. Zhang, Z. Xu, L. Cao, X. Yao, *Mater. Lett.* **2007**, 61, 1130; b) F. Ya-Jun, X. Zhuo, L. Zhen-Rong, Z. Lin, Y. Xi, *J. Inorg. Mater.* **2006**, 21, 1127; c) L. Zhang, Z. Xu, Z. Li, S. Xia, X. Yao, *J. Electroceram.* **2008**, 21, 605; d) Z. Dai, J. Xie, W. Liu, X. Wang, L. Zhang, Z. Zhou, J. Li, X. Ren, *ACS Appl. Mater. Interfaces* **2020**, 12, 30289; e) Z. Wang, L. Zhang, R. Kang, W. Yang, L. He, P. Mao, X. Lou, L. Zhang, J. Wang, *Chem. Eng. J.* **2021**, 431, 133716; f) Z. Wang, R. Kang, W. Liu, L. Zhang, L. He, S. Zhao, H. Duan, Z. Yu, F. Kang, Q. Sun, T. Zhang, P. Mao, J. Wang, L. Zhang, *Chem. Eng. J.* **2022**, 427, 131989.
- [86] J. Koruza, A. J. Bell, T. Frömling, K. G. Webber, K. Wang, J. Rödel, *Journal of Materiomics* **2018**, 4, 13.
- [87] X. Lv, J. Zhu, D. Xiao, X.-x. Zhang, J. Wu, *Chem. Soc. Rev.* **2020**, 49, 671.
- [88] A. Safari, Q. Zhou, Y. Zeng, J. D. Leber, *Jpn. J. Appl. Phys.* **2023**, 62, S10801.
- [89] H. Wei, H. Wang, Y. Xia, D. Cui, Y. Shi, M. Dong, C. Liu, T. Ding, J. Zhang, Y. Ma, N. Wang, Z. Wang, Y. Sun, R. Wei, Z. Guo, *J. Mater. Chem. C* **2018**, 6, 12446.
- [90] S. Zhang, F. Li, F. Yu, X. Jiang, H.-Y. Lee, J. Luo, T. R. Shrout, *J. Korean Ceram. Soc* **2018**, 55, 419.
- [91] I. Milisavljevic, Y. Wu, *BMC Materials* **2020**, 2, 2.
- [92] C. Hu, X. Meng, M.-H. Zhang, H. Tian, J. E. Daniels, P. Tan, F. Huang, L. Li, K. Wang, J.-F. Li, Q. Lu, W. Cao, Z. Zhou, *Sci. Adv.* **2020**, 6, eaay5979.
- [93] G. L. Messing, S. Trolier-McKinstry, E. M. Sabolsky, C. Duran, S. Kwon, B. Brahmarouti, P. Park, H. Yilmaz, P. W. Rehrig, K. B. Eitel, E. Suvaci, M. Seabaugh, K. S. Oh, *Crit. Rev. Solid State Mater. Sci.* **2004**, 29, 45.
- [94] J. Wu, S. Zhang, F. Li, *Appl. Phys. Lett.* **2022**, 121, 120501.
- [95] H. Leng, Y. Yan, X. Li, S. K. Karan, M. Fanton, S. Priya, *J. Mater. Chem. C* **2023**, 11, 2229.
- [96] H. Leng, Y. Yan, B. Wang, T. Yang, H. Liu, X. Li, R. Sriramdas, K. Wang, M. Fanton, R. J. Meyer, L.-Q. Chen, S. Priya, *Acta Mater.* **2022**, 234, 118015.
- [97] a) S. Yang, F. Tian, C. Li, M. Wang, J. Zhang, Q. Zhu, J. Wu, J. Li, X. Gao, F. Li, *J. Appl. Phys.* **2023**, 133, 094104; b) S. Yang, J. Li, Y. Liu, M. Wang, L. Qiao, X. Gao, Y. Chang, H. Du, Z. Xu, S. Zhang, F. Li, *Nat. Commun.* **2021**, 12, 1414.
- [98] a) X. Ren, Y. Wang, M. Tang, X. Liu, Z. Xu, Y. Yan, *J. Am. Ceram. Soc.* **2023**, 106, 5331; b) M. Wang, S. Yang, J. Wu, J. Li, L. Qiao, X. Liu, C. Wang, X. Feng, C. Li, F. Li, *Appl. Phys. Lett.* **2023**, 122, 222903.
- [99] M. Tang, X. Liu, Y. Wang, X. Ren, Z. Xu, Y. Yan, *J. Appl. Phys.* **2023**, 133, 184102.
- [100] Y. Yan, L. D. Geng, H. Liu, H. Leng, X. Li, Y. U. Wang, S. Priya, *Nat. Commun.* **2022**, 13, 3565.
- [101] a) Y. Sun, L. Jiang, R. Chen, R. Li, H. Kang, Y. Zeng, Y. Yan, S. Priya, Q. Zhou, *IEEE Trans. Ultrason. Ferroelectr. Freq. Control.* **2022**, 69, 3095; b) L. Bian, K. Zhu, Q. Wang, J. Ma, J. Fan, X. Qi, G. Jiang, B. Zhao, R. Zhang, B. Yang, W. Cao, *J. Adv. Dielectr.* **2022**, 12, 2244003.
- [102] G.-T. Hwang, M. Byun, C. K. Jeong, K. J. Lee, *Adv. Healthcare Mater.* **2015**, 4, 646.
- [103] J. W. Judy, *Smart Mater. Struct.* **2001**, 10, 1115.
- [104] Y. Qiu, V. J. Gigliotti, M. Wallace, F. Griggio, E. M. C. Demore, S. Cochran, S. Trolier-McKinstry, *Sensors* **2015**, 15, 8020.
- [105] Y. He, H. Wan, X. Jiang, C. Peng, *Biosensors* **2023**, 13, 55.
- [106] L. Yang, D.-Y. Zheng, K.-X. Guo, W.-N. Zhao, Z.-H. Peng, G.-G. Peng, T. Zhou, *J. Mater. Sci.: Mater. Electron.* **2018**, 29, 18011.
- [107] C. Cai, D. Zhang, W. Liu, J. Wang, S. Zhou, Y. Su, X. Sun, D. Lin, *Materials* **2018**, 11, 2392.
- [108] S. Zhou, D. Lin, Y. Su, L. Zhang, W. Liu, *J. Adv. Ceram.* **2021**, 10, 98.
- [109] a) M. Wang, Y. Zhou, *Microsystem Technologies* **2017**, 23, 1761; b) V. M. Mastronardi, F. Guido, M. Amato, M. De Vittorio, S. Petroni, *Microelectron. Eng.* **2014**, 121, 59.
- [110] a) B. Stadlober, M. Zirkel, M. Irimia-Vladu, *Chem. Soc. Rev.* **2019**, 48, 1787; b) Y. Xin, C. Guo, X. Qi, H. Tian, X. Li, Q. Dai, S. Wang, C. Wang, *Ferroelectrics* **2016**, 500, 291; c) L. Zhang, Z. Y. Cheng, *J. Adv. Dielectr.* **2011**, 01, 389; d) L. Zhang, X. Shan, P. Bass, Y. Tong, T. D. Rolin, C. W. Hill, J. C. Brewer, D. S. Tucker, Z. Y. Cheng, *Sci. Rep.* **2016**, 6, 35763; e) C. Dagdeviren, S.-W. Hwang, Y. Su, S. Kim, H. Cheng, O. Gur, R. Haney, F. G. Omenetto, Y. Huang, J. A. Rogers, *Small* **2013**, 9, 3398.
- [111] a) L. Lu, W. Ding, J. Liu, B. Yang, *Nano Energy* **2020**, 78, 105251; b) X. Chen, X. Han, Q.-D. Shen, *Adv. Electron. Mater.* **2017**, 3, 1600460; c) X. Lu, L. Hou, L. Zhang, Y. Tong, G. Zhao, Z. Y. Cheng, *Sens. Actuators, A* **2017**, 261, 196.
- [112] Y. Liu, W.-G. Liu, D.-B. Lin, X.-L. Niu, S. Zhou, J. Zhang, S.-B. Ge, Y.-C. Zhu, X. Meng, Z.-L. Chen, *Nanomaterials* **2022**, 12, 588.
- [113] a) C. Peng, M. Chen, H. Wang, J. Shen, X. Jiang, *IEEE Sens. J.* **2020**, 21, 2642; b) Z. Qian, P. A. Lewin, P. E. Bloomfield, *IEEE Trans. Ultrason. Ferroelectr. Freq. Control.* **1997**, 44, 1148; c) F. S. Foster, K. A. Harasiewicz, M. D. Sherar, *IEEE Trans. Ultrason. Ferroelectr. Freq. Control.* **2000**, 47, 1363; d) B. M. Trindade, Y. Ono, E. D. Lemaire, I. AlMohimeed, in *2014 IEEE International Ultrasonics Symposium*, **2014**, pp. 2112–2115; e) Z. Zhou, J. Li, W. Xia, X. Zhu, T. Sun, C. Cao, L. Zhang, *Phys. Chem. Chem. Phys.* **2020**, 22, 5711.
- [114] T. E. Hooper, J. I. Roscow, A. Mathieson, H. Khanbareh, A. J. Goetzee-Barral, A. J. Bell, *J. Eur. Ceram. Soc.* **2021**, 41, 6115.
- [115] A. Safari, V. F. Janas, A. Bandyopadhyay, *AIChE J.* **1997**, 43, 2849.
- [116] P. Eltouby, I. Shyha, C. Li, J. Khaliq, *Ceram. Int.* **2021**, 47, 17813.
- [117] a) P. Kabakov, T. Kim, Z. Cheng, X. Jiang, S. Zhang, *Annu. Rev. Mater. Res.* **2023**, 53, 165; b) H. Kim, X. Jiang, *Appl. Sci.* **2023**, 13, 615.
- [118] Y. Yang, K. Zhu, E. Sun, P. Liu, R. Zhang, W. Cao, *Sens. Actuators, A* **2022**, 346, 113873.
- [119] X. Zhou, Q. Yue, Q. Zhang, J. Ma, M. Chen, J. Wang, F. Wang, Y. Tang, D. Lin, H. Luo, X. Zhao, *Composites Communications* **2022**, 36, 101399.
- [120] E. Yalcin, N. K. Gözüaçık, S. Alkoy, H. A. Sari, M. Y. Kaya, Ç. Öncel, E. Menşur, *Sens. Actuators, A* **2023**, 357, 114389.
- [121] J. Lv, X. Xie, X. Zhu, Z. Li, Z. Han, Y. Cui, B. Zhang, X. Jian, *Appl. Acoust.* **2022**, 188, 108540.
- [122] P. Lin, L. Zhang, C. Fei, D. Li, R. Wu, Q. Chen, C. Hou, Y. Yang, *Compos. Struct.* **2020**, 245, 112364.
- [123] P. Lin, Y. Zhu, Z. Chen, C. Fei, D. Chen, S. Zhang, D. Li, W. Feng, Y. Yang, C. Chai, *Compos. Struct.* **2022**, 285, 115249.
- [124] a) K. Zhu, J. Ma, Y. Liu, B. Shen, D. Huo, Y. Yang, X. Qi, E. Sun, R. Zhang, *Micromachines* **2022**, 13, 1715; b) H. Hang, X. Jiang, D. Lin, F. Wang, X. a. Wang, H. Luo, *Curr. Appl. Phys.* **2023**, 47, 1; c) H. Wan, C. Luo, C.-C. Chung, Y. Yamashita, X. Jiang, *Appl. Phys. Lett.* **2021**, 118, 102904.
- [125] a) J. Xiong, Z. Wang, X. Yang, R. Su, X. Long, C. He, *RSC Adv.* **2021**, 11, 12826; b) J. Ma, K. Zhu, D. Huo, X. Qi, E. Sun, R. Zhang, *Appl. Phys. Lett.* **2021**, 118, 022901.
- [126] a) L. W. Bradley, Y. S. Yaras, B. Karahasanoglu, B. Atasoy, F. L. Degertekin, *IEEE Sens. J.* **2023**, 23, 6672; b) F. Craciun, F. Cordero, E. Mercadelli, N. Ilic, C. Galassi, C. Baldisserri, J. Bobic, P. Stagnaro, G. Canu, M. T. Buscaglia, A. Dzunuzovic, M. V. Petrovic, *Composites, Part B* **2023**, 263, 110835; c) B. Karahasanoglu, L. W. Bradley, H. H. Snyder, B. Atasoy, Y. S. Yaras, F. L. Degertekin, in *2023 IEEE International Conference on Flexible and Printable Sensors and Systems (FLEPS)*, **2023**, pp. 1–4.
- [127] W. Wang, S. W. Or, Q. Yue, Y. Zhang, J. Jiao, B. Ren, D. Lin, C. M. Leung, X. Zhao, H. Luo, *Sens. Actuators, A* **2013**, 192, 69.
- [128] a) Y. Zhang, L. Wang, L. Qin, C. Zhong, S. Hao, *IEEE Trans. Ultrason. Ferroelectr. Freq. Control.* **2021**, 68, 1791; b) S. Hao, C. Zhong, Y.

- Zhang, Y. Chen, L. Wang, L. Qin, *ACS Appl. Electron. Mater.* **2023**, *5*, 2686.
- [129] T. Kim, Z. Cui, W. Y. Chang, H. Kim, Y. Zhu, X. Jiang, *IEEE Trans Ind Electron* **2020**, *67*, 6955.
- [130] a) C. Peng, M. Chen, H. K. Sim, Y. Zhu, X. Jiang, *IEEE Sens. J.* **2021**, *21*, 2642; b) C. Peng, M. Chen, H. K. Sim, Y. Zhu, X. Jiang, in *2020 IEEE 15th International Conference on Nano/Micro Engineered and Molecular System (NEMS)*, **2020**, pp. 143–146.
- [131] a) N. Jia, T. Wang, J. Duan, K. Qiang, S. Xia, H. Du, F. Li, Z. Xu, *ACS Appl. Mater. Interfaces* **2022**, *14*, 8137; b) N. Jia, T. Wang, L. Ning, Z. Ma, Y. Dang, C. C. Li, H. Du, F. Li, Z. Xu, *ACS Appl. Mater. Interfaces* **2023**, *15*, 36611.
- [132] W. Chen, J. Liu, S. Lei, Z. Yang, Q. Zhang, Y. Li, J. Huang, Y. Dong, H. Zheng, D. Wu, T. Ma, *IEEE Trans. Biomed. Eng.* **2023**, *70*, 2841.
- [133] T. Tang, Z. Shen, J. Wang, S. Xu, J. Jiang, J. Chang, M. Guo, Y. Fan, Y. Xiao, Z. Dong, H. Huang, X. Li, Y. Zhang, D. Wang, L.-Q. Chen, K. Wang, S. Zhang, C.-W. Nan, Y. Shen, *Natl Sci Rev* **2023**, *10*, nwad177.
- [134] a) E. J. Curry, T. T. Le, R. Das, K. Ke, E. M. Santorella, D. Paul, M. T. Chorsi, K. T. M. Tran, J. Baroody, E. R. Borges, B. Ko, A. Golabchi, X. Xin, D. Rowe, L. Yue, J. Feng, M. D. Morales-Acosta, Q. Wu, I. P. Chen, X. T. Cui, J. Pachter, T. D. Nguyen, *Proc. Natl. Acad. Sci. USA* **2020**, *117*, 214; b) V. Sencadas, C. Ribeiro, A. Heredia, I. K. Bdkin, A. L. Kholkin, S. Lanceros-Mendez, *Appl. Phys. A* **2012**, *109*, 51.
- [135] a) Y. Inuzuka, K. Onishi, S. Kinoshita, Y. Nakashima, T. Nagata, H. Yamane, T. Nakai, T. Kataoka, S. Ito, Y. Tajitsu, *Jpn. J. Appl. Phys.* **2012**, *51*, 09LD15; b) Y. Tajitsu, S. Kawai, M. Kanesaki, M. Date, E. Fukada, *Ferroelectrics* **2004**, *304*, 195.
- [136] a) S. Gong, B. Zhang, J. Zhang, Z. L. Wang, K. Ren, *Adv. Funct. Mater.* **2020**, *30*, 1908724; b) G. Zhao, B. Huang, J. Zhang, A. Wang, K. Ren, Z. L. Wang, *Macromol. Mater. Eng.* **2017**, *302*, 1600476; c) J. Tian, F. Jiang, Q. Zeng, M. PourhosseiniAsl, C. Han, K. Ren, *IEEE Sens. J.* **2023**, *23*, 6264.
- [137] E. J. Curry, K. Ke, M. T. Chorsi, K. S. Wrobel, A. N. Miller, A. Patel, I. Kim, J. Feng, L. Yue, Q. Wu, C.-L. Kuo, K. W. H. Lo, C. T. Laurencin, H. Ilies, P. K. Purohit, T. D. Nguyen, *Proc. Natl. Acad. Sci. USA* **2018**, *115*, 909.
- [138] Y. Liu, G. Zvidotor, T. T. Le, T. Vinikoor, K. Morgan, E. J. Curry, R. Das, A. McClinton, E. Eisenberg, L. N. Apuzzo, K. T. M. Tran, P. Prasad, T. J. Flanagan, S.-W. Lee, H.-M. Kan, M. T. Chorsi, K. W. H. Lo, C. T. Laurencin, T. D. Nguyen, *Sci. Transl. Med.* **2022**, *14*, eabi7282.
- [139] R. Das, T. T. Le, B. Schiff, M. T. Chorsi, J. Park, P. Lam, A. Kemerley, A. M. Supran, A. Eshed, N. Luu, N. G. Menon, T. A. Schmidt, H. Wang, Q. Wu, M. Thirunavukkarasu, N. Maulik, T. D. Nguyen, *Biomaterials* **2023**, *301*, 122270.
- [140] R. Das, E. J. Curry, T. T. Le, G. Awale, Y. Liu, S. Li, J. Contreras, C. Bednarsz, J. Millender, X. Xin, D. Rowe, S. Emadi, K. W. H. Lo, T. D. Nguyen, *Nano Energy* **2020**, *76*, 105028.
- [141] a) L. H. Chen, C. C. Chan, X. M. Ang, W. Yuan, P. Zu, W. C. Wong, Y. Zhang, K. C. Leong, *IEEE J. Sel. Top. Quantum Electron.* **2012**, *18*, 1042; b) G. de Marzo, V. M. Mastronardi, L. Algieri, F. Vergari, F. Pisano, L. Fachechi, S. Marras, L. Natta, B. Spagnolo, V. Brunetti, F. Rizzi, F. Pisanello, M. De Vittorio, *Adv. Electron. Mater.* **2022**, *9*, 2200069; c) C. Li, S. Lu, C. Zhong, X. Song, *IEEE Sens. J.* **2022**, *22*, 6669; d) G. d. Marzo, V. M. Mastronardi, L. Algieri, F. Vergari, F. Pisano, L. Fachechi, L. Natta, G. Ascanio, F. Rizzi, F. Pisanello, M. D. Vittorio, in *2022 IEEE 22nd International Conference on Nanotechnology (NANO)*, **2022**, pp. 136–139.
- [142] T. Vijayakanth, S. Shankar, G. Finkelstein-Zuta, S. Rencus-Lazar, S. Gilead, E. Gazit, *Chem. Soc. Rev.* **2023**, *52*, 6191.
- [143] a) Z. Zhang, X. Li, Z. Peng, X. Yan, S. Liu, Y. Hong, Y. Shan, X. Xu, L. Jin, B. Liu, X. Zhang, Y. Chai, S. Zhang, A. K. Y. Jen, Z. Yang, *Nat. Commun.* **2023**, *14*, 4094; b) M. Ali, M. J. Bathaei, E. Istif, S. N. H. Karimi, L. Beker, *Adv. Healthcare Mater.* **2023**, *12*, 2300318.
- [144] a) Y. Yang, X. Song, X. Li, Z. Chen, C. Zhou, Q. Zhou, Y. Chen, *Adv. Mater.* **2018**, *30*, 1706539; b) Z. Chen, Z. Li, J. Li, C. Liu, C. Lao, Y. Fu, C. Liu, Y. Li, P. Wang, Y. He, J. *Eur. Ceram. Soc.* **2019**, *39*, 661.
- [145] J. Park, D.-G. Lee, S. Hur, J. M. Baik, H. S. Kim, H.-C. Song, *Actuators* **2023**, *12*, 177.
- [146] D. Sun, Y. Lu, T. Karaki, *Resources Chemicals and Materials* **2023**, *2*, 128.
- [147] Y. Zeng, L. Jiang, Q. He, R. Wodnicki, Y. Yang, Y. Chen, Q. Zhou, *J. Phys. D: Appl. Phys.* **2022**, *55*, 013002.
- [148] a) Y. Yang, Z. Chen, X. Song, Z. Zhang, J. Zhang, K. K. Shung, Q. Zhou, Y. Chen, *Adv. Mater.* **2017**, *29*, 1605750; b) R. Wodnicki, H. Kang, Y. Sun, L. Jiang, H. Lu, Q. Zhou, in *2020 IEEE International Ultrasonics Symposium (IUS)*, **2020**, pp. 1–4.
- [149] Z. Chen, X. Song, L. Lei, X. Chen, C. Fei, C. T. Chiu, X. Qian, T. Ma, Y. Yang, K. Shung, Y. Chen, Q. Zhou, *Nano Energy* **2016**, *27*, 78.
- [150] Y. Zeng, L. Jiang, Y. Sun, Y. Yang, Y. Quan, S. Wei, G. Lu, R. Li, J. Rong, Y. Chen, Q. Zhou, *Micromachines* **2020**, *11*, 713.
- [151] X. Chen, X. Qian, K.-H. Lam, C. T. Chiu, R. Chen, Z. Chen, K. K. Shung, P. Yu, Q. Zhou, *Adv. Funct. Mater.* **2019**, *29*, 1902912.
- [152] H. Lu, H. Cui, G. Lu, L. Jiang, R. Hensleigh, Y. Zeng, A. Rayes, M. K. Panduranga, M. Acharya, Z. Wang, A. Irimia, F. Wu, G. P. Carman, J. M. Morales, S. Putterman, L. W. Martin, Q. Zhou, X. Zheng, *Nat. Commun.* **2023**, *14*, 2418.
- [153] a) Y. Chen, X. Bao, C.-M. Wong, J. Cheng, H. Wu, H. Song, X. Ji, S. Wu, *Ceram. Int.* **2018**, *44*, 22725; b) D. Yao, H. Cui, R. Hensleigh, P. Smith, S. Alford, D. Bernero, S. Bush, K. Mann, H. F. Wu, M. Chin-Nieh, G. Youmans, X. Zheng, *Adv. Funct. Mater.* **2019**, *29*, 1903866; c) T. Roloff, R. Mitkus, J. N. Lion, M. Sinapius, *Sensors* **2022**, *22*, 6964.
- [154] Z. Wang, X. Yuan, J. Yang, Y. Huan, X. Gao, Z. Li, H. Wang, S. Dong, *Nano Energy* **2020**, *73*, 104737.
- [155] Y. Chen, D. Zhang, H. Luo, Z. Peng, L. Zeng, M. Yuan, X. Ji, *Ceram. Int.* **2023**.
- [156] C. Yang, N. Chen, X. Liu, Q. Wang, C. Zhang, *RSC Adv.* **2021**, *11*, 20662.
- [157] Y. M. Yousry, V.-K. Wong, R. Ji, Y. Chen, S. Chen, X. Zhang, D. B. K. Lim, L. Shen, K. Yao, *Adv. Funct. Mater.* **2023**, *33*, 2213582.
- [158] C. Fei, J. Ma, C. T. Chiu, J. A. Williams, W. Fong, Z. Chen, B. Zhu, R. Xiong, J. Shi, T. K. Hsiai, K. K. Shung, Q. Zhou, *Appl. Phys. Lett.* **2015**, *107*, 123505.
- [159] P. Lin, Y. Zhu, D. Chen, C. Fei, C. Zheng, Z. Chen, R. Wu, D. Li, S. Zhang, W. Feng, Z. Jiang, L. Wen, C. Chai, Y. Yang, *Struct Multidiscipl Optim* **2022**, *65*, 101.
- [160] Z. Li, D.-Q. Yang, S.-L. Liu, S.-Y. Yu, M.-H. Lu, J. Zhu, S.-T. Zhang, M.-W. Zhu, X.-S. Guo, H.-D. Wu, X.-L. Wang, Y.-F. Chen, *Sci. Rep.* **2017**, *7*, 42863.
- [161] K. Zhu, J. Ma, X. Qi, B. Shen, Y. Liu, E. Sun, R. Zhang, *Sensors* **2022**, *22*, 8025.
- [162] M. S. Osman, H. Chen, K. Creamer, J. Minotto, J. Liu, S. Mirg, J. Christian, X. Bai, S. Agrawal, S. R. Kothapalli, *IEEE Trans. Ultrason. Ferroelectr. Freq. Control.* **2022**, *69*, 2672.
- [163] J. Zhao, Z. Li, C. Fei, C. Hou, D. Wang, L. Lou, D. Chen, D. Li, Z. Chen, Y. Yang, *IEEE Trans. Ultrason. Ferroelectr. Freq. Control.* **2022**, *69*, 1952.
- [164] C. M. Sayers, C. E. Tait, *Ultrasonics* **1984**, *22*, 57.
- [165] H. Kim, J. Yoo, D. Heo, Y. S. Seo, H. G. Lim, H. H. Kim, *IEEE Trans. Ultrason. Ferroelectr. Freq. Control.* **2022**, *69*, 1960.
- [166] A. Amry Amin, I. Mohamad Pauzi, S. Suhairy, A. Mohd Noorul Ikhsan, in *RnD Seminar 2010: Research and Development Seminar 2010*, Bangi, Malaysia **2010**.
- [167] H. Fujii, C. Nakaya, H. Takeuchi, T. Kondo, Y. Ishikawa, *Jpn. J. Appl. Phys.* **1995**, *34*, 312.

- [168] a) Z. Li, S. Yang, M. Zhou, C. Hou, D. Chen, C. Fei, D. Li, Y. Quan, Y. Yang, *J. Adv. Dielectr.* **2023**, *13*, 2350001; b) Z. Li, S. Yang, D. Wang, H. Shan, D. Chen, C. Fei, M. Xiao, Y. Yang, *Appl. Phys. Lett.* **2021**, *119*, 073501; c) H. Sun, S. Wang, S. Huang, L. Peng, Q. Wang, W. Zhao, *Sci. Rep.* **2020**, *10*, 1469; d) Z. Li, R. Guo, C. Fei, D. Li, D. Chen, C. Zheng, R. Wu, W. Feng, Y. Yang, *Appl. Acoust.* **2021**, *175*, 107787.
- [169] Z. Li, J. Zhao, C. Hou, C. Fei, C. Zheng, L. Lou, D. Chen, D. Li, Y. Yang, *IEEE Electron Device Lett.* **2022**, *43*, 946.
- [170] Z. Li, R. Guo, D. Chen, C. Fei, X. Yang, D. Li, C. Zheng, J. Chen, R. Wu, W. Feng, Z. Xu, Y. Yang, *IEEE Trans. Ultrason. Ferroelectr. Freq. Control.* **2021**, *68*, 1546.
- [171] Z. Li, S. Yang, C. Fei, R. Guo, D. Chen, C. Zheng, Y. Yang, *IEEE Trans. Ultrason. Ferroelectr. Freq. Control.* **2022**, *69*, 254.
- [172] Z. Li, D. Wang, C. Fei, P. Jiang, S. Zhang, D. Chen, D. Li, C. Zhen, R. Wu, X. Peng, Y. Xu, Z. Chen, W. Feng, Y. Yang, *IEEE Sens. J.* **2021**, *21*, 8935.
- [173] Z. Li, C. Fei, S. Yang, C. Hou, J. Zhao, Y. Li, C. Zheng, H. Wu, Y. Quan, T. Zhao, D. Chen, D. Li, G. Niu, W. Ren, M. Xiao, Y. Yang, *Adv. Funct. Mater.* **2022**, *32*, 2209173.
- [174] a) B. Salmon, D. Le Denmat, *Clin Oral Investig* **2012**, *16*, 643; b) J. Marotti, S. Heger, J. Tinschert, P. Tortamano, F. Chuembou, K. Radermacher, S. Wolfart, *Oral Surgery, Oral Medicine, Oral Pathology and Oral Radiology* **2013**, *115*, 819.
- [175] C. Shi, X. Luo, J. Guo, Z. Najdovski, T. Fukuda, H. Ren, *IEEE Journal of Biomedical and Health Informatics* **2018**, *22*, 806.
- [176] C. Fei, Y. Yang, F. Guo, P. Lin, Q. Chen, Q. Zhou, L. Sun, *IEEE Trans. Biomed. Eng.* **2018**, *65*, 2087.
- [177] J. Chen, C. Fei, D. Lin, P. Gao, J. Zhang, Y. Quan, D. Chen, D. Li, Y. Yang, *Frontiers in Materials* **2022**, *8*, 733358.
- [178] K. A. Snook, Z. Jian-Zhong, C. H. F. Alves, J. M. Cannata, C. Wo-Hsing, R. J. Meyer, T. A. Ritter, K. K. Shung, *IEEE Trans. Ultrason. Ferroelectr. Freq. Control.* **2002**, *49*, 169.
- [179] J. Sauvage, M. Flesch, G. Férin, A. Nguyen-Dinh, J. Porée, M. Tanter, M. Pernot, T. Deffieux, *Physics in Medicine & Biology* **2018**, *63*, 215012.
- [180] C. H. Seo, J. T. Yen, *IEEE Trans. Ultrason. Ferroelectr. Freq. Control.* **2009**, *56*, 837.
- [181] a) J. Joontaek, K. Sangwon, L. Wonjun, C. Hongsoo, *J. Micromech. Microeng.* **2013**, *23*, 125037; b) H. Bouzari, M. Engholm, T. L. Christiansen, M. B. Stuart, S. I. Nikolov, E. V. Thomsen, J. A. Jensen, in *2015 IEEE International Ultrasonics Symposium (IUS)*, **2015**, pp. 1–4; c) M. Schou, A. S. Havreland, M. Engholm, M. B. Stuart, E. V. Thomsen, J. A. Jensen, in *2018 IEEE International Ultrasonics Symposium (IUS)*, **2018**, pp. 1–4.
- [182] A. Fenster, D. B. Downey, *IEEE Eng Med Biol Mag* **1996**, *15*, 41.
- [183] J. Jung, W. Lee, W. Kang, E. Shin, J. Ryu, H. Choi, *J. Micromech. Microeng.* **2017**, *27*, 113001.
- [184] a) W. Jiangfeng, G. K. Fedder, L. R. Carley, *IEEE J. Solid-State Circuits* **2004**, *39*, 722; b) J. Xie, C. Lee, H. Feng, *J. Microelectromech. Syst.* **2010**, *19*, 317.
- [185] B. A. Greenlay, R. J. Zemp, *IEEE Trans. Ultrason. Ferroelectr. Freq. Control.* **2017**, *64*, 93.
- [186] J. Joontaek, L. Wonjun, K. Woojin, S. Eunjung, R. Jungho, C. Hongsoo, *J. Micromech. Microeng.* **2017**, *27*, 113001.
- [187] V. Pashaei, A. Roman, S. Mandal, in *2018 IEEE Biomedical Circuits and Systems Conference (BioCAS)*, **2018**, pp. 1–4.
- [188] I. AlMohimeed, Y. Ono, *Sensors* **2020**, *20*, 3616.
- [189] Y. Zeng, L. Jiang, Y. Sun, Y. Yang, Y. Quan, S. Wei, G. Lu, R. Li, J. Rong, Y. Chen, Q. Zhou, *Micromachines* **2020**, *11*, 713.
- [190] J. Elloian, J. Jadwiszczak, V. Arslan, J. D. Sherman, D. O. Kessler, K. L. Shepard, *Sci. Rep.* **2022**, *12*, 16184.
- [191] M. Tanabe, K. Sato, T. Uda, M. Kobayashi, *Jpn. J. Appl. Phys.* **2023**, *62*, S1034.
- [192] C. Dagdeviren, L. Zhang, *Methods and Apparatus for Imaging with Conformable Ultrasound Patch*, US patent, Cambridge, United States **2020**.
- [193] G. R. Harris, R. C. Preston, A. S. DeReggi, *IEEE Trans. Ultrason. Ferroelectr. Freq. Control.* **2000**, *47*, 1321.
- [194] I. AlMohimeed, H. Turkistani, Y. Ono, in *2013 IEEE International Ultrasonics Symposium (IUS)*, **2013**, pp. 1137–1140.
- [195] a) A. Huang, Y. Ono, in *2016 IEEE-EMBS International Conference on Biomedical and Health Informatics (BHI)*, **2016**, pp. 188; b) E. Yeung, I. AlMohimeed, Y. Ono, in *2019 IEEE SENSORS*, **2019**, pp. 1–4.
- [196] S. Steinberg, A. Huang, Y. Ono, S. Rajan, *IEEE Instrumentation & Measurement Magazine* **2022**, *25*, 6.
- [197] a) Y. Qi, N. T. Jafferis, K. Lyons, C. M. Lee, H. Ahmad, M. C. McAlpine, *Nano Lett.* **2010**, *10*, 524; b) W. Liu, D. Wu, *Sensors* **2020**, *20*, 3333.
- [198] J. Kim, W. Chang, S. Huang, X. Jiang, in *2016 IEEE 16th International Conference on Nanotechnology (IEEE-NANO)*, **2016**, pp. 191–192.
- [199] S. Jiang, Y. Shen, S. Wang, Y. Zhi, B. Han, *Frontiers in Materials* **2022**, *9*, 958775.
- [200] a) Y. Kato, T. Sekitani, Y. Noguchi, T. Yokota, M. Takamiya, T. Sakurai, T. Someya, *IEEE Trans. Electron Devices* **2010**, *57*, 995; b) A. Decharat, S. Wagle, A. Habib, S. Jacobsen, F. Melandsø, *Smart Mater. Struct.* **2018**, *27*, 025001.
- [201] a) O. Casula, C. Poidevin, G. Cattiaux, P. Dumas, *Ultrasonics* **2006**, *44*, e647; b) G. Toullelan, O. Casula, E. Abittan, P. Dumas, *AIP Conf. Proc.* **2008**, *975*, 794.
- [202] C. R. Bowen, L. R. Bradley, D. P. Almond, P. D. Wilcox, *Ultrasonics* **2008**, *48*, 367.
- [203] C. Mo, S. Rs, U. Cd, V. Sp, S. B., L. H., B. Er, G. Ws, *Studies in health technology and informatics* **2008**, *132*, 95.
- [204] R. S. Singh, S. Natarajan, M. Lee, A. E. Dann, B. P. Cox, D. B. Bennett, E. R. Brown, H. Lee, W. S. Grundfest, M. O. Culjat, in *2009 IEEE International Ultrasonics Symposium*, **2009**, pp. 1852–1855.
- [205] A. Dann, D. Bennett, R. Singh, J.-J. Lemaire, W. Grundfest, M. Culjat, *Fabrication of a Conformal Ring-Annular Ultrasound Array*, Vol. 7629, SPIE Medical Imaging, San Diego, CA **2010**.
- [206] a) Y. Yang, H. Tian, B. Yan, H. Sun, C. Wu, Y. Shu, L.-G. Wang, T.-L. Ren, *RSC Adv.* **2013**, *3*, 24900; b) Z. Wang, Q.-T. Xue, Y.-Q. Chen, Y. Shu, H. Tian, Y. Yang, D. Xie, J.-W. Luo, T.-L. Ren, *Sensors* **2015**, *15*, 2538.
- [207] C. J. L. Lane, *Case Studies in Nondestructive Testing and Evaluation* **2014**, *1*, 13.
- [208] K. Nakahata, S. Tokumasu, A. Sakai, Y. Iwata, K. Ohira, Y. Ogura, *Nephrol Dial Transplant* **2016**, *82*, 13.
- [209] T. C. WU, M. KOBAYASHI, C. C. CHENG, C. H. YANG, *19th World Conference on Non-Destructive Testing*, **2016**.
- [210] J.-H. Lee, I.-J. Cho, K. Ko, E.-S. Yoon, H.-H. Park, T. S. Kim, *Microsystem Technologies* **2017**, *23*, 2321.
- [211] H. Ding, S. Akhbari, B. E. Eovino, Y. Wu, J. Xie, L. Lin, in *2018 IEEE Micro Electro Mechanical Systems (MEMS)*, **2018**, pp. 396–399.
- [212] S. Sun, M. Zhang, C. Gao, B. Liu, W. Pang, in *2018 IEEE International Ultrasonics Symposium (IUS)*, **2018**, pp. 1–4.
- [213] A. Smiley, M. Howell, G. T. Clement, A. J. Fleischman, *Biomedical Physics & Engineering Express* **2019**, *5*, 025025.
- [214] D.-C. Pang, C.-M. Chang, *Sensors* **2017**, *17*, 1443.
- [215] a) S. Joshi, S. Yazadi, V. Henneken, R. Dekker, R. Sanders, in *2015 IEEE 17th Electronics Packaging and Technology Conference (EPTC)*, **2015**, pp. 1–4; b) P. Hamelmann, M. Mischi, F. A. Kolen, O. E. H. J. van Laar, R. Vullings, W. M. J. Bergmans, *Sensors* **2019**, *19*, 1195.
- [216] S. Xu, L. Zhang, C. Wang, H. Hu, X. Li, *Stretchable Ultrasonic Transducer Devices*, US Patent, Oakland, CA, US, **2018**.
- [217] B. Li, T. Wang, D. Luo, P. Peng, Y. Wang, L. Liu, H. Wang, H. Liu, *Adv. Mater. Technol.* **2023**, *2201814*.

- [218] H. Liu, J. Geng, Q. Zhu, L. Zhang, F. Wang, T. Chen, L. Sun, *Sensors* **2019**, *20*, 86.
- [219] a) L. Jiang, G. Lu, Y. Yang, Y. Zeng, Y. Sun, R. Li, M. S. Humayun, Y. Chen, Q. Zhou, *Energy Environ. Sci.* **2021**, *14*, 1490; b) L. Jiang, B. Wu, X. Wei, X. Lv, H. Xue, G. Lu, Y. Zeng, J. Xing, W. Wu, J. Wu, *Mater. Horiz.* **2022**, *9*, 2180.
- [220] W. Liu, C. Zhu, D. Wu, *IEEE Electron Device Lett.* **2021**, *42*, 240.
- [221] H. Hu, Y. Ma, X. Gao, D. Song, M. Li, H. Huang, X. Qian, R. Wu, K. Shi, H. Ding, M. Lin, X. Chen, W. Zhao, B. Qi, S. Zhou, R. Chen, Y. Gu, Y. Chen, Y. Lei, C. Wang, C. Wang, Y. Tong, H. Cui, A. Abdal, Y. Zhu, X. Tian, Z. Chen, C. Lu, X. Yang, J. Mu, et al., *Nat. Biomed. Eng.* **2023**.
- [222] J. Lu, X. Jiang, in *2019 IEEE International Ultrasonics Symposium (IUS)*, **2019**, pp. 1753–1756.
- [223] S. Jiang, T. Zhang, Y. Zhou, P. Lai, Y. Huang, *The Innovation* **2023**, *4*, 100447.
- [224] D. Seo, R. M. Neely, K. Shen, U. Singhal, E. Alon, J. M. Rabaey, J. M. Carmena, M. M. Maharbiz, *Neuron* **2016**, *91*, 529.
- [225] Q. Zhu, L. Zhang, H. Liu, T. Chen, L. Sun, X. Le, J. Xie, in *2018 IEEE 13th Annual International Conference on Nano/Micro Engineered and Molecular Systems (NEMS)*, **2018**, pp. 345–348.
- [226] Q. Ren, J. Chen, X. Liu, S. Zhang, Y. Gu, *Sensors* **2022**, *22*, 8100.
- [227] a) L. Song, S. Glinsek, E. Defay, *Appl. Phys. Rev.* **2021**, *8*, 041315; b) T. Liu, A. Dangi, J. N. Kim, S.-R. Kothapalli, K. Choi, S. Trolier-McKinstry, T. Jackson, *Sensors* **2021**, *21*, 1014.
- [228] L. Zhen, Z. Liu, Z. Liu, Q. Wang, J. Liu, Z. Yao, B. Yang, *IEEE Sensors Journal* **2023**, *23*, 5270.
- [229] S. Xu, Y. Zhang, J. Cho, J. Lee, X. Huang, L. Jia, J. A. Fan, Y. Su, J. Su, H. Zhang, H. Cheng, B. Lu, C. Yu, C. Chuang, T.-i. Kim, T. Song, K. Shigeta, S. Kang, C. Dagdeviren, I. Petrov, P. V. Braun, Y. Huang, U. Paik, J. A. Rogers, *Nat. Commun.* **2013**, *4*, 1543.
- [230] H. Liu, J. Geng, Q. Zhu, L. Zhang, F. Wang, T. Chen, L. Sun, *Sensors* **2020**, *20*, 86.
- [231] M. H. Behfar, D. D. Vito, A. Korhonen, D. Nguyen, B. M. Amin, T. Kurkela, M. Tuomikoski, M. Mäntysalo, *IEEE Trans. Compon., Packag., Manuf. Technol.* **2021**, *11*, 1022.
- [232] F. Xu, Y. Zhu, *Adv. Mater.* **2012**, *24*, 5117.
- [233] J.-H. Kim, S.-R. Kim, H.-J. Kil, Y.-C. Kim, J.-W. Park, *Nano Lett.* **2018**, *18*, 4531.
- [234] A. Kalra, A. Lowe, A. M. Al-Jumaily, *J. Mater. Sci. Eng.* **2016**, *5*, 1.
- [235] a) Z. Ma, C. Bourquard, Q. Gao, S. Jiang, T. De Lure-Grimmel, R. Huo, X. Li, Z. He, Z. Yang, G. Yang, Y. Wang, E. Lam, Z.-h. Gao, O. Supponen, J. Li, *Science* **2022**, *377*, 751; b) K. Nan, V. R. Feig, B. Ying, J. G. Howarth, Z. Kang, Y. Yang, G. Traverso, *Nat. Rev. Mater.* **2022**, *7*, 908.
- [236] a) B. Ying, R. Z. Chen, R. Zuo, J. Li, X. Liu, *Adv. Funct. Mater.* **2021**, *31*, 2104665; b) B. Ying, X. Liu, *iScience* **2021**, *24*, 103174.
- [237] a) C. Zhang, X. Geng, F. Yao, L. Liu, Z. Guo, Y. Zhang, Y. Wang, *Appl. Sci.* **2023**, *13*, 5664; b) J. Lim, *Biomed. Eng. Lett.* **2022**, *12*, 219; c) C. Chen, M. A. P. Pertijs, *IEEE Open Journal of the Solid-State Circuits Society* **2021**, *1*, 104.
- [238] X. Xu, H. Venkataraman, S. Oswal, E. Bartolome, K. Vasanth, in *2010 IEEE International Ultrasonics Symposium*, **2010**, pp. 310–313.
- [239] a) J. M. Rothberg, T. S. Ralston, A. G. Rothberg, J. Martin, J. S. Zahorian, S. A. Alie, N. J. Sanchez, K. Chen, C. Chen, K. Thiele, D. Grosjean, J. Yang, L. Bao, R. Schneider, S. Schaez, C. Meyer, A. Neben, B. Ryan, J. R. Petrus, J. Lutsky, D. McMahonill, G. Corteville, M. R. Hageman, L. Miller, K. G. Fife, *Proc. Natl. Acad. Sci. USA* **2021**, *118*, e2019339118; b) D. Chen, X. Cui, Q. Zhang, D. Li, W. Cheng, C. Fei, Y. Yang, *Micromachines* **2022**, *13*, 114; c) E. Alcaín, P. R. Fernández, R. Nieto, A. S. Montemayor, J. Vilas, A. Galiana-Bordera, P. M. Martinez-Girones, C. Prieto-de-la-Lastra, B. Rodriguez-Vila, M. Bonet, C. Rodriguez-Sanchez, I. Yahyaoui, N. Malpica, S. Borromeo, F. Machado, A. Torrado-Carvajal, *Electronics* **2021**, *10*, 3118.
- [240] J. Lee, K. R. Lee, B. E. Eovino, J. H. Park, L. Y. Liang, L. Lin, H. J. Yoo, J. Yoo, *IEEE J. Solid-State Circuits* **2021**, *56*, 1910.
- [241] I. Zamora, E. Ledesma, A. Uranga, N. Barniol, *IEEE Access* **2020**, *8*, 142785.
- [242] Y. M. Hopf, B. Ossenkoppele, M. Soozande, E. Noothout, Z. Y. Chang, H. J. Vos, J. G. Bosch, M. D. Verweij, N. d. Jong, M. A. P. Pertijs, *IEEE Solid State Circuits Lett.* **2022**, *5*, 166.
- [243] I. Zamora, E. Ledesma, A. Uranga, N. Barniol, *IEEE Electron Device Lett.* **2022**, *43*, 1113.
- [244] D. Giusti, F. Quaglia, D. Rahul, V. S. Rao, A. Savoia, M. Shaw, D. H. S. Wee, in *2022 IEEE 24th Electronics Packaging Technology Conference (EPTC)*, **2022**, pp. 280–285.
- [245] R. Bharath, P. Kumar, C. Dusa, V. Akkala, S. Puli, H. Ponduri, K. D. Krishna, P. Rajalakshmi, S. N. Merchant, M. A. Mateen, U. B. Desai, *J. Imaging* **2015**, *1*, 193.
- [246] S. Shomaji, P. Dehghanzadeh, A. Roman, D. Forte, S. Bhunia, S. Mandal, *IEEE Consumer Electronics Magazine* **2019**, *8*, 12.
- [247] T. Noda, T. Azuma, Y. Ohtake, I. Sakuma, N. Tomii, *IEEE Trans. Ultrason. Ferroelectr. Freq. Control.* **2022**, *69*, 3232.
- [248] B. W. Drinkwater, P. D. Wilcox, *Nephrol Dial Transplant* **2006**, *39*, 525.
- [249] Y. Zheng, X. Zhao, S.-J. Song, J. Zhang, *Wave Motion* **2020**, *94*, 102494.
- [250] C. K. S. Park, T. Trumpour, A. Aziz, J. S. Bax, D. Tessier, L. Gardi, A. Fenster, *Sci. Rep.* **2023**, *13*, 14390.
- [251] B. H. McGhee, E. J. Bridges, *Critical Care Nurse* **2002**, *22*, 60.
- [252] C. Dagdeviren, *Science* **2016**, *354*, 1109.
- [253] A. Huang, M. Yoshida, Y. Ono, S. Rajan, in *2017 IEEE International Ultrasonics Symposium (IUS)*, **2017**, pp. 1–4.
- [254] X. Gao, X. Chen, H. Hu, X. Wang, W. Yue, J. Mu, Z. Lou, R. Zhang, K. Shi, X. Chen, M. Lin, B. Qi, S. Zhou, C. Lu, Y. Gu, X. Yang, H. Ding, Y. Zhu, H. Huang, Y. Ma, M. Li, A. Mishra, J. Wang, S. Xu, *Nat. Commun.* **2022**, *13*, 7757.
- [255] P. Hamelmann, R. Vullings, A. F. Kolen, J. W. M. Bergmans, J. O. E. H. v. Laar, P. Tortoli, M. Mischi, *IEEE Trans. Ultrason. Ferroelectr. Freq. Control.* **2020**, *67*, 226.
- [256] I. Song, J. Yoon, J. Kang, M. Kim, S. W. Jang, N.-Y. Shin, Y. Yoo, *Appl. Sci.* **2019**, *9*, 2202.
- [257] J. M. Cannata, T. Chilipka, H.-C. Yang, S. Han, S. W. Ham, V. L. Rowe, F. A. Weaver, K. K. Shung, D. Vilkomerson, *J. Ultrasou. Med.* **2012**, *31*, 1795.
- [258] H. Jin, Z. Zheng, Z. Cui, Y. Jiang, G. Chen, W. Li, Z. Wang, J. Wang, C. Yang, W. Song, X. Chen, Y. Zheng, *Nat. Commun.* **2023**, *14*, 4692.
- [259] a) Y. Ma, Y. Zhang, S. Cai, Z. Han, X. Liu, F. Wang, Y. Cao, Z. Wang, H. Li, Y. Chen, X. Feng, *Adv. Mater.* **2020**, *32*, 1902062; b) H.-R. Lim, H. S. Kim, R. Qazi, Y.-T. Kwon, J.-W. Jeong, W.-H. Yeo, *Adv. Mater.* **2020**, *32*, 1901924.
- [260] a) N. Nazmi, M. A. Abdul Rahman, S.-I. Yamamoto, S. A. Ahmad, H. Stanzuri, S. A. Mazlan, *Sensors* **2016**, *16*, 1304; b) S. Đorđević, S. Stančin, A. Meglič, V. Milutinović, S. Tomažič, *Sensors* **2011**, *11*, 9411.
- [261] K. Kim, W. R. Wagner, *Ann. Biomed. Eng.* **2016**, *44*, 621.
- [262] P. N. T. Wells, H.-D. Liang, *J. R. Soc., Interface* **2011**, *8*, 1521.
- [263] A. Ozturk, J. R. Grajo, M. Dhyani, B. W. Anthony, A. E. Samir, *Abdominal Radiology* **2018**, *43*, 773.
- [264] F. Zabiollahy, B. M. Trindade, Y. Ono, E. D. Lemaire, in *2016 IEEE EMBS International Student Conference (ISC)*, **2016**, pp. 1–4.
- [265] I. AlMohimeed, M. Agarwal, Y. Ono, in *2018 IEEE Canadian Conference on Electrical & Computer Engineering (CCECE)*, **2018**, pp. 1–4.
- [266] I. AlMohimeed, Y. Ono, in *2019 IEEE International Conference on Flexible and Printable Sensors and Systems (FLEPS)*, **2019**, pp. 1–3.
- [267] X. Xue, B. Zhang, S. Moon, G.-X. Xu, C.-C. Huang, N. Sharma, X. Jiang, *Biosensors* **2023**, *13*, 134.

- [268] Y. Bai, H. Jantunen, J. Juuti, *Adv. Mater.* **2018**, *30*, 1707271.
- [269] H. Liu, J. Zhong, C. Lee, S.-W. Lee, L. Lin, *Appl. Phys. Rev.* **2018**, *5*, 041306.
- [270] L. Mateu, T. Dräger, I. Mayordomo, M. Pollak, in *WearableSensors* (Eds.: E. Sazonov, M. R. Neuman), Academic Press, Oxford **2014**, pp. 235–298.
- [271] J. Andreu-Perez, D. R. Leff, H. M. D. Ip, G. Yang, *IEEE Trans. Biomed. Eng.* **2015**, *62*, 2750.
- [272] X. Huang, L. Wang, H. Wang, B. Zhang, X. Wang, R. Y. Z. Stening, X. Sheng, L. Yin, *Small* **2019**, 1902827.
- [273] J. Deng, X. Sun, H. Peng, *EcoMat* **2023**, *5*, e12343.
- [274] S. Lee, Q. Shi, C. Lee, *APL Mater.* **2019**, *7*, 031302.
- [275] S. Ozeri, D. Shmilovitz, *Ultrasonics* **2010**, *50*, 556.
- [276] Q. Shi, T. Wang, C. Lee, *Sci. Rep.* **2016**, *6*, 24946.
- [277] L. Jiang, Y. Yang, R. Chen, G. Lu, R. Li, D. Li, M. S. Humayun, K. K. Shung, J. Zhu, Y. Chen, Q. Zhou, *Nano Energy* **2019**, *56*, 216.
- [278] a) D. B. Christensen, S. Roundy, *J. Intell Mater Syst Struct* **2015**, *27*, 1092; b) Q. He, J. Liu, B. Yang, X. Wang, X. Chen, C. Yang, *Sens. Actuators, A* **2014**, *219*, 65.
- [279] D. K. Piech, B. C. Johnson, K. Shen, M. M. Ghanbari, K. Y. Li, R. M. Neely, J. E. Kay, J. M. Carmena, M. M. Maharbiz, R. Muller, *Nat. Biomed. Eng.* **2020**, *4*, 207.
- [280] C. Chen, Z. Wen, J. Shi, X. Jian, P. Li, J. T. W. Yeow, X. Sun, *Nat. Commun.* **2020**, *11*, 4143.
- [281] a) T. Maleki, N. Cao, S. H. Song, C. Kao, S. Ko, B. Ziaie, *IEEE Trans. Biomed. Eng.* **2011**, *58*, 3104; b) J. Moore, S. Castellanos, S. Xu, B. Wood, H. Ren, Z. T. H. Tse, *Ann. Biomed. Eng.* **2019**, *47*, 22.
- [282] L. Jiang, Y. Yang, R. Chen, G. Lu, R. Li, J. Xing, K. K. Shung, M. S. Humayun, J. Zhu, Y. Chen, Q. Zhou, *Adv. Funct. Mater.* **2019**, *29*, 1902522.
- [283] S. Selvarajan, A. Kim, S. H. Song, *IEEE Access* **2020**, *8*, 68219.
- [284] E. Mehdizadeh, G. Piazza, in *Proc. IEEE Int. Ultrason. Symp. (IUS)*, IEEE, Washington, DC, USA **2017**, pp. 1–4.
- [285] a) R. J. Coffey, *Artif. Organs* **2009**, *33*, 208; b) J. M. Bronstein, M. Tagliati, R. L. Alterman, A. M. Lozano, J. Volkmann, A. Stefani, F. B. Horak, M. S. Okun, K. D. Foote, P. Krack, R. Pahwa, J. M. Henderson, M. I. Hariz, R. A. Bakay, A. Rezaei, W. J. Marks Jr., E. Moro, J. L. Vitek, F. M. Weaver, R. E. Gross, M. R. DeLong, *Arch Neurol* **2011**, *68*, 165.
- [286] a) N. E. O'Connell, L. Marston, S. Spencer, L. H. DeSouza, B. M. Wand, *Cochrane Database Syst Rev* **2018**, *3*, CD008208; b) N. Obidin, F. Tasnim, C. Dagdeviren, *Adv. Mater.* **2020**, *32*, 1901482; c) J. Rivnay, H. Wang, L. Frenno, K. Deisseroth, G. G. Malliaras, *Sci. Adv.* **2017**, *3*, e1601649.
- [287] a) A. Marino, G. G. Genchi, V. Mattoli, G. Ciofani, *Nano Today* **2017**, *14*, 9; b) A. Carpentier, M. Canney, A. Vignot, V. Reina, K. Beccaria, C. Horodyckid, C. Karachi, D. Leclercq, C. Lafon, J.-Y. Chapelon, L. Capelle, P. Cornu, M. Sanson, K. Hoang-Xuan, J.-Y. Delattre, A. Idbah, *Sci. Transl. Med.* **2016**, *8*, 343.
- [288] a) Y. Tufail, A. Yoshihiro, S. Pati, M. M. Li, W. J. Tyler, *Nature Protocols* **2011**, *6*, 1453; b) A. Haritonova, D. Liu, E. S. Ebbini, *IEEE Transactions on Ultrasonics, Ferroelectrics, and Frequency Control* **2015**, *62*, 2031; c) A. Marino, S. Arai, Y. Hou, E. Sinibaldi, M. Pellegrino, Y.-T. Chang, B. Mazzolai, V. Mattoli, M. Suzuki, G. Ciofani, *ACS Nano* **2015**, *9*, 7678; d) R. M. Neely, D. K. Piech, S. R. Santacruz, M. M. Maharbiz, J. M. Carmena, *Current Opinion in Neurobiology* **2018**, *50*, 64; e) W. Qiu, A. Bouakaz, E. E. Konofagou, H. Zheng, *IEEE Transactions on Ultrasonics, Ferroelectrics, and Frequency Control* **2021**, *68*, 6.
- [289] a) A. Javid, S. Ilham, M. Kiani, *IEEE Trans Biomed Circuits Syst* **2023**, *1*; b) J. Blackmore, S. Shrivastava, J. Sallet, C. R. Butler, R. O. Cleveland, *Ultrasound in Medicine & Biology* **2019**, *45*, 1509.
- [290] a) A. Fomenko, C. Neudorfer, R. F. Dallapiazza, S. K. Kalia, A. M. Lozano, *Brain Stimul* **2018**, *11*, 1209; b) S. Wang, W. Meng, Z. Ren, B. Li, T. Zhu, H. Chen, Z. Wang, B. He, D. Zhao, H. Jiang, *Front Physiol* **2020**, *11*, 787.
- [291] a) C. Rojas, M. Tedesco, P. Massobrio, A. Marino, G. Ciofani, S. Martinoia, R. Raiteri, *J. Neural Eng.* **2018**, *15*, 036016; b) D. P. Darrow, *Neurotherapeutics* **2019**, *16*, 88.
- [292] J. Lee, K. Ko, H. Shin, S.-J. Oh, C. J. Lee, N. Chou, N. Choi, M. Tack Oh, B. Chul Lee, S. Chan Jun, I.-J. Cho, *Microsyst. Nanoeng.* **2019**, *5*, 28.
- [293] a) J. Kim, S. Lee, *IEEE ASME Trans Mechatron* **2016**, *21*, 2284; b) O. Naor, S. Krupa, S. Shoham, *J. Neural Eng.* **2016**, *13*, 031003.
- [294] D. K. Piech, J. E. Kay, B. E. Boser, M. M. Maharbiz, in *2017 39th Annual International Conference of the IEEE Engineering in Medicine and Biology Society (EMBC)*, **2017**, pp. 221–225.
- [295] V. Falanga, R. R. Isseroff, A. M. Soulika, M. Romanelli, D. Margolis, S. Kapp, M. Granick, K. Harding, *Nat. Rev. Dis. Primers* **2022**, *8*, 50.
- [296] a) W. J. Ennis, C. Lee, K. Gellada, T. F. Corbiere, T. J. Koh, *Plast. Reconstr. Surg.* **2016**, *138*, 94s; b) R. Luo, J. Dai, J. Zhang, Z. Li, *Adv. Healthcare Mater.* **2021**, *10*, 2100557.
- [297] a) A. Harrison, V. Alt, *Injury* **2021**, *52*, S91; b) C. McCarthy, G. Camci-Unal, *Micromachines* **2021**, *12*, 1488.
- [298] a) V. S. Bachu, J. Kedda, I. Suk, J. J. Green, B. Tyler, *Ann. Biomed. Eng.* **2021**, *49*, 1975; b) L. Li, X. Zhang, J. Zhou, L. Zhang, J. Xue, W. Tao, *Small* **2022**, *18*, 2107705.
- [299] P. Chen, P. Wu, X. Wan, Q. Wang, C. Xu, M. Yang, J. Feng, B. Hu, Z. Luo, *Nano Energy* **2021**, *86*, 106123.
- [300] X. Shi, Y. Chen, Y. Zhao, M. Ye, S. Zhang, S. Gong, *Biomater. Sci.* **2022**, *10*, 692.
- [301] P. Chen, C. Xu, P. Wu, K. Liu, F. Chen, Y. Chen, H. Dai, Z. Luo, *ACS Nano* **2022**, *16*, 16513.
- [302] B. C. Seah, B. M. Teo, *Int. J. Nanomed.* **2018**, *13*, 7749.
- [303] B. E. Polat, D. Hart, R. Langer, D. Blankschtein, *J. Controlled Release* **2011**, *152*, 330.
- [304] A. Azagury, L. Khoury, G. Eenden, J. Kost, *Adv. Drug Delivery Rev.* **2014**, *72*, 127.
- [305] M. T. Chorsi, T. T. Le, F. Lin, T. Vinikoor, R. Das, J. F. Stevens, C. Mundrane, J. Park, K. T. M. Tran, Y. Liu, J. Pfund, R. Thompson, W. He, M. Jain, M. D. Morales-Acosta, O. R. Bilal, K. Kazerounian, H. Illies, T. D. Nguyen, *Sci. Adv.* **2023**, *9*, eadg6075.
- [306] J. Li, Y. Xie, X. Zou, Z. Li, W. Liu, G. Liu, M. Ma, Y. Zheng, *Mater Today Bio* **2023**, *20*, 100665.
- [307] a) D. L. Miller, N. B. Smith, M. R. Bailey, G. J. Czarnota, K. Hynynen, I. R. S. Makin, M. Bioeffects Committee of the American Institute of Ultrasound, *J. Ultrasou. Med.* **2012**, *31*, 623; b) K. G. Baker, V. J. Robertson, F. A. Duck, *Physical Therapy* **2001**, *81*, 1351.
- [308] a) G. ter Haar, *Progress in Biophysics and Molecular Biology* **2007**, *93*, 111; b) M. R. Bailey, V. A. Khokhlova, O. A. Sapozhnikov, S. G. Kargl, L. A. Crum, *Acoust. Phys.* **2003**, *49*, 369; c) S.-J. Kang, J. J. Pak, *Nano* **2017**, *5*, 22; d) Y. Zhou, *Gastroenterology Research and Practice* **2014**, *2014*, 11; e) Y. Wang, J. Li, J. Zhou, Y. Qiu, J. Song, *Ultrasonics* **2022**, *121*, 106678.
- [309] M. D. Langer, G. K. Lewis Jr., *Proc. SPIE Int. Soc. Opt. Eng.* **2015**, *9467*, 946701.
- [310] H. D. Tiwari, K. Jae-Hyung, W. H. Cho, in *2018 IEEE International Symposium on Circuits and Systems (ISCAS)*, **2018**, pp. 1–5.
- [311] H. Liu, J. Geng, Q. Zhu, L. Zhang, F. Wang, T. Chen, L. Sun, *Sensors* **2020**, *20*, 86.
- [312] Y. Tian, W. Sang, H. Tian, L. Xie, G. Wang, Z. Zhang, W. Li, Y. Dai, *Adv. Funct. Mater.* **2022**, *32*, 2205690.
- [313] a) W. Wang, W. Sun, Y. Du, W. Zhao, L. Liu, Y. Sun, D. Kong, H. Xiang, X. Wang, Z. Li, Q. Ma, *ACS Nano* **2023**, *17*, 9793; b) R. Luo, B. Shi, D. Luo, Z. Li, *Sci. Bull.* **2023**, *68*, 1740; c) Z. Li, in *Handbook of Triboelectric Nanogenerators* (Eds.: Z. L. Wang, Y. Yang, J. Zhai, J. Wang), Springer International Publishing, Cham **2023**, pp. 597–626.

- [314] a) Y. Zou, P. Tan, B. Shi, H. Ouyang, D. Jiang, Z. Liu, H. Li, M. Yu, C. Wang, X. Qu, L. Zhao, Y. Fan, Z. L. Wang, Z. Li, *Nat. Commun.* **2019**, *10*, 2695; b) W.-G. Kim, D.-W. Kim, I.-W. Tcho, J.-K. Kim, M.-S. Kim, Y.-K. Choi, *ACS Nano* **2021**, *15*, 258; c) H. Ouyang, Z. Li, *Sci. Bull.* **2019**, *64*, 1565.
- [315] R. Hinchet, H.-J. Yoon, H. Ryu, M.-K. Kim, E.-K. Choi, D.-S. Kim, S.-W. Kim, *Science* **2019**, *365*, 491.
- [316] a) R. Bouchard, O. Sahin, S. Emelianov, *IEEE Trans. Ultrason. Ferroelectr. Freq. Control.* **2014**, *61*, 450; b) M. Wu, N. Awasthi, N. M. Rad, J. P. W. Pluim, R. G. P. Lopata, *Sensors* **2021**, *21*, 7947; c) S. Wang, Y. Zhao, Y. Xu, *Vis Comput Ind Biomed Art* **2020**, *3*, 24.
- [317] H. Chen, S. Agrawal, M. Osman, J. Minotto, S. Mirg, J. Liu, A. Dangi, Q. Tran, T. Jackson, S.-R. Kothapalli, *BME Front.* **2022**, *2022*, 9871098.
- [318] K. Roy, S. Agrawal, A. Dangi, T. Liu, H. Chen, T. N. Jackson, R. Pratap, S. R. Kothapalli, in *2020 IEEE International Ultrasonics Symposium (IUS)*, **2020**, pp. 1–4.
- [319] J. Zhang, A. Wiacek, Z. Feng, K. Ding, M. A. Lediju Bell, *Biomed. Opt. Express* **2023**, *14*, 4349.
- [320] Y. H. Liu, L. X. Chen, C. Y. Li, F. S. Lin, H. Y. Su, C. T. Tsai, L. W. Wang, Y. H. Wang, C. H. Huang, *IEEE Sens. J.* **2022**, *22*, 2070.
- [321] J. Zhang, A. Wiacek, E. González, Z. Feng, K. Ding, M. A. L. Bell, in *2022 IEEE International Ultrasonics Symposium (IUS)*, **2022**, pp. 1–4.
- [322] a) H. Kim, J. Song, S. Kim, S. Lee, Y. Park, S. Lee, S. Lee, J. Kim, *Biosensors* **2023**, *13*, 470; b) S. H. D. Wong, G. R. Deen, J. S. Bates, C. Maiti, C. Y. K. Lam, A. Pachauri, R. AlAnsari, P. Bělský, J. Yoon, J. M. Dodda, *Adv. Funct. Mater.* **2023**, *33*, 2213560; c) D. Ryu, D. H. Kim, J. T. Price, J. Y. Lee, H. U. Chung, E. Allen, J. R. Walter, H. Jeong, J. Cao, E. Kulikova, H. Abu-Zayed, R. Lee, K. L. Martell, M. Zhang, B. R. Kampmeier, M. Hill, J. Lee, E. Kim, Y. Park, H. Jang, H. Arafa, C. Liu, M. Chisembele, B. Vwalika, N. Sindano, M. B. Spelke, A. S. Paller, A. Premkumar, W. A. Grobman, J. S. A. Stringer, et al., *Proc. Natl. Acad. Sci. USA* **2021**, *118*, e2100466118.
- [323] L. Zhao, C. Liang, Y. Huang, G. Zhou, Y. Xiao, N. Ji, Y.-T. Zhang, N. Zhao, *NPJ Digit Med* **2023**, *6*, 93.
- [324] J. R. Sempionatto, M. Lin, L. Yin, E. De la paz, K. Pei, T. Sona-ard, A. N. de Loyola Silva, A. A. Khorshed, F. Zhang, N. Tostado, S. Xu, J. Wang, *Nat. Biomed. Eng.* **2021**, *5*, 737.
- [325] Y. Fang, X. Zhao, T. Tat, X. Xiao, G. Chen, J. Xu, J. Chen, *Matter* **2021**, *4*, 1102.
- [326] Q. Shi, Z. Sun, X. Le, J. Xie, C. Lee, *ACS Nano* **2023**, *17*, 4985.
- [327] Z. Tan, H. Zhang, X. Wu, J. Xing, Q. Zhang, J. Zhu, *Phys. Rev. Lett.* **2023**, *130*, 246802.
- [328] L. Li, L. Zhao, R. Hassan, H. Ren, *Machines* **2023**, *11*, 325.
- [329] a) J.-H. Kim, C. Marcus, R. Ono, D. Sadat, A. Mirzazadeh, M. Jens, S. Fernandez, S. Zheng, T. Durak, C. Dagdeviren, *Nat. Electron.* **2022**, *5*, 794; b) J.-H. Lee, K. H. Cho, K. Cho, *Adv. Mater.* **2023**, *35*, 2209673.
- [330] X. Huang, M. A. L. Bell, K. Ding, *IEEE Transactions on Medical Imaging* **2021**, *40*, 3178.
- [331] X. Ma, Y. Liu, J. Ruan, C. Tao, J. Yuan, Y. Chang, W. Cao, *IEEE Trans. Ultrason. Ferroelectr. Freq. Control.* **2022**, *69*, 751.
- [332] S. Han, G. Jiang, Y. Zhu, Y. Liu, H. Zhang, L. Bian, D. Liu, Y. Sun, L. Zheng, B. Yang, W. Cao, *J. Adv. Dielectr.* **2023**, 2350012.
- [333] Q. Zhang, X. Pang, Z. Zhang, M. Su, J. Hong, H. Zheng, W. Qiu, K. H. Lam, *IEEE Trans. Ultrason. Ferroelectr. Freq. Control.* **2019**, *66*, 1102.
- [334] Z. Jiang, C. Hou, C. Fei, Z. Li, Z. G. Ye, *IEEE Trans. Ultrason. Ferroelectr. Freq. Control.* **2022**, *69*, 795.
- [335] C. Zou, Y. Li, S. Hou, Z. Liu, H. Tang, S. Chen, J. Peng, *IEEE Trans. Ultrason. Ferroelectr. Freq. Control.* **2022**, *69*, 744.
- [336] W. Wang, S. W. Or, Q. Yue, Y. Zhang, J. Jiao, C. M. Leung, X. Zhao, H. Luo, *Sens. Actuators, A* **2013**, *196*, 70.
- [337] J. Xing, L. Jiang, C. Zhao, Z. Tan, Q. Xu, J. Wu, Q. Chen, D. Xiao, J. Zhu, *Journal of Materiomics* **2020**, *6*, 513.
- [338] C. Fei, T. Zhao, D. Wang, Y. Quan, P. Lin, D. Li, Y. Yang, J. Cheng, C. Wang, C. Wang, Q. Zhou, *Micromachines* **2018**, *9*, 291.
- [339] P. Lin, C. Fei, S. Hou, T. Zhao, Q. Chen, Y. Quan, K. K. Shung, Q. Zhou, *IEEE Sens. J.* **2018**, *18*, 5685.
- [340] C. Fei, T. Zhao, J. Zhang, Y. Quan, D. Wang, X. Yang, Q. Chen, P. Lin, D. Li, Y. Yang, S. Dong, W. Ren, K. K. Shung, Q. Zhou, *J. Alloys Compd.* **2018**, *743*, 365.
- [341] X. Yan, K. H. Lam, X. Li, R. Chen, W. Ren, X. Ren, Q. Zhou, K. K. Shung, *IEEE Trans. Ultrason. Ferroelectr. Freq. Control.* **2013**, *60*, 1272.
- [342] J. M. Cannata, T. A. Ritter, C. Wo-Hsing, R. H. Silverman, K. K. Shung, *IEEE Trans. Ultrason. Ferroelectr. Freq. Control.* **2003**, *50*, 1548.
- [343] T. Zhang, J. Ou-Yang, X. Yang, W. Wei, B. Zhu, *Electron. Mater. Lett.* **2019**, *15*, 1.
- [344] Y. Chen, X. P. Jiang, H. S. Luo, J. Y. Dai, H. L. W. Chan, *IEEE Trans. Ultrason. Ferroelectr. Freq. Control.* **2010**, *57*, 2601.
- [345] J. Ma, S. Xue, X. Zhao, F. Wang, Y. Tang, Z. Duan, T. Wang, W. Shi, Q. Yue, H. Zhou, H. Luo, B. Fang, *Appl. Phys. Lett.* **2017**, *111*, 092903.
- [346] B. Zhu, Z. Zhang, T. Ma, X. Yang, Y. Li, K. K. Shung, Q. Zhou, *Appl. Phys. Lett.* **2015**, *106*, 173504.
- [347] Y. Quan, C. Fei, W. Ren, L. Wang, G. Niu, J. Zhao, J. Zhuang, J. Zhang, K. Zheng, P. Lin, X. Sun, Q. Chen, Z. G. Ye, T. Karaki, *IEEE Trans. Ultrason. Ferroelectr. Freq. Control.* **2021**, *68*, 1979.
- [348] Y. Zhang, X. Zhao, W. Wang, B. Ren, D. Liu, H. Luo, *IEEE Trans. Ultrason. Ferroelectr. Freq. Control.* **2011**, *58*, 1774.
- [349] L. Jiang, H. Chen, Y. Zeng, Z. Tan, J. Wu, J. Xing, J. Zhu, *ACS Appl. Mater. Interfaces* **2022**, *14*, 30979.
- [350] Q. Ke, W. H. Liew, H. Tao, J. Wu, K. Yao, *IEEE Trans. Ultrason. Ferroelectr. Freq. Control.* **2019**, *66*, 1395.
- [351] R. Liu, D. Knapik, K. A. Harasiewicz, F. S. Foster, J. G. Flanagan, C. J. Pavlin, G. E. Trope, in *1999 IEEE Ultrasonics Symposium. Proceedings. International Symposium (Cat. No. 99CH37027)*, Vol. 2, **1999**, pp. 973–976, vol. 972.
- [352] J. H. Cha, J. H. Chang, *Sens. Actuators, A* **2014**, *217*, 39.
- [353] S. Hou, X. Yang, C. Fei, X. Sun, Q. Chen, P. Lin, D. Li, Y. Yang, Q. Zhou, *J. Electron. Mater.* **2018**, *47*, 6842.
- [354] Q. Yue, D. Liu, J. Deng, X. Zhao, D. Lin, W. Di, X. Li, W. Wang, X. a. Wang, H. Luo, *Sens. Actuators, A* **2015**, *234*, 34.
- [355] S. Zhang, F. Li, N. P. Sherlock, J. Luo, H. Jae Lee, R. Xia, R. J. Meyer Jr, W. Hackenberger, T. R. Shrout, *J. Cryst. Growth* **2011**, *318*, 846.
- [356] X. Zhou, K. Zhou, D. Zhang, C. Bowen, Q. Wang, J. Zhong, Y. Zhang, *Nanoenergy Advances* **2022**, *2*, 269.
- [357] Y. Kato, S. Furukawa, K. Samejima, N. Hironaka, M. Kashino, *Front. Neuroeng.* **2012**, *5*, 11.
- [358] S. Gupta, W. T. Navaraj, L. Lorenzelli, R. Dahiya, *Npj Flex Electron* **2018**, *2*, 8.
- [359] L. Gillan, J. Hiltunen, M. H. Behfar, K. Rönkä, *Jpn. J. Appl. Phys.* **2022**, *61*, SE0804.
- [360] S. G. Kirtania, A. W. Elger, M. R. Hasan, A. Wisniewska, K. Sekhar, T. Karacolak, P. K. Sekhar, *Micromachines* **2020**, *11*, 847.
- [361] Memscyclopedia.org, **2023**.
- [362] a) J. Zhu, L. Zhang, Y. Zhao, L.-J. Yin, J.-W. Zha, Z.-M. Dang, *J. Appl. Polym. Sci.* **2022**, *139*, 51595; b) T. Xu, W. Shen, X. Lin, Y. M. Xie, *Polymers* **2020**, *12*, 3010.
- [363] Smooth-On.
- [364] a) M. Pharr, J.-Y. Sun, Z. Suo, *J. Appl. Phys.* **2012**, *111*; b) 3M, 3M, **2022**.
- [365] a) R. M. Grigorescu, F. Ciuprina, P. Ghioca, M. Ghiurea, L. Iancu, B. Spurcaci, D. M. Panaitescu, *J. Phys. Chem. Solids* **2016**, *89*, 97; b) mexopolimeros.



Lin Zhang received his Bachelor's degree in electronic science and technology, Master's degree in microelectronics and solid state electronics at Xi'an Jiaotong University, China, and his Ph.D. in materials engineering at Auburn University, USA. He was involved in research efforts in Materials Engineering at Auburn University, NanoEngineering at UC San Diego, and Electronic Science and Technology at Xi'an Jiaotong University. He joined the MIT Media Lab as Research Scientist since 2019. His scientific interests focus on smart and conformable electronics, include piezoelectric composites for sensors and transducers, dielectric composites for energy storage, and other flexible/stretchable electronics.



Wenya Du received her Bachelor's degree in electronic information engineering at the North China Institute of Aerospace Engineering, China, and her Master's degree in materials engineering at Auburn University, USA. From June 2022, she started her graduate study at Conformable Decoders research group at the MIT Media Lab with the support from the National Science Foundation Graduate Research Fellowship Program (NSF GRFP). She focuses on the high performance conformable piezoelectric electronics for women's healthcare monitoring.



Jin-Hoon Kim received his B.S. and Ph.D. in material science and engineering at Yonsei University, South Korea. He joined Conformable Decoders group in MIT Media Lab as a postdoctoral researcher in 2021. His research interest lies in development of mechanically soft multi-modal sensor arrays for monitoring the biological and environmental signals throughout the human body.



Chia-Chen (Debbie) Yu earned her B.S. degree from the Department of Electrical Engineering at the California Institute of Technology and her M.S. degree from the Electrical Engineering and Computer Science at the Massachusetts Institute of Technology. She earned her Ph.D. in Media Arts and Sciences at Massachusetts Institute of Technology. Her research interest lies in designing and building wearable and implantable conformable devices that actively engage in rehabilitating, monitoring, or improving our bodily functions. She is currently working on developing conformable ultrasound devices for health applications.



Canan Dagdeviren is an associate professor of media arts and sciences and LG career development professor of media arts and sciences at Massachusetts Institute of Technology, where she leads a research group, called Conformable Decoders. Prof. Dagdeviren earned her Ph.D. in materials science and engineering from the University of Illinois at Urbana-Champaign. Her collective research aims to design and fabricate conformable, hybrid electromechanical systems to convert the patterns of nature and the human body into beneficial signals and energy.